Deformation Mechanisms of Single Crystals of FCC Medium Entropy Alloys

2021

Ashif Equbal

Contents

Chapter 1 1

Introduction 1

1.1. Background 1

1.2. Four core effects of HEAs 4

1.3. Plastic deformation mechanism of FCC alloys 9

1.4. Solid Solution Strengthening (S.S.S.) 11

1.5. Temperature dependence of Yield stress of FCC High Entropy alloys 12

1.6. Alloy Selection for the Present Study 14

1.7. Research Objectives 15

1.8. Thesis Outline 16

Chapter 2 22

Deformation Mechanism of Single Crystal FCC Cr-Fe-Co-Ni Medium Entropy alloy 22

2.1. Introduction 22

2.2. Experimental Procedures 24

2.3. Results 27

2.4. Discussions 47

2.5. Conclusions 55

References 57

Chapter 3 61

Deformation Mechanism of single crystal FCC Fe-Co-Ni Medium Entropy alloy 61

3.1. Introduction 61

3.2. Experimental Procedures 63

3.3. Results 66

3.4. Discussions 81

3.5. Conclusions 89

References 91

Chapter 4 94

Mean Square Atomic Displacement: A scaling factor to predict Solid Solution Strengthening in HEAs/MEAs and determine the fitting parameters of the equation used to determine 0K CRSS. 94

4.1. Introduction 94

4.2. Experimental procedures 97

4.3. Results and Discussions 98

4.4. Conclusion 109

References 110

Chapter 5 112

Summary and Conclusions 112

Acknowledgements 116

Chapter 1

Introduction

1.1. Background

Since the beginning of humankind, there was a quest to find and develop different materials and alloys. The progress from natural metals and natural alloys to the accidental discovery of arsenical bronzes is a remarkable story. From binary alloys to ternary to multi-component civilization has come a long way in terms of alloy design. Nonetheless, there was one element in major proportion in all these alloys. Even superalloys are identified with a principal component.

In 2004 Jien-Wei Yeh[1] in Taiwan and Brian Cantor[2] in the United Kingdom, as well as a dependent publication in 2003 by S.Ranganathan[3] in India, ignited research on a unique alloy concept, "high entropy alloys (H.E.A.s) or multi principal element alloys (MPEAs),". This new concept of alloy design withdrew tremendous attention from various research groups across the globe and placed a new milestone in the history of alloy development. High entropy alloys contain five or more principal elements in equiatomic proportions, where each element constitutes 20 at% of the total composition. Cantor[2] reported the first F.C.C. high entropy alloy containing Cr, Mn, Fe, Co and Ni, forming a solid solution with a typical dendrite structure in the as-cast condition. A wide range of multi-component alloys was investigated based on this composition by adding different elements like Cu, Ti, Nb, V, W, Mo, Ta and Ge. Cantor made an important conclusion that the total number of phases is

always less than the allowed maximum number by Gibbs phase rule in equilibrium condition. J. W. Yeh [1,4] believed that high mixing entropy leads to solid solution formation and reduces the number of phases. In 2003, S Ranganathan wrote an article, "Alloyed pleasures-multi cocktail", in which he said that multi-component alloys represent a new frontier in metallurgy[3]. Yeh et al. [1,5] first coined the word high entropy alloys (H.E.A.s). Definition of high entropy alloys was based on high mixing entropy and configurational entropy, responsible for forming a random solid solution. Boltzmann's equation describes the configurational entropy of a system:

$$\Delta S_{conf} = k \ln w \tag{1.1}$$

Where k is Boltzman's constant and w is the number of ways in which the available energy can be mixed. In the case of n component system, the contribution of each component per mole fraction, configurational entropy is given by

$$\Delta S_{conf} = - R\sum_{i=1}^{n} Xi \ln Xi \tag{1.2}$$

where R is the gas constant, n is the number of elements, and Xi is the mole fraction of the constituent elements. For equiatomic compositions, we can write equation 1.2 as

$$\Delta S_{conf} = R \ln n \tag{1.3}$$

R is the gas constant, and n is the number of elements in an equiatomic solid solution.

For solid solutions composed of 5 elements or more in the equiatomic compositions, configurational entropy using equation 1.3 is calculated is $1.61R$ and for $N= 4$ $\Delta Sconf = 1.39R$. Thus it is reasonable to think that $\Delta S_{conf} = 1.5R$ is borderline between high and

medium entropy alloys, as shown in Figure 1.1. In Table 1.1, configurational entropies is listed for traditional alloys at their liquid state.

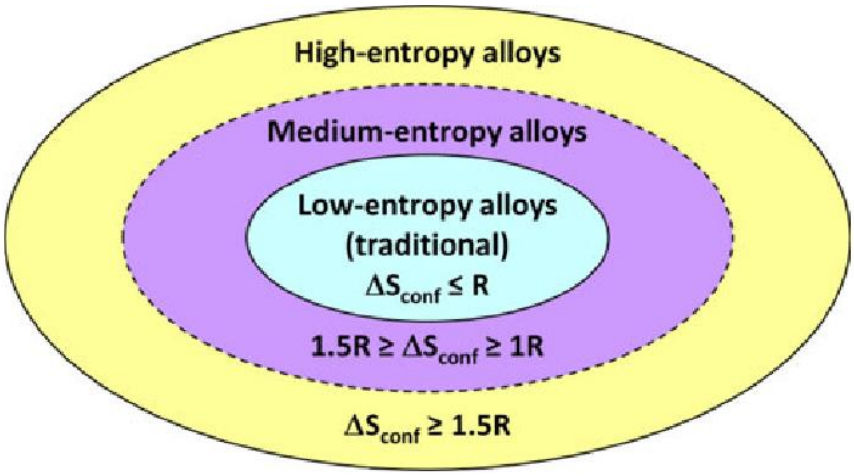

Figure 1-1 shows the alloys based on configurational entropy[5]

System	Alloys	ΔS_{conf} at liquid state
Low alloy steel	440	0.22R low
Stainless steel	304,306	0.96R Low, 1.15R medium
High Speed steel	M2	0.73R Low
Mg Alloy	AZ91D	0.35R low
Al alloy	2024,7075	0.29R low,0.43R low
Cu alloy	7-3 brass	.61R low
Ni-based alloy	Inconel 718, Hastelloy X	1.31R medium, 1.37R medium

Table 1.1

1.2. Four core effects of HEAs

1.2.1. High entropy effect

The high entropy effect is essential because it can enhance solid solutions' formation and simplify the microstructure. As Gibbs free energy of mixing,

$$\Delta G_{mix} = \Delta H_{mix} - T\Delta S_{mix} \quad (1.4)$$

where ΔH_{mix} and ΔS_{mix} are the enthalpies of mixing and entropy of mixing, respectively.

More elements would lower the mixing free energy, especially at a higher temperature, by contributing larger ΔS_{mix}. Because of this, H.E.A.s forms mostly as F.C.C. or B.C.C. solid solutions. Although there are numerous possible states in the solid-state of an alloy, the equilibrium state has the lowest free energy of mixing according to the second law of thermodynamics. There are three possible categories of competing states: elemental phases, intermetallic compounds, and solid solution phases underneath the lowest melting point of the alloy [6]. The elemental phase is the terminal solid solution based on one metal element. An intermetallic compound is a stoichiometric compound with specific superlattices, such as NiAl having a B2 structure and Ni3Ti with a D024 structure. A solid solution is a phase with the complete mixing or significant mixing of all elements in the structure of B.C.C. (body-centred cubic), F.C.C. (Face centred cubic), or H.C.P. (hexagonal close-packed). However, some reports have shown that high entropy effect does not necessarily suppress the formation of compounds. For example, the addition of Boron in the AlCoCrCuFeNi alloy led to the formation of (Cr, Fe)-rich borides [5], and high-temperature annealing experiments showed

that the formed borides were stable [5]. It was suggested that the large negative enthalpy for the formation of borides could override the high entropy effect in such systems. In a different study on the equiatomic Co-Cr-Fe-Mn-Ni having single-phase F.C.C. crystal, Otto et al.[7] evaluated its phase stability under prolonged annealing time intervals for 500 days at intermediate temperature 500°C and high-temperature 900°C. They found that the single-phase solid solution decomposes into different phases (L10-NiMn, B2-FeCo and Cr-rich B.C.C. phase) at 500°C, whereas the solid solution remained stable F.C.C. phase at 900°C. These observations might be understood in a manner conforming to Equation 1.4. For any system, the enthalpy of mixing dominates at low temperatures, whereas the high configuration entropy is effective at high temperatures. Therefore, it has been suggested that the competition between entropy and enthalpy determines the phase formation in the H.E.A.s.

1.2.2. Severe Lattice Distortion Effect

High entropy alloys contain different kinds of elements in the square matrix, and because of that, there is a large lattice strain due to atomic size differences, as shown in Figure 1.2. For plastic deformation of metallic materials, the fundamental mechanism that governs mechanical properties is dislocation slips. Due to the lattice distortion in H.E.A.s, dislocations are expected to possess unusual dislocation core structure, and the Peierls potential fluctuates, which significantly affects the mechanical properties of H.E.A.s as reported by various research groups[5,8,9]. For example, Wu et al. [10] reported a systematic study on the mechanical properties of equiatomic Cr-Mn-Fe-Co-Ni and its other derivatives such as Co-Cr-Fe-Ni, Co-Fe-Ni, all having single-phase F.C.C. structures. They found that

strong temperature dependence of the yield strength was essentially due to lattice friction resulting from the lattice distortion. Okamoto et al.[11] has given a new theory of Mean Square Atomic Displacement(MSAD) and suggests that lattice distortion depends not only on the size of a given atom but also on the environment surrounded by each element of that alloy.

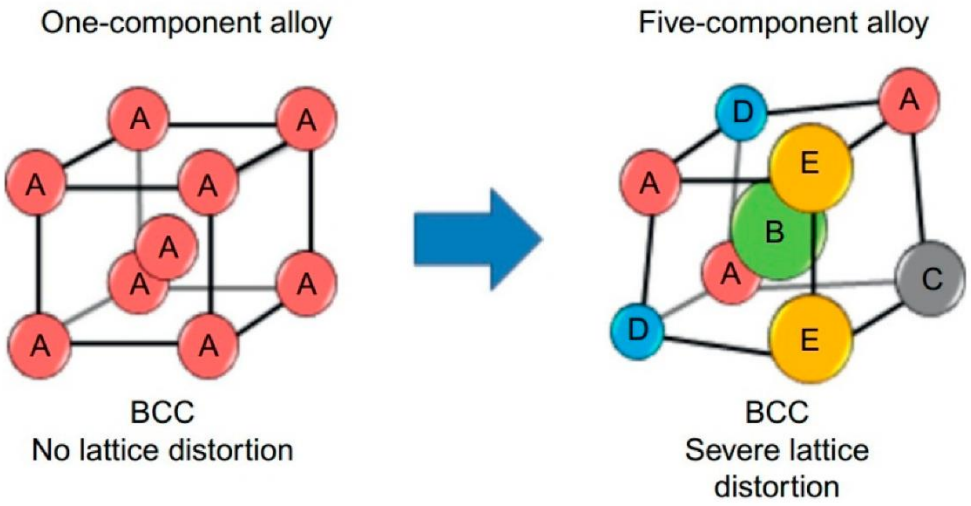

Figure1.2 Schematic diagram showing lattice distortion exists in five-elements B.C.C. lattice[5].

1.2.3. Sluggish Diffusion Effect

H/MEAs mainly contain the random solid solution or ordered solid solution and could be considered as whole-solute matrices. As a result, the diffusion of an atom in a whole-solute matrix would be very dissimilar from that in the matrix of traditional alloys. A vacancy in the whole-solute matrix is surrounded and competed by different-element atoms during diffusion. due to larger lattice potential energy (L.P.E.) fluctuation between lattice sites, slower diffusion and higher activation energy would occur in HEA.s, as proposed by Tsai et

al.[12]. The abundant low-LPE sites can serve as traps and hinder the diffusion of atoms. This leads to the sluggish diffusion effect. They also showed that the activation energy(*Q*) for the diffusion of each element in Cantor alloy was higher than that in metals and traditional alloys. Figure 1.3 compares the activation energies for the diffusion of Co, Cr, Fe, Mn, Ni atoms in different matrices. Ni was reported to have the highest activation energy(A.E.) in cantor alloy, Q ~317.5 kJ mol^{-1}. In additional work, Liu et al.[13] reported a grain coarsening behavior of Co-Cr-Fe-Mn-Ni and found activation energy for the grain growth, Q ~321 kJ mol^{-1}, similar to the value mentioned earlier, which supports the possibility of sluggish diffusion.

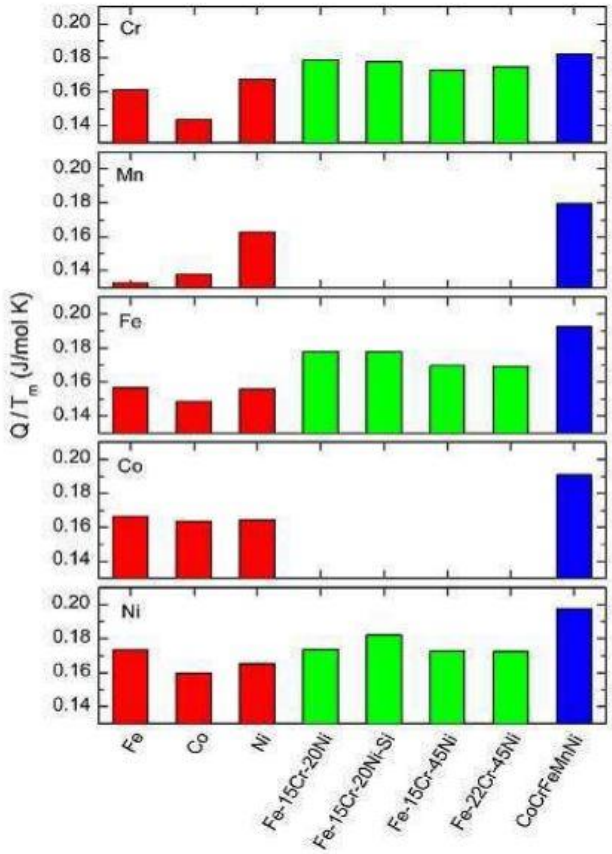

Figure 1.3 Activation energy for the diffusion of Co, Cr, Fe, Mn, and Ni in different matrices. Activation energy is normalized by the melting temperature[5].

1.2.4. Cocktail effects

Cocktail effects in H.E.A.s are used to emphasize the enhancement of properties by at least five major elements. This is because of phase size, shape, distribution, phase boundaries and properties of each phase. For example, Figure 1.4 shows the cocktail effects introduced by the interaction of constituent's elements in the AlCoCrCuFeAl alloy, in which phase transformation from F.C.C. to B.C.C. occurs as a function of Al content beyond the critical values.

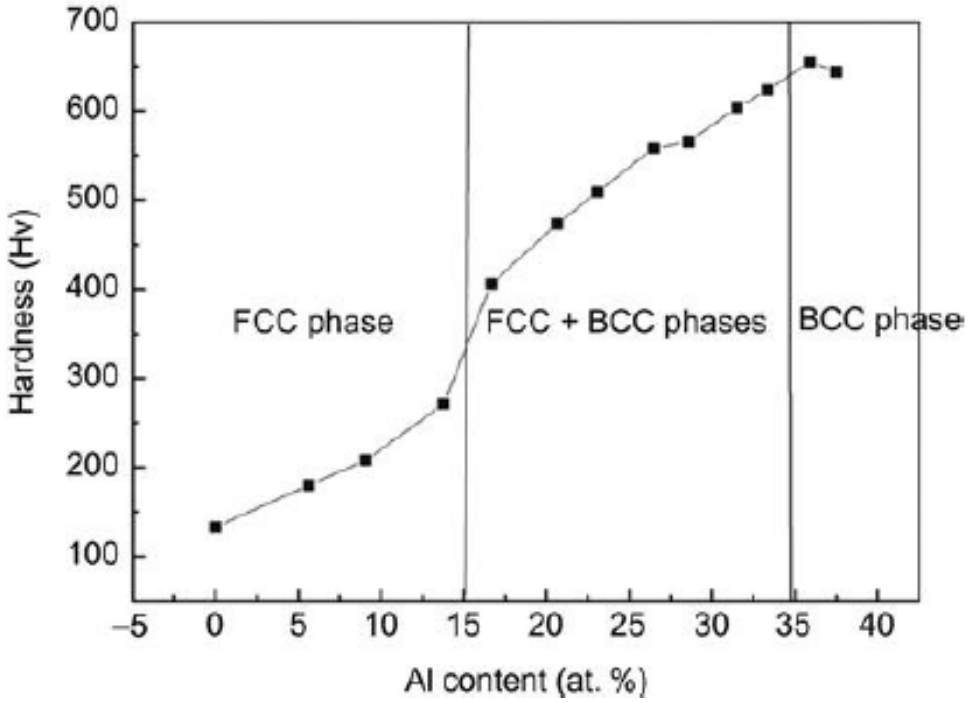

Figure 1.4 Effect of Al content on the hardness of AlxCoCrFeCuNi H.E.A. [5].

1.3. Plastic deformation mechanism of FCC alloys

Slip and Twinning are the major deformation modes for crystalline materials under the action of applied stress. The surface of polished metal crystals, then plastically deformed, becomes covered with one or more parallel lines called slip lines. The plane on which these lines appear is called glide planes or slip planes, while the shear direction is called slip or glide direction. In most metals, the planes on which slip takes place are usually those with the closet atomic packing, while the slip direction is always the closed pack direction in the slip plane. Figure 1.5(a) shows a cross-section of typical slip geometry. Critical resolve shear stress(CRSS) is determined using this geometry required to move a dislocation plastically while applying the stress on a metal crystal. In other words, crystals of a given metal start deforming plastically when the resolved shear stress on the slip plane in the slip direction reaches a critical value τ_0. Figure 1.5(b) shows the closed packed planes in F.C.C. crystal where dislocation can move.

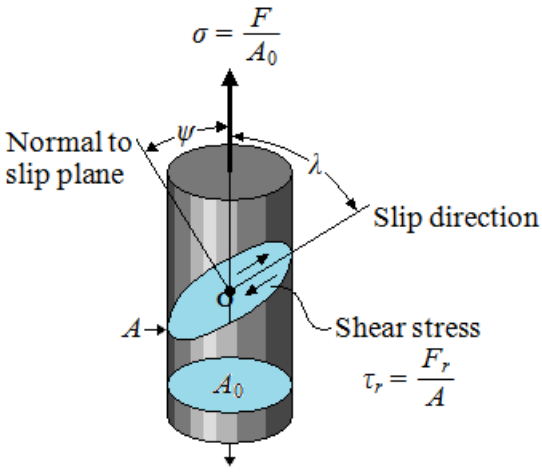

Fig 1.5(a) Cross-section of slip geometrry

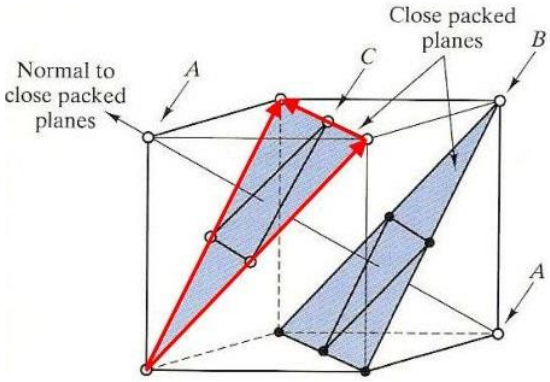

Fig 1.5(b) Closed packed FCC

From Figure1.5(a), CRSS is $\tau_0 = \sigma_0 \cos\psi . cos\lambda$. This is called Schmid's Law.

Twinning Deformation - When deformed, some metals undergo a sudden localized shear process called Twinning, which involves a small but well-defined volume within the crystal. This contrasts with the slip process, which is limited to one crystal plane and is thus a two-dimensional character, although it occurs by shear. Twinning proceeds by the atoms translation for the accommodation of deformation; thus, it is a polar mechanism that cannot be reversible, while the slip is reversible. Blewitt et al. [14] have observed Twinning as a mode of deformation of a single crystal copper at low temperature. Suzuki and Barrett[15] have made similar observations on Au-Ag alloys. For materials with low stacking fault energy, dissociation into partial is more favourable and partial dislocation separation is more extensive, making it difficult for dissociated dislocations to associate and thus impeding the cross slip and climb of dislocations. As a result, the primary deformation mode is more easily change from dislocation glide to mechanical Twinning. Such mechanical Twinning effectively increases the dislocation storage capacity and provides steady work hardening, improving strength and ductility by postponing the onset of plastic instability by necking. F.C.C. High Entropy alloys also displayed twinning phenomena at a lower temperature as they are mostly low stacking fault energy materials[16–18]. Apart from twinning mode, a martensitic transformation (hcp phase) is also reported in low stacking fault energy alloys. Recently in Cr-Mn-Fe-Co-Ni H.E.A., deformation twinning is observed at room temperature and in Cr-Co-Ni M.E.A., twinning deformation observed at room temperature and 77K[16,18–21]. In Figure 1.6(a) and (b), twinning deformation and martensitic transformation (hcp phase) are demonstrated in between the matrix.

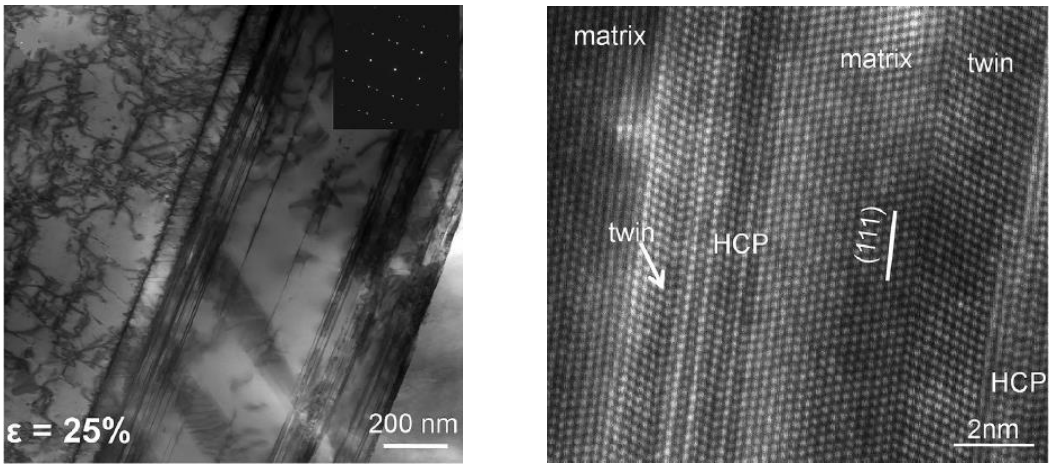

Figure 1.6 (a) and (b) shows the twinning and hcp phase of FCC polycrystal Cr-Co-Ni Medium Entropy alloys.

1.4. Solid Solution Strengthening (S.S.S.)

Solid solution strengthening shoots from the interaction of lattice dislocations with solutes. As a dislocation moves in the crystal, the distortion it persuades on the lattice interacts with the distortions around substitutional solutes [22]. Substitutional solutes in cubic materials distort a lattice both geometrically due to size mismatch with atoms of the host lattice and chemically by introducing a different local bonding environment[24,25]. It is suggested that theories of solute strengthening in alloys can be broadly divided into two categories of strong-pinning and weak-pinning models. The strong-pinning models, such as the ones proposed by Friedel[23] and Fleischer[24], treat the solutes as individual point obstacles that pin the dislocations. On the other hand, the weak-pinning models, initially proposed by Mott[25] and Labusch[26], consider the collective effect of a field of randomly distributed solids on the dislocations.

High Entropy alloys are equiatomic and all the constituents are primary, making it difficult to define 'solute' and 'solvent' separately. Classical theories of S.S.S. can not define the mechanism of solute strengthening in H.E.A.s. Recently, many researchers investigated the S.S.S. theories of high entropy alloys[27–29].

1.5. Temperature dependence of Yield stress of FCC High Entropy alloys

Compared to decades-old theories of strengthening in dilute solid solutions, the mechanical behaviour of concentrated solid solutions is poorly understood. Z. Wu et al. [10] investigated derivatives of Cantor alloy (Cr-Mn-Fe-Co-Ni) in binary, ternary and quaternary alloys to clarify the mechanical behaviour of these HEAs. They found out that Cr-Co-Ni, Cr-Mn-Co-Ni and Cr-Fe-Co-Ni show strong temperature dependence with decreasing temperature (Fig 1.7). It is generally believed that Peierls barriers are high in bcc metals and relatively low in fcc metals and that a significant factor contributing to this difference is the relative widths of the dislocations. Their studies suggest that the dislocations in equiatomic FCC alloys may be narrower than those in pure FCC metals, leading to a more substantial Peierls barrier and temperature dependence of strength. However, the temperature dependence of the equiatomic alloys, while stronger than that of pure FCC metals, is not as strong as that of BCC metals. Specifically, from room temperature to liquid nitrogen temperature, the yield stress of the equiatomic F.C.C. alloys increases by 1.3– 2.0 times compared to 3.5 for bcc metals such as iron[30] and tantalum[31]. Thus, the Peierls barrier height of the FCC equiatomic alloys is likely intermediate to pure FC. and BCC metals. However, a detailed investigation is required

to understand the deformation mechanism of FCC high and medium entropy alloys and single-crystal data is needed to solve this problem.

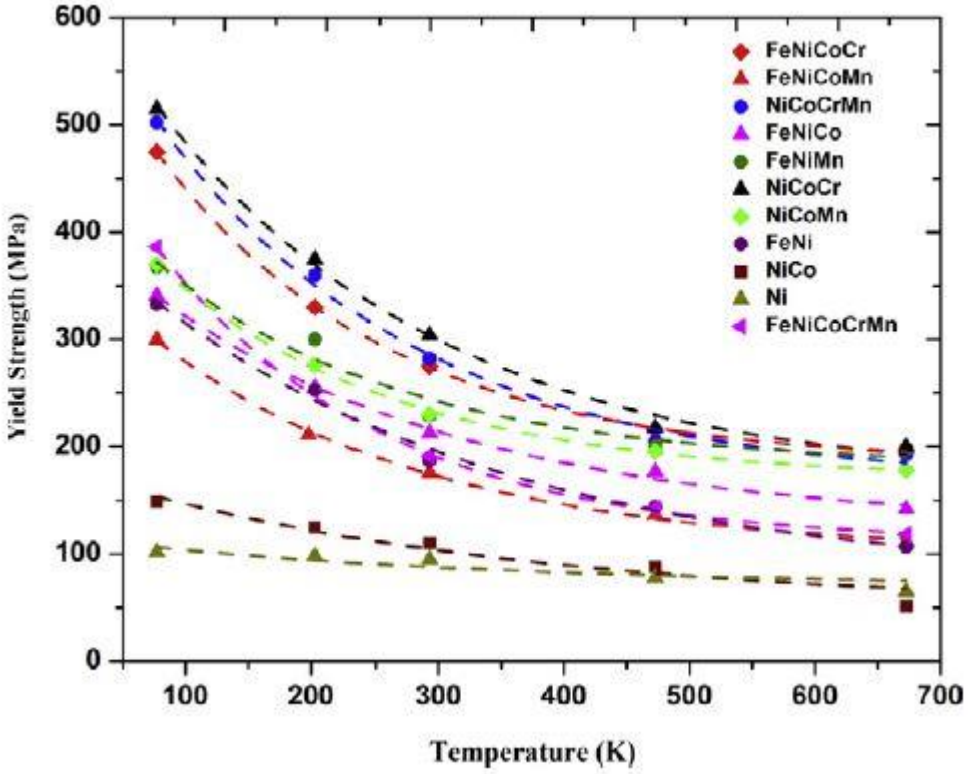

Figure 1.7 Temperature dependence of Yield strength of FCC High Entropy alloys[10]

1.6. Alloy Selection for the Present Study

To understand the fundamentals of the deformation mechanism of F.C.C. HEAs, Kawamura et al. [16] investigated the 5-elements Cr-Mn-Fe-Co-Ni high entropy alloy, also known as Cantor alloy, by using a single crystal. They studied deformation behavior in compression and tension in a wide range of temperatures with defined orientations. Cr-Mn-Fe-Co-Ni and its other derivatives show excellent mechanical properties at lower temperatures [16,32–35]. A detailed investigation is still limited in single-crystal to understand the deformation behavior fully.

Therefore, we selected the derivatives of Cantor alloy viz 4-elements Cr-Fe-Co-Ni and 3-elements Fe-Co-Ni F.C.C. single-crystal medium entropy alloy to understand the deformation mechanism at a wide range of temperatures in compression and tension.

1.7. Research Objectives

The purpose of the present study is as follows:

1. Investigate the deformation mechanism of 4-elements single-crystal equiatomic Cr-Fe-Co-Ni Medium entropy alloy in the temperature range of 13K-1373K.
2. Investigate the deformation mechanism of 3-elements single-crystal equiatomic Fe-Co-Ni Medium Entropy alloy in the temperature range of 13K-1373K.
3. To study the correlation of the strength of FCC MEAs with mean square atomic displacement(MSAD) and determination of fitting parameters for temperature dependence of CRSS.

1.8. Thesis Outline

Chapter 1 is the "*Introduction,*" The concepts of high entropy alloys, plastic deformation of FCC metals and alloys, research objective, and the thesis outline are introduced.

Chapter 2 studies "*Deformation mechanism of 4-elements single-crystal equiatomic Cr-Fe-Co-Ni in the temperature range of 13K-1373K,*" where mechanical properties and deformation mechanism of Cr-Fe-Co-Ni at different temperatures and strain rates are investigated and discussed.

Chapter 3 studies " *Deformation mechanism of 3-elements single-crystal equiatomic Fe-Co-Ni in the temperature range of 13K-1373K,*" " where mechanical properties and deformation mechanism of Fe-Co-Ni at different temperatures and strain rates are investigated and discussed.

Chapter 4 studies "*Mean square atomic displacement: a scaling factor to predict the strength of High/Medium entropy alloys,*" where the concept of MSAD and its correlation with CRSS at 0K is discussed. Fitting parameters for the temperature dependence of CRSS are discussed.

Chapter 5 is the "*Summary and Conclusions,*" which shows the summary and conclusions of the thesis.

References

[1] J.W. Yeh, S.K. Chen, S.J. Lin, J.Y. Gan, T.S. Chin, T.T. Shun, C.H. Tsau, S.Y. Chang, Nanostructured high-entropy alloys with multiple principal elements: Novel alloy design concepts and outcomes, Adv. Eng. Mater. 6 (2004) 299–303. https://doi.org/10.1002/adem.200300567.

[2] B. Cantor, I.T.H. Chang, P. Knight, A.J.B. Vincent, Microstructural development in equiatomic multicomponent alloys, Mater. Sci. Eng. A. 375–377 (2004) 213–218. https://doi.org/10.1016/j.msea.2003.10.257.

[3] S. Ranganathan, Alloyed pleasures: Multimetallic cocktails, Curr. Sci. 85 (2003) 1404–1406.

[4] M.C. Gao, J.-W. Yeh, P.K. Liaw, Y. Zhang, High-Entropy Alloys, n.d.

[5] B.S. Murty, J.W. Yeh, S. Ranganathan, High-Entropy Alloys, n.d.

[6] M.H. Tsai, J.W. Yeh, High-entropy alloys: A critical review, Mater. Res. Lett. 2 (2014) 107–123. https://doi.org/10.1080/21663831.2014.912690.

[7] F. Otto, A. Dlouhý, K.G. Pradeep, M. Kuběnová, D. Raabe, G. Eggeler, E.P. George, Decomposition of the single-phase high-entropy alloy CrMnFeCoNi after prolonged anneals at intermediate temperatures, Acta Mater. 112 (2016) 40–52. https://doi.org/10.1016/j.actamat.2016.04.005.

[8] S. Yoshida, T. Bhattacharjee, Y. Bai, N. Tsuji, Friction stress and Hall-Petch relationship in CoCrNi equi-atomic medium entropy alloy processed by severe plastic deformation and subsequent annealing, Scr. Mater. 134 (2017) 33–36. https://doi.org/10.1016/j.scriptamat.2017.02.042.

[9] R.S. Mishra, N. Kumar, M. Komarasamy, Lattice strain framework for plastic deformation in complex concentrated alloys including high entropy alloys, Mater. Sci. Technol. (United Kingdom). 31 (2015) 1259–1263. https://doi.org/10.1179/1743284715Y.0000000050.

[10] Z. Wu, H. Bei, G.M. Pharr, E.P. George, Temperature dependence of the mechanical properties of equiatomic solid solution alloys with face-centered cubic crystal structures, Acta Mater. 81 (2014) 428–441. https://doi.org/10.1016/j.actamat.2014.08.026.

[11] N.L. Okamoto, K. Yuge, K. Tanaka, H. Inui, E.P. George, Atomic displacement in the CrMnFeCoNi high-entropy alloy - A scaling factor to predict solid solution strengthening, A.I.P. Adv. 6 (2016). https://doi.org/10.1063/1.4971371.

[12] K.Y. Tsai, M.H. Tsai, J.W. Yeh, Sluggish diffusion in Co-Cr-Fe-Mn-Ni high-entropy alloys, Acta Mater. 61 (2013) 4887–4897. https://doi.org/10.1016/j.actamat.2013.04.058.

[13] W.H. Liu, Y. Wu, J.Y. He, T.G. Nieh, Z.P. Lu, Grain growth and the Hall-Petch relationship in a high-entropy FeCrNiCoMn alloy, Scr. Mater. 68 (2013) 526–529. https://doi.org/10.1016/j.scriptamat.2012.12.002.

[14] T.H. Blewitt, R.R. Coltman, J.K. Redman, Low-temperature deformation of copper single crystals, J. Appl. Phys. 28 (1957) 651–660. https://doi.org/10.1063/1.1722824.

[15] H. Suzuki, C.S. Barrett, Deformation twinning in silver-gold alloys, Acta Metall. (1958). https://doi.org/10.1016/0001-6160(58)90002-6.

[16] M. Kawamura, M. Asakura, N.L. Okamoto, K. Kishida, H. Inui, E.P. George, Plastic

deformation of single crystals of the equiatomic Cr−Mn−Fe−Co−Ni high-entropy alloy in tension and compression from 10 K to 1273 K, Acta Mater. 203 (2021). https://doi.org/10.1016/j.actamat.2020.10.073.

[17] Y. Wang, B. Liu, K. Yan, M. Wang, S. Kabra, Y.L. Chiu, D. Dye, P.D. Lee, Y. Liu, B. Cai, Probing deformation mechanisms of a FeCoCrNi high-entropy alloy at 293 and 77 K using in situ neutron diffraction, Acta Mater. 154 (2018) 79–89. https://doi.org/10.1016/j.actamat.2018.05.013.

[18] G. Laplanche, A. Kostka, C. Reinhart, J. Hunfeld, G. Eggeler, E.P. George, Reasons for the superior mechanical properties of medium-entropy CrCoNi compared to high-entropy CrMnFeCoNi, Acta Mater. 128 (2017) 292–303. https://doi.org/10.1016/j.actamat.2017.02.036.

[19] W. Abuzaid, H. Sehitoglu, Critical resolved shear stress for slip and twin nucleation in single crystalline FeNiCoCrMn high entropy alloy, Mater. Charact. 129 (2017) 288–299. https://doi.org/10.1016/j.matchar.2017.05.014.

[20] J. Liu, C. Chen, Y. Xu, S. Wu, G. Wang, H. Wang, Y. Fang, L. Meng, Deformation twinning behaviors of the low stacking fault energy high-entropy alloy: An in-situ T.E.M. study, Scr. Mater. 137 (2017) 9–12. https://doi.org/10.1016/j.scriptamat.2017.05.001.

[21] Z. Li, S. Zhao, R.O. Ritchie, M.A. Meyers, Mechanical properties of high-entropy alloys with emphasis on face-centered cubic alloys, Prog. Mater. Sci. 102 (2019) 296–345. https://doi.org/10.1016/j.pmatsci.2018.12.003.

[22] M. Frank, S.S. Nene, Y. Chen, B. Gwalani, E.J. Kautz, A. Devaraj, K. An, R.S. Mishra,

Correlating work hardening with co-activation of stacking fault strengthening and transformation in a high entropy alloy using in-situ neutron diffraction, Sci. Rep. 10 (2020) 1–10. https://doi.org/10.1038/s41598-020-79492-8.

[23] G.P.M. Leyson, W.A. Curtin, Friedel vs. Labusch: The strong/weak pinning transition in solute strengthened metals, Philos. Mag. 93 (2013) 2428–2444. https://doi.org/10.1080/14786435.2013.776718.

[24] R.L. Fleischert, SUBSTITUTIONAL SOLUTION HARDENING*, n.d.

[25] N.F. Mott, CXVII. A theory of work-hardening of metal crystals, London, Edinburgh, Dublin Philos. Mag. J. Sci. 43 (1952) 1151–1178. https://doi.org/10.1080/14786441108521024.

[26] R. Labusch, R. LABUSCH: A Statistical Theory of Solid Solution Hardening A Statistical Theory of Solid Solution Hardening, 1970.

[27] C. Varvenne, A. Luque, W.A. Curtin, Theory of strengthening in fcc high entropy alloys, Acta Mater. 118 (2016) 164–176. https://doi.org/10.1016/j.actamat.2016.07.040.

[28] I. Toda-Caraballo, A general formulation for solid solution hardening effect in multicomponent alloys, Scr. Mater. 127 (2017) 113–117. https://doi.org/10.1016/j.scriptamat.2016.09.009.

[29] G. Bracq, M. Laurent-Brocq, C. Varvenne, L. Perrière, W.A. Curtin, J.M. Joubert, I. Guillot, Combining experiments and modeling to explore the solid solution strengthening of high and medium entropy alloys, Acta Mater. 177 (2019) 266–279. https://doi.org/10.1016/j.actamat.2019.06.050.

[30] M.M. Hutchison, The temperature dependence of the yield stress of polycrystalline iron, Philos. Mag. 8 (1963) 121–127. https://doi.org/10.1080/14786436308212493.

[31] F.J. Zerilli, R.W. Armstrong, Description of tantalum deformation behavior by dislocation mechanics based constitutive relations, J. Appl. Phys. 68 (1990) 1580–1591. https://doi.org/10.1063/1.346636.

[32] Z. Wu, Y.F. Gao, H. Bei, Single crystal plastic behavior of a single-phase, face-center-cubic-structured, equiatomic FeNiCrCo alloy, Scr. Mater. 109 (2015) 108–112. https://doi.org/10.1016/j.scriptamat.2015.07.031.

[33] J. Antonaglia, X. Xie, Z. Tang, C.W. Tsai, J.W. Qiao, Y. Zhang, M.O. Laktionova, E.D. Tabachnikova, J.W. Yeh, O.N. Senkov, M.C. Gao, J.T. Uhl, P.K. Liaw, K.A. Dahmen, Temperature Effects on Deformation and Serration Behavior of High-Entropy Alloys (H.E.A.s), J.O.M. 66 (2014) 2002–2008. https://doi.org/10.1007/s11837-014-1130-9.

[34] R. Carroll, C. Lee, C.W. Tsai, J.W. Yeh, J. Antonaglia, B.A.W. Brinkman, M. Leblanc, X. Xie, S. Chen, P.K. Liaw, K.A. Dahmen, Experiments and Model for Serration Statistics in Low-Entropy, Medium-Entropy, and High-Entropy Alloys, Sci. Rep. 5 (2015). https://doi.org/10.1038/srep16997.

[35] B. Gludovatz, A. Hohenwarter, D. Catoor, E.H. Chang, E.P. George, R.O. Ritchie, A fracture-resistant high-entropy alloy for cryogenic applications, Science (80-.). 345 (2014) 1153–1158. https://doi.org/10.1126/science.1254581.

Chapter 2

Deformation Mechanism of Single Crystal FCC Cr-Fe-Co-Ni Medium Entropy alloy

2.1. Introduction

Cantor alloy consists of Cr-Mn-Fe-Co-Ni is a single-phase FCC solid solution and is widely investigated because of its exceptional mechanical properties at low temperatures [1]. Many researchers focused on the strength and ductility of equiatomic HEAs. Cr-Fe-Co-Ni is one of the derivatives of Cantor alloy, firstly introduced by Brain Cantor [2]. Cr-Fe-Co-Ni is a single-phase FCC structure medium entropy alloy, which increases strength and ductility with decreasing temperature[3]. The high yield strengths of single-phase HEAs and medium entropy alloys comprising fewer than five elements should be mainly due to the solid solution hardening[4]. Many theoretical investigations have been done, and various models and correlations have been proposed for the yield strength at 0K and temperature dependence of CRSS or yield strength[4–6]. Improved tensile elongation at lower temperatures has been reported, and twining deformation is responsible for this behavior[7,8].

Considere criterion suggests that twinning decreases the mean free path for dislocation motion, increasing strain level over which work hardening persists. Despite the above progress, previous experimental observations are based on mechanical testing of polycrystalline materials, which cannot answer some of the fundamental questions related to single-crystal plasticity. In polycrystalline materials, the stress state of individual grains

becomes very complex and individual grains are no longer subjected to a uniaxial stress state even when the specimen is deformed uniaxially. Because the slip systems in neighbouring grains are oriented differently, the need for an individual grain to accommodate the slip fields in the neighbouring grains will make the slip systems operating near a grain boundary frequently different from those elsewhere. Grain boundaries can act as obstacles to dislocation movement, and such an interaction is affected by many factors such as temperature and grain size. All of these make it challenging to understand the deformation mechanisms of the alloy mechanistically. The reason for choosing this Cr-Fe-Co-Ni alloy is that its mechanical properties are similar to Cantor alloy and no manganese content allowed us to fabricate a single crystal using an optical floating zone facility. Moreover, this study of the deformation mechanism will develop a clear understanding of the behavior of such FCC equiatomic alloys.

This chapter aims to understand the deformation mechanism of equiatomic Cr-Fe-Co-Ni medium entropy alloy in bulk single-crystal in tension and compression in the temperature range of 13K-1373K.

2.2. Experimental Procedures

2.2.1. Starting Material

Cylindrical ingots, 10 mm in diameter and 80 mm long, were prepared by arc-melting in argon atmosphere high-purity (> 99.9%) Cr, Fe, Co, and Ni in equiatomic ratios. Each ingot was flipped and re-melted at least four times to ensure chemical homogeneity. This ingot was then used to grow single crystals of the quaternary MEA by the Floating Zone method in the Ar atmosphere at the growth rate of 10 mm/h and 15 rpm. Figure 2.1 (a) shows a grown single crystal specimen after the floating zone. The single crystals were annealed at 1473 K for 72 h, followed by water quenching. A small piece of this sample was cut, and EBSD was done to check the quality of a single crystal. Elemental mapping was done using EDX, and Figure 2.1 (b) confirms the chemical homogeneity of the single crystal. Crystallographic orientations were determined by the X-ray back-reflection Laue method, and oriented test specimens were cut from the crystal by spark-machining for uniaxial tests in compression (dimensions: 2 ×2 ×5 mm^3) and tension (gage section dimensions: 2 ×2 ×5 mm^3). The surfaces of the compression and tensile test specimens were mechanically polished, followed by electro-polishing with a solution of nitric acid and methanol (1:3 by volume). The compression-axis orientations and tensile axis tested were $[\bar{1}23]$. Compression and tensile tests were conducted on an Instron-type testing machine in a vacuum in the temperature range from 13 to 1373 K at an engineering strain rate of 1 ×10 −4 s^{-1}. The strain-rate sensitivity of flow stress was measured by suddenly changing the strain rate up or down by one or two orders of magnitude in the range of 1 ×10^{-5} to 5 ×10^{-3} s −1 at selected temperatures.

Deformation offsets on the specimen surface (caused by slip or twinning) were examined by optical microscopy and in a scanning electron microscope (SEM) equipped with an electron backscatter diffraction (EBSD) detector. Dislocation and dislocation core structures were examined by transmission electron microscopy (TEM) and scanning transmission electron microscopy (STEM), respectively, with JEOL JEM-20 0 0FX, JEM-210 0F, and JEM-ARM200F electron microscopes operated at 200 kV. Thin foils for TEM/STEM observations were prepared by electro-polishing with a solution of methanol, nitric acid and ethylene glycol (20:5:2 by volume).

Figure 2.1(a) Single-crystal Cr-Fe-Co-Ni

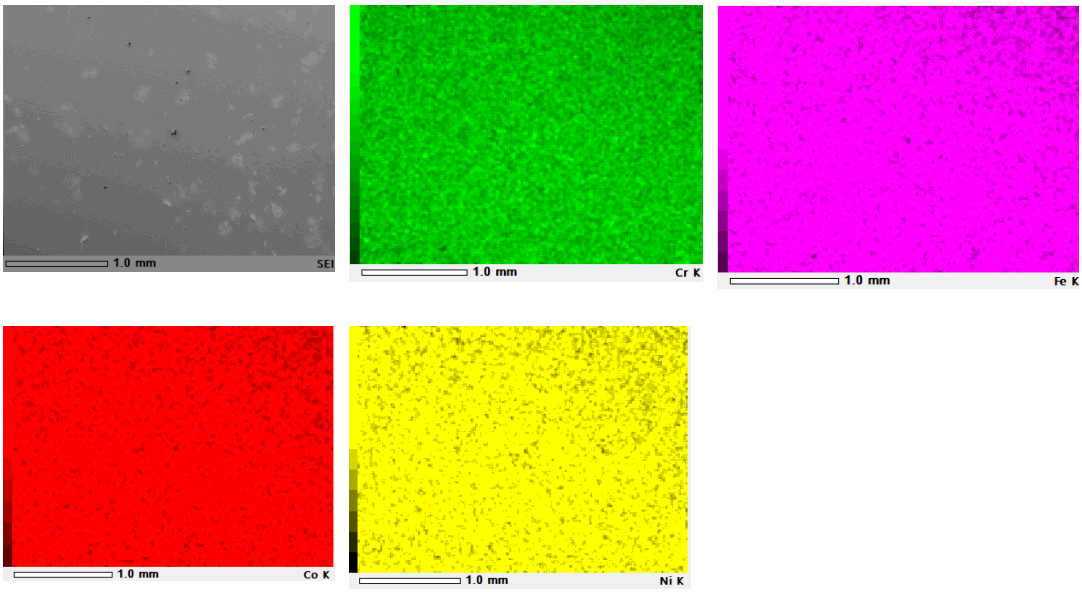

Figure 2.1(b) Elemental mapping of single crystal Cr-Fe-Co-Ni

2.2.2. Compression deformation

Rectangular specimens for compression tests in the range of 13K-1373K, having dimensions 2x2x5 mm^3, were cut from the $[\bar{1}23]$ oriented crystal using an electric discharge wire cutting machine. Uniaxial compression tests were carried out in the vacuum atmosphere at high temperatures (400K-1373K) and cryogenic temperature (13K- 212K). Room temperature and 77K compression test was done separately by using an Instron-type testing machine. The strain-rate sensitivity of flow stress was measured by suddenly changing the strain rate up or down by one or two orders of magnitude in the range of 1×10^{-5} to 5×10^{-3}/ s at selected temperatures.

2.2.3. Tensile deformation

Dog bone shape specimens were cut from the oriented crystal using an electric discharge wire cutting machine. Next, uniaxial tensile tests were performed at room temperature and 77K at an Instron-type testing machine at a strain rate of $1x10^{-4}$ s^{-1}. For 77K, the tensile test specimen was immersed in liquid nitrogen temperature, and a pre-test was done before starting the actual test.

2.3. Results

2.3.1. Compression deformation behavior

Stress-strain curves of jump test of a single crystal with $[\bar{1}23]$ orientation deformed at a temperature range from 13K-1373K is shown in Figure 2.3 (a) & (b), and slip markings on the surface of compression specimen for RT and 77K is shown in Figure 2.4 (a) and (b). Strain rate sensitivity was measured in the easy-glide region to minimize the work hardening effect. Optical microscopy images of slip markings confirm the (111) $[\bar{1}01]$ slip systems at room temperature and 77K. Slip markings on the surface are straight from one end of the specimen to others, which is possible because of this system's low stacking fault energy where dislocation easily glide in the system.

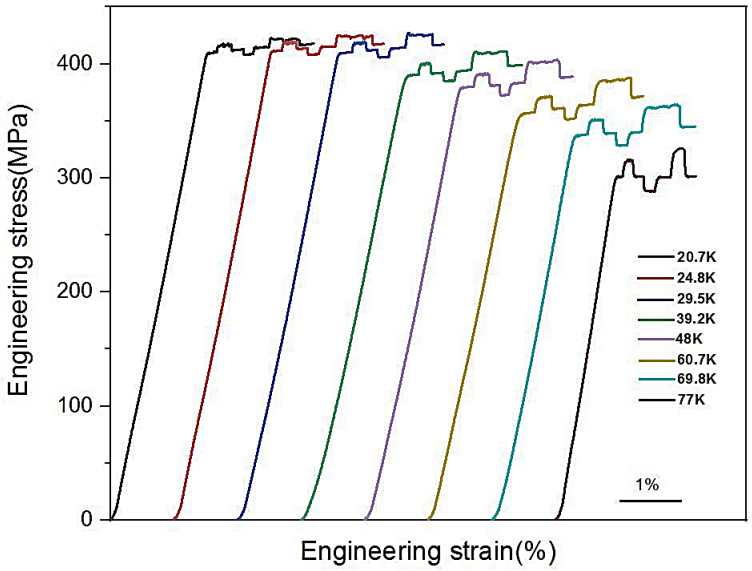

Figure 2.3 (a) Stress-strain curves obtained for $[\bar{1}23]$-oriented single crystals deformed in compression at selected temperatures

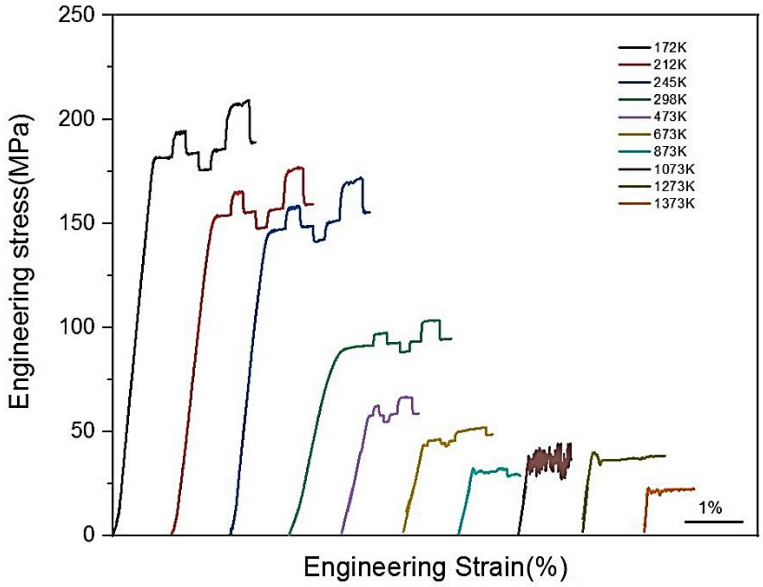

Figure 2.3 (b) Stress-strain curves obtained for $[\bar{1}23]$-oriented single crystals deformed in compression at selected temperatures

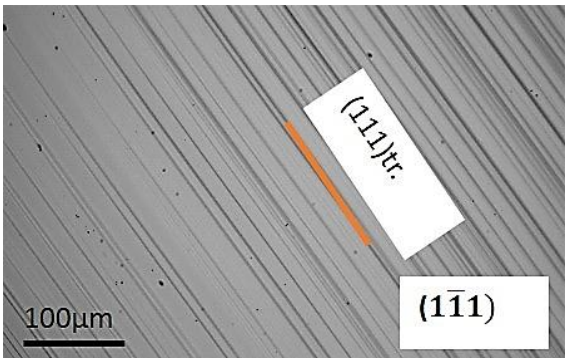

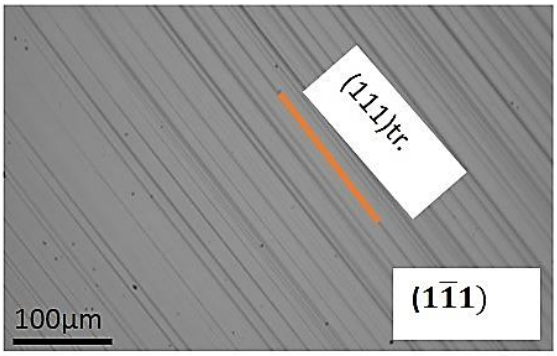

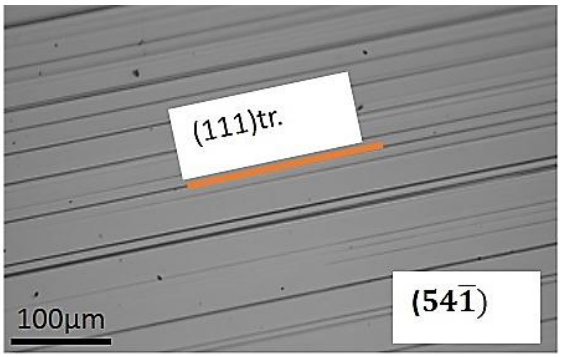

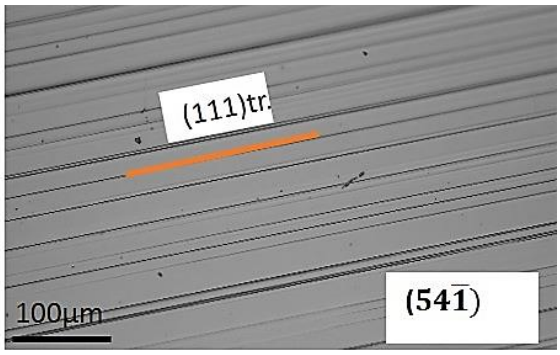

Figure 2.4(a) Slip markings of RT

Figure 2.4(b) Slip markings of 77K

2.3.2. Temperature dependence of CRSS

The temperature dependence of the CRSS curve of single-crystal Cr-Fe-Co-Ni at a strain rate of $1x10^{-4}$ s^{-1} is shown in Figure 2.5(b). The absolute values of CRSS at each temperature are much more extensive for the Cr-Fe-Co-Ni MEA than other binary FCC alloys reported previously, and the same phenomena are also reported for quinary Cr-Mn-Fe-Co-Ni HEA by Kawamura et al.[7]. CRSS values were calculated by multiplying the 0.2% of yield strength to the Schmid factor. Below 50K temperature, the curve starts getting dull and such phenomena is also observed in FCC binary alloys such as Cu-15Al, Cu-10Al alloys, Cu-5Al and Cu-2Al alloys, which is described as inertia effect[9]. At shallow temperature, the

phonon frictional force becomes so low that dislocation velocities can reach very high values. The inertia effects are sufficiently significant to help dislocation pass through solute atoms, termed underdamped dislocation motion[10]. A slight increase in CRSS values is noticed around 1073K, and a serration is noticed in the S-S curve, which is also observed in Cu-Al alloys (Fig 2.5-a) and our previously reported result of Cantor alloy.[7] Serration occurs at this temperature because, at a high temperature of 1073K, there is an interaction between solute atoms and dislocation known as Portvin-Le Chatlier (PLC) effect. 0K CRSS for Cr-Fe-Co-Ni is estimated to be 213MPa by extrapolating the temperature dependence curve using equation 2.3 (a), higher than single-crystal cantor alloy (0K CRSS 168MPa). And much higher than other binary FCC alloys. (Figure2.5(a))

$$\tau_{crss} = \tau_{ath} + \tau_{th} \times \left[1 - \left(\frac{T}{T_{TA}}\right)^{\frac{1}{q}}\right]^{\frac{1}{p}} \qquad 2.3\ (a)$$

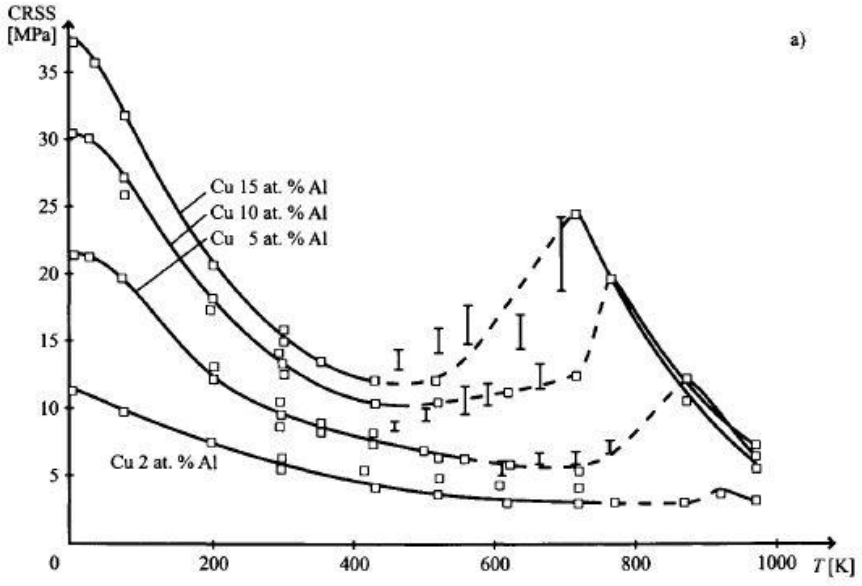

Figure 2.5 (a) CRSS as a function of the temperature of Cu-Al alloys

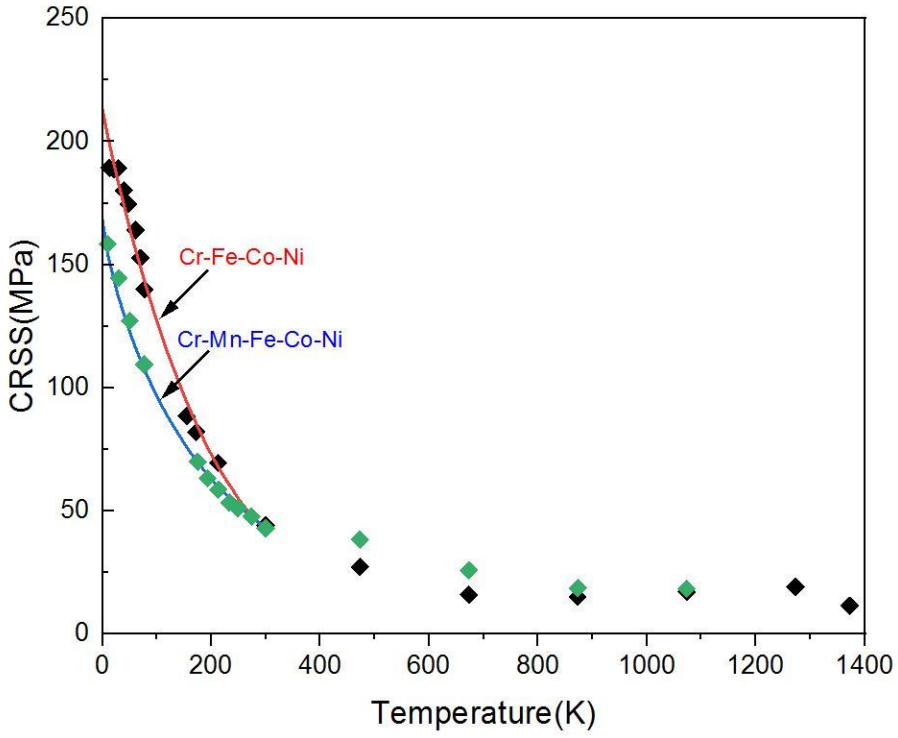

Figure 2.5 (b) Temperature dependence of CRSS of Cr-Fe-Co-Ni and Cr-Mn-Fe-Co-Ni

2.3.3. Strain rate sensitivity of flow stress and Activation Volume

The strain rate sensitivity of flow stress measured for $[\bar{1}23]$ oriented single crystal of equiatomic Cr-Fe-Co-Ni MEA in the easy-glide region at a temperature range between 12.4K and 473K are plotted in Fig 2.6 as a function of strain rate. Stress and strain are converted into shear stress and shear strain by using Schmid factor(0.46). The flow stress of Cr-Fe-Co-Ni equiatomic MEA increased at a higher strain rate, and strain rate sensitivity (SRS) is more prominent at low temperatures up to 60.7K. Below this temperature, SRS of flow stress becomes smaller, as shown in Fig 2.6. This decrease in SRS of flow stress is

strong evidence of the occurrence of the inertia effect [11], through which the dullness of the temperature dependence of CRSS occurs in Fig 2.5(a).

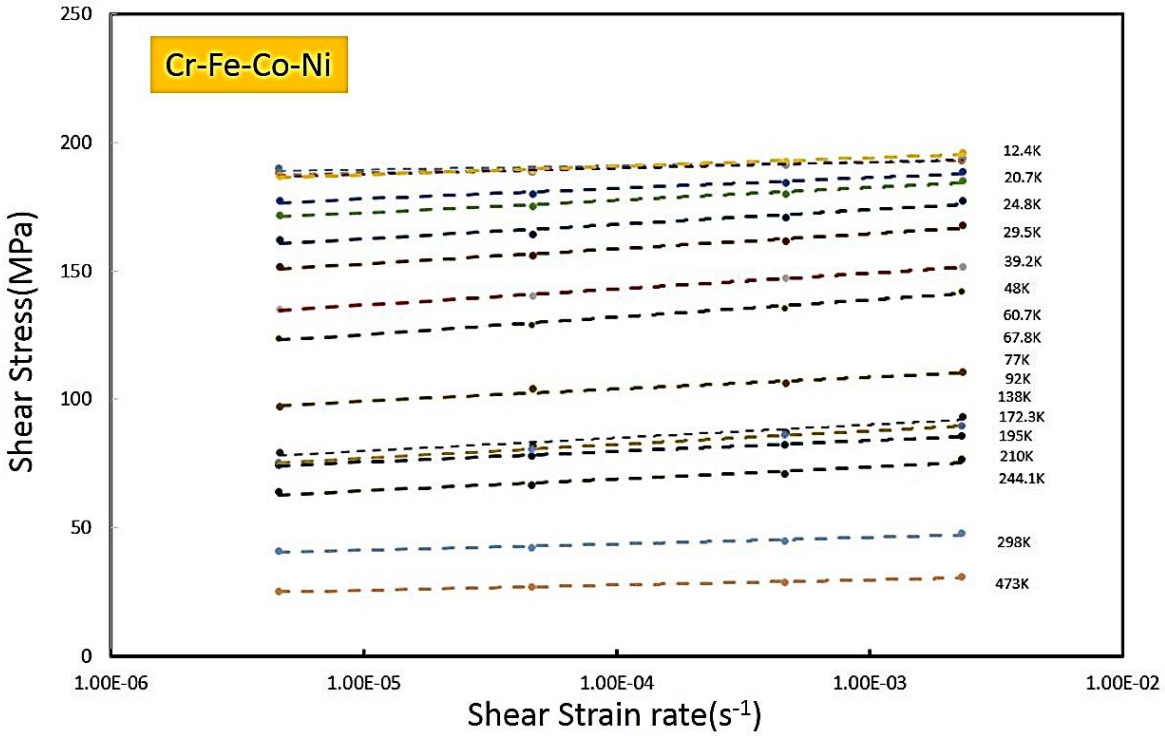

Figure 2.6 Strain Rate sensitivity of Cr-Fe-Co-Ni

The activation volume (V) is determined with the strain rate sensitivity of flow stress measured at different temperatures by using equation 2.3(b)

$$V = kT\delta \ln(\dot{\epsilon}) / \delta\tau \qquad 2.3(b)$$

Where k is Boltzmann's constant, T is test temperature, $\dot{\epsilon}$ is shear strain rate, and $\delta\tau$ is shear stress. The values of activation volume are measured at each temperature and are plotted in Fig 2.7. Activation volumes at a temperature below 50K are less dependent on temperature. At room temperature, the activation volume is 248.7 b^3, close to the activation volume

measured for quinary Cr-Mn-Fe-Co-Ni equiatomic single-crystal HEA, which is 232.7 b^3. At 12.4K and 77K, activation volumes are 22.4 b^3 and 33.74 b^3 which is more than Cr-Mn-Fe-Co-Ni HEA 5.4 b3 for 10K but less than 40.2 b^3 for 77K. The low-temperature region value of activation volume increases slightly, suggesting the inertia effects phenomenon below 50K (Figure 2.7(a)). Even slope of strain rate sensitivity plot shows a decreasing value around 50K in the low-temperature region, as shown in Figure 2.7(b).

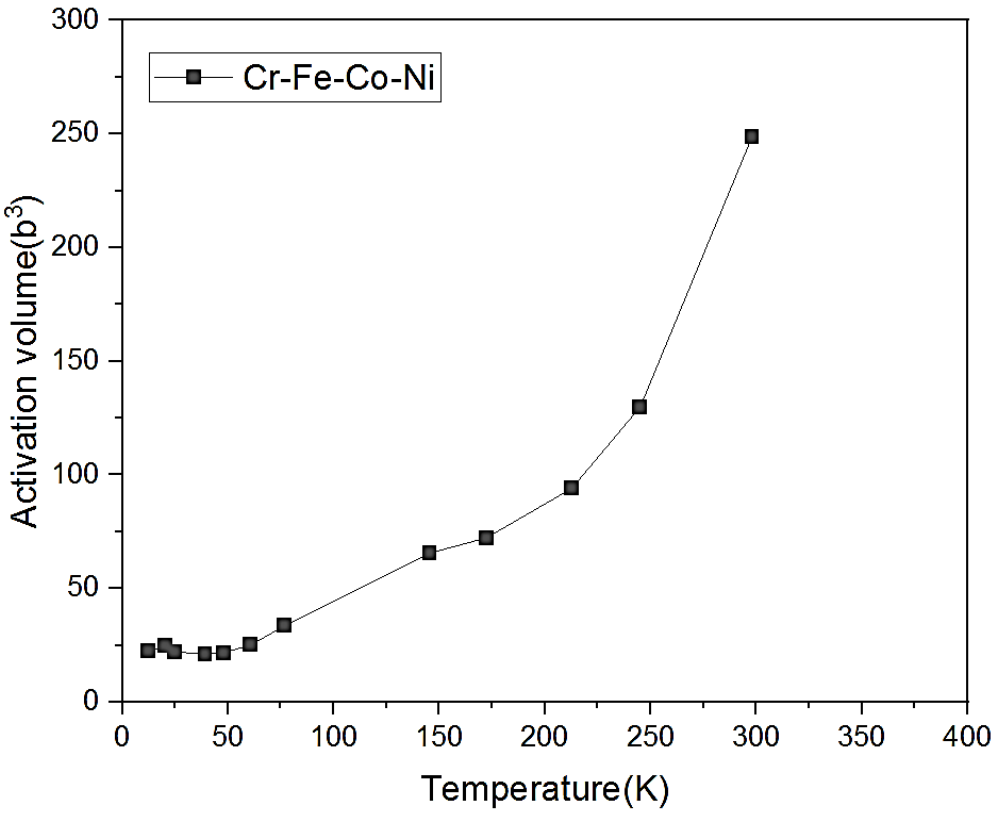

Figure 2.7 (a) Activation Volume as a function of Temperature

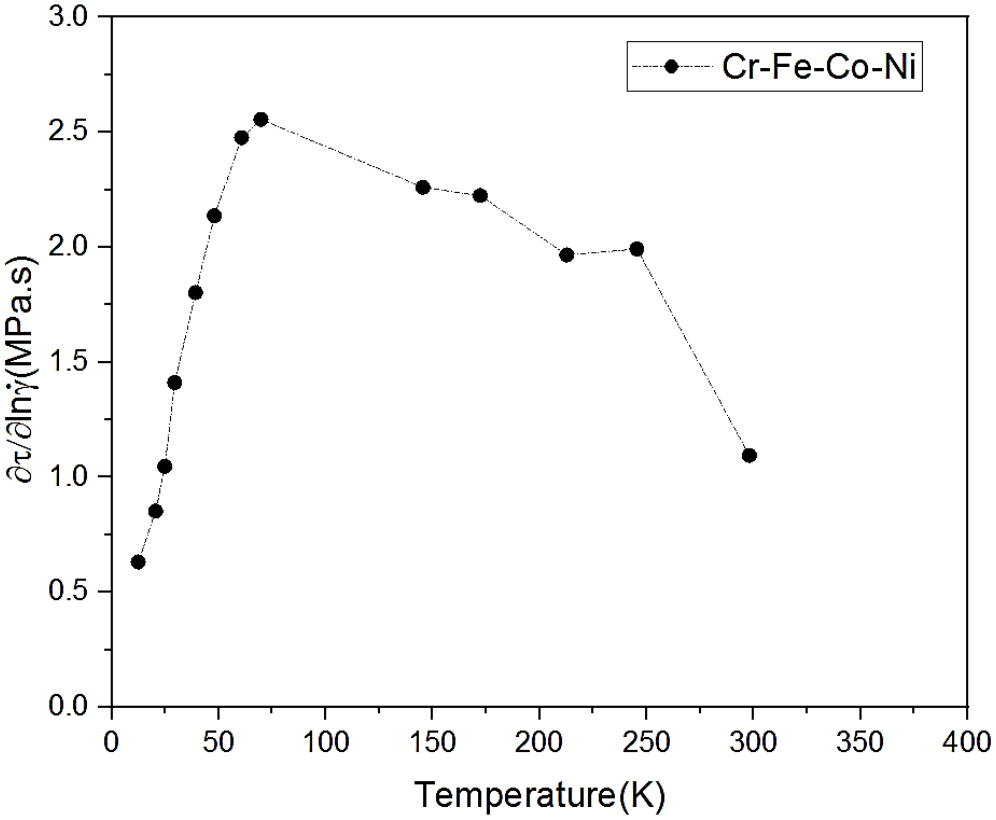

Figure 2.7 (b) Gradient of SRS as a function of temperature

2.3.4. Dislocation Structures and stacking fault energy

A typical dislocation structure observed in an [$\bar{1}23$] oriented single crystal of quaternary Cr-Fe-Co-Ni MEA deformed in compression up to 3% of plastic strain at RT. is shown in figure 2.8(a). A thin foil of deformed specimen was cut parallel to the (111) slip plane. Planar arrays of dislocations are observed without any evidence of dislocation cell formation that indicates the low stacking fault energy of this MEA. However, the weak beam image in Fig 2.8(b) shows a widespread partial dislocation. Stacking fault energy is measured by measuring the

separation width from weak beam image and is estimated to be 20 ± 4 mJ/m^2, and shown in Figure 2.9. This is consistent with the value reported by S.F. Liu et al. [12].

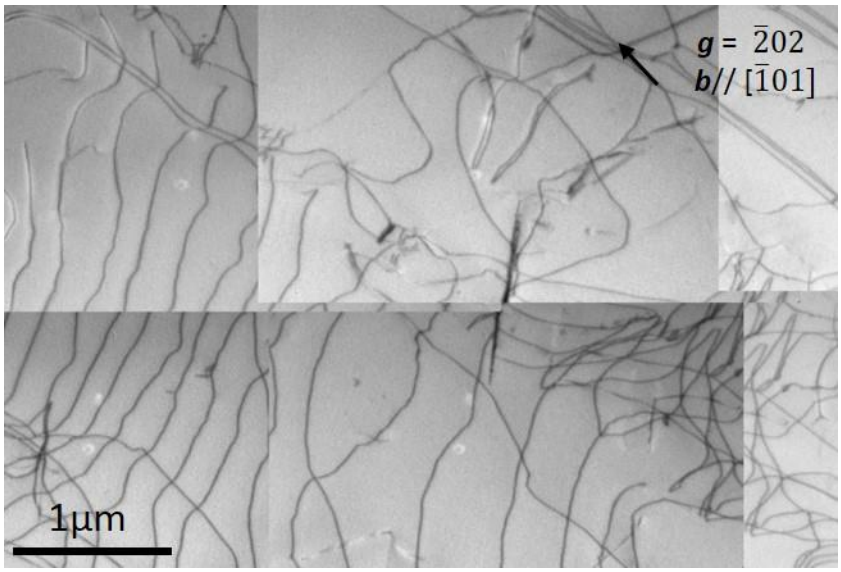

Figure 2.8 (a) Bright-field image of dislocation structure

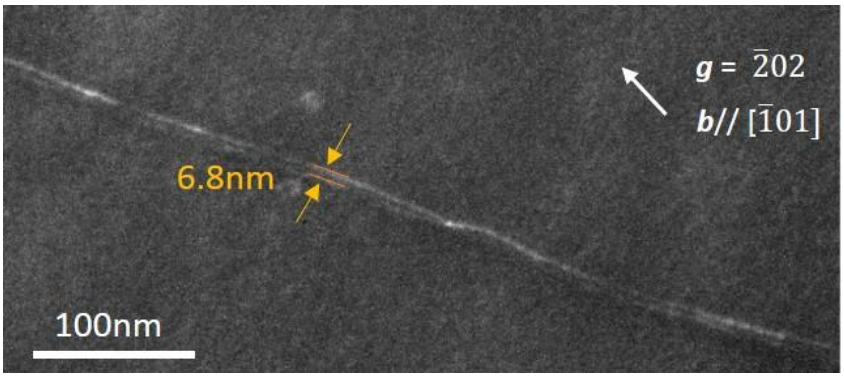

Figure 2.8 (b) weak beam image of dislocation dissociation

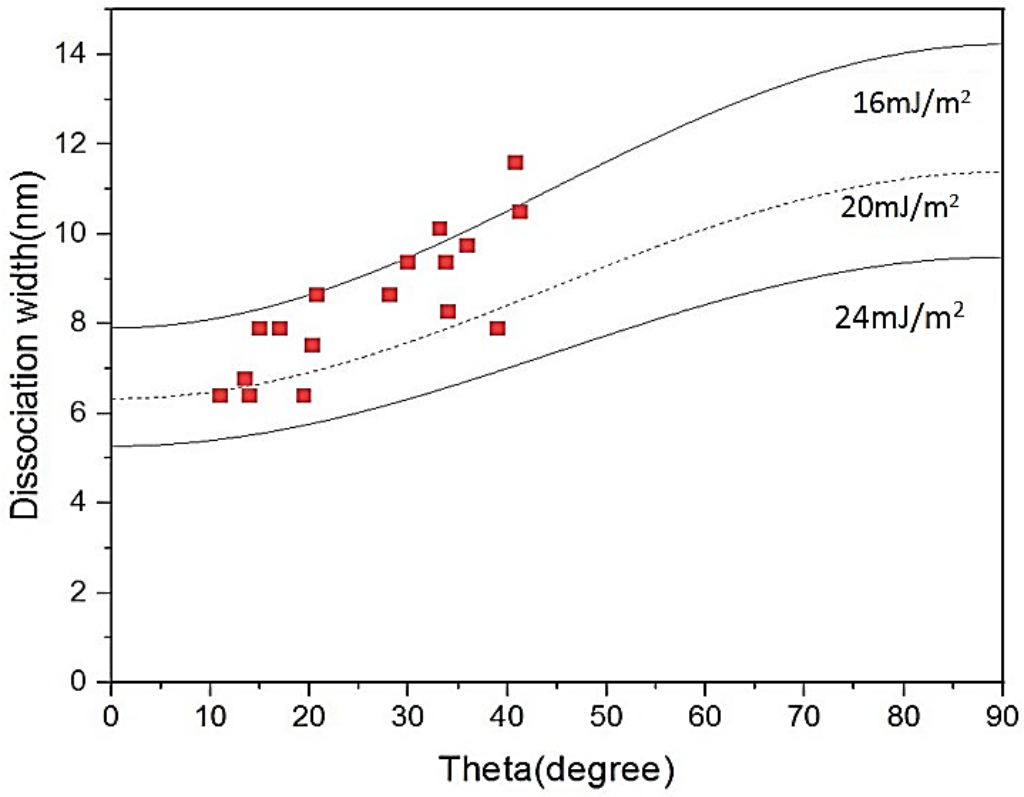

Figure 2.9 Separation distance of partial measured from a weak-beam image of Cr-Fe-Co-Ni

2.3.5. Tensile deformation behavior

Engineering Stress-Strain curves of [$\bar{1}$23] oriented Cr-Fe-Co-Ni single crystal deformed at RT and 77K are shown in Figure 2.10. These specimens were deformed at an engineering strain rate of 1 x 10^{-4}/s until fracture occurred. At room temperature, Stage 1 (easy glide, low work hardening) extends to about 10% plastic strain, followed by stage 2 work hardening (high work hardening) until necking occurs at the ultimate tensile strength around 300 MPa. The hardening rate in stage 2 is about G/254 when normalized by shear modulus (G), which is well within the range of many conventional FCC alloys and consistent with Cantor alloy[7]. During stage 1, slip markings corresponding to the (111) [110] primary slip system gradually

fill the entire gage length. During stage 2, in addition to the primary slip system, the conjugate slip system starts to operate with its extent increase with increasing strain. The CRSS in tension at room temperature is 46MPa, consistent with the CRSS obtained in compression deformation. This tension-compression symmetry in Cr-Fe-Co-Ni MEA suggests that its dislocation structure and response to applied stress is "normal" for the FCC metals, and this is also found true in Cantor alloy. SEM- EBSD on the deformed specimen after facture shows no sign of twinning deformation at RT., as shown in Fig 2.10.

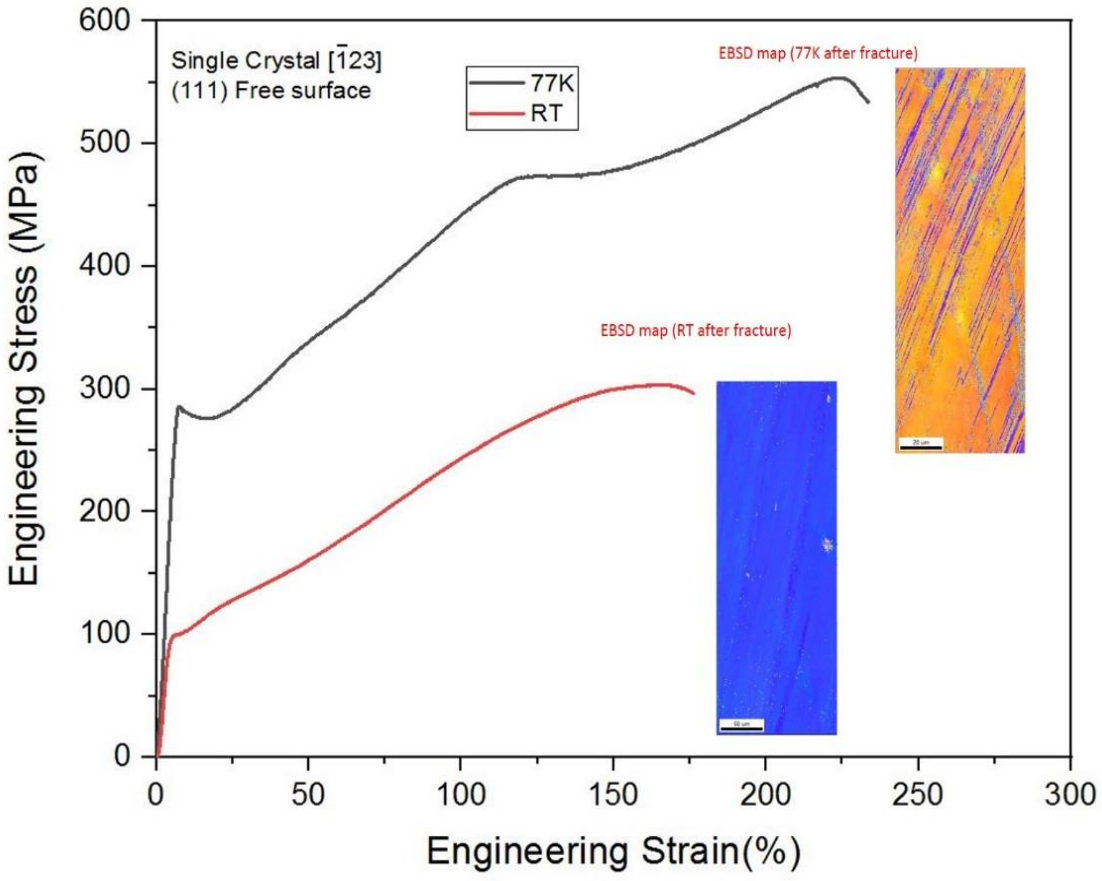

Figure 2.10 Engineering S-S curve of single-crystal Cr-Fe-Co-Ni at RT and 77K till fracture

At 77K, the CRSS increases significantly to 140 MPa from 46 MPa at RT while exhibiting no compression-tension asymmetry. Our results of CRSS at 77K is higher than Z. Wu et al. results on Cr-Fe-Co-Ni single crystal (CRSS is 96-112 MPa at 77K). Possible reasons for this discrepancy could be inhomogeneity and deviations from the equiatomic composition and quality of a single crystal. Stage I (easy glide, low work-hardening rate) extends up to 12%, followed by stage II (high work-hardening rate). The work hardening rate at 77 K in stage II (G /217) is similar to that at room temperature (G /254). However, the tensile stress-strain curve at 77 K (Fig 2.10) exhibits a sudden change in the work-hardening rate at a plastic strain of about 80% in stage II. This sudden change in the work-hardening rate was confirmed to be associated with the onset of deformation twinning by repeatedly observing the microstructure after interrupted tests, as shown in Fig. 2.12. A similar trend was seen in Cantor alloy single crystal tensile deformation at 77K.

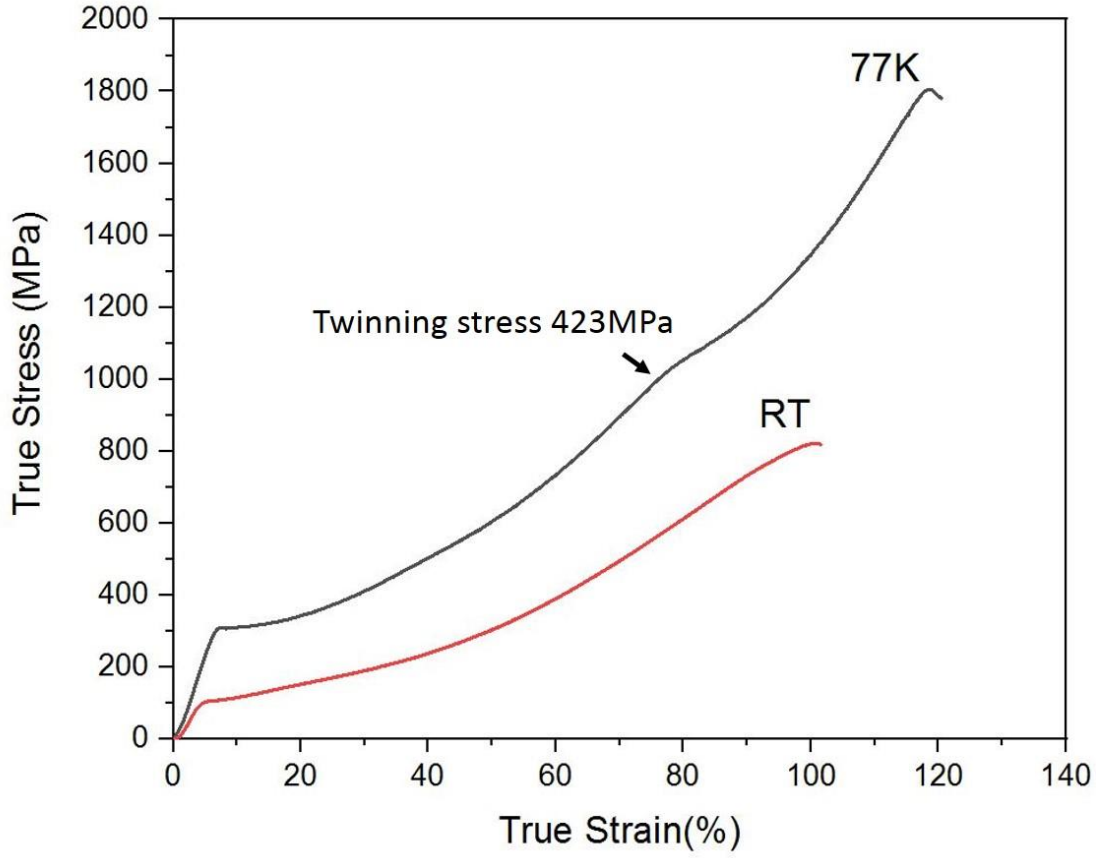

Figure 2.11 True S-S curve of tensile deformation of Cr-Fe-Co-Ni single crystal at RT and 77K

A tensile test of the $[\bar{1}23]$-oriented single crystal at 77 K was interrupted at points A −D in Fig. 2.12 to examine deformation microstructures by EBSD (Fig. 2.13 (a)). No evidence is obtained for deformation twinning up to point B. Beyond that, surface markings appear corresponding to deformation twinning on the (1 1 1) conjugate planes once the tensile axis orientation 'overshoots' and reaches approximately the $[\ 1\bar{3}\ 12\ 25]$ orientation as shown in a standard triangle in Figure 2.13(b). There could be a small experimental error of a few (at most, several) degrees in identifying the tensile axis orientation of $[1\bar{3}\ 12\ 25]$ since the

specimen needed to be removed from the tensile testing machine for the orientation measurement by EBSD.

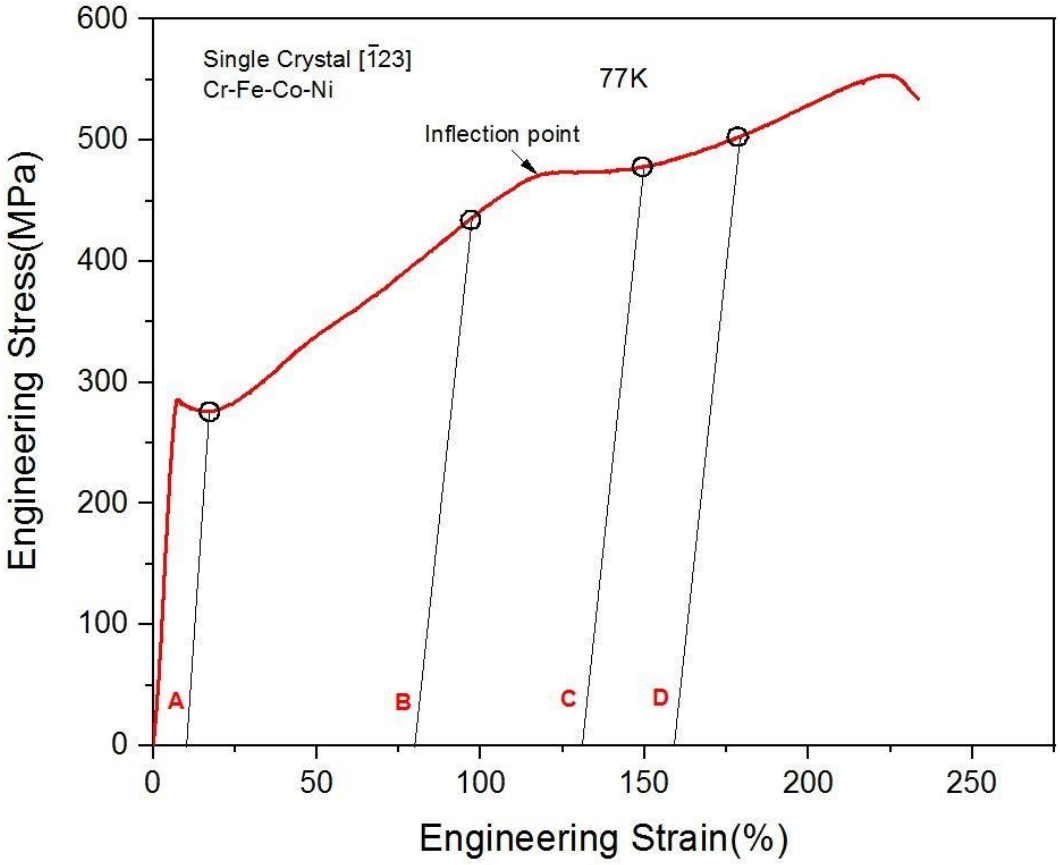

Figure 2.12 Engineering S-S curve for a [$\bar{1}$23]-oriented single crystal of Cr-Fe-Co-Ni deformed in tension at 77 K, in which the test was repeatedly interrupted at points A −D for microstructure observations.

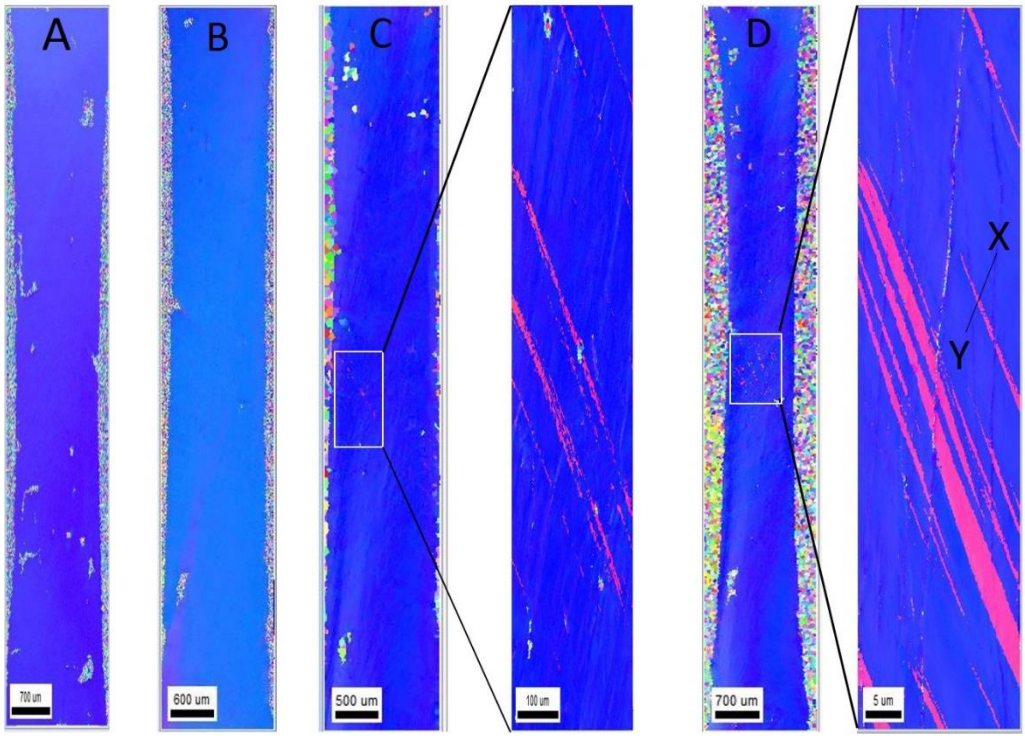

Figure 2.13 (a). EBSD orientation maps at the A-D points of tensile S-S curve

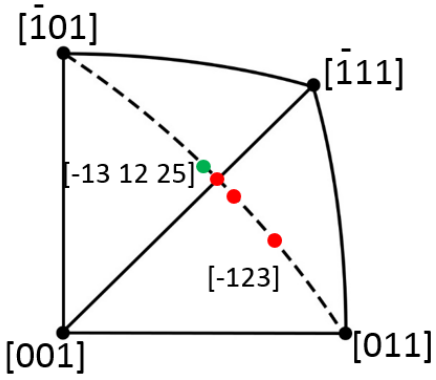

Figure 2.13 (b). Tensile axis rotation during deformation shown in stereographic projection

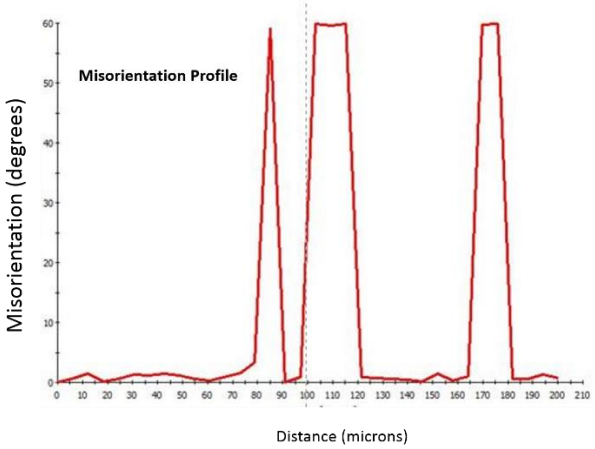

Figure 2.13 (c). Misorientation along the line X-Y in the EBSD map showing deformation twinning

Of interest to note is that the tensile elongation to failure is much greater at 77 K than at room temperature, as shown in Fig 2.10; this is due to the occurrence of deformation twinning at 77 K. Laplanche et al.[8] postulated that twinning is stress-controlled, and in low stacking fault energy alloys, twinning stress is less affected by deformation temperature; since the occurrence of cross slip is difficult, it is possible to make the case that twinning could not occur at room temperature because the true stress never reached the high value of 1040 MPa needed to activate twinning at 77 K. Figure Fig. 2.11 shows true stress (σ_t) - true strain (ε_t) curves converted from the engineering stress curves of Fig. 2.10 for [$\bar{1}23$] oriented single crystals deformed in tension at room temperature and 77 K. The true stress for the onset of deformation twinning is 1044 MPa, which can be converted into a twinning shear stress of 423 MPa with the use of the Schmid factor (0.405) for ($11\bar{1}$) [$1\bar{2}\bar{1}$] conjugate twinning in the [$1\bar{3}$ 12 25] tensile-axis orientation. Fig. 2.14 (a) shows an optical micrograph of the specimen after unloading from point C in Fig. 2.12. Surface markings corresponding to deformation twinning on the (111) conjugate planes are observed to intersect those corresponding to the previously activated (111) [101] primary slip system, causing the primary slip lines to be bent by the twinning shear.

A typical TEM image of deformation twins viewed end-on in Fig. 2.14 (b) indicates that twins are mostly nanometer scale. The average twin thickness for Cr-Fe-Co-Ni is 4.6nm. On average, the volume fraction of conjugate twins is relatively high (0.44). Thus, the twin thickness and distribution are more miniature than observed in single crystal cantor alloy after 77 K deformation by Kawamura et al. [16]. However, our twin volume fraction (0.44) is slightly less than their value (0.58), indicating tensile elongation is less than single-crystal

cantor alloy. A typical high-resolution HAADF STEM image of deformation twins in Fig. 2.15 demonstrates that apart from the formation of profuse nano twins and stacking faults, an HCP structure in the form of thin layers also formed. HCP layers are visible in atomic-scale HAADF STEM image viewed along <110> type. Many of the twins are observed with thin HCP layers, and also twins are observed in between the matrix. Though HCP layers are not widely spread but could be detected locally. Histograms of the distribution of twin thickness and HCP layer are shown in Figure 2.16(a) and (b). The average twin thickness and HCP layer is 1.41nm and 0.50nm, respectively.

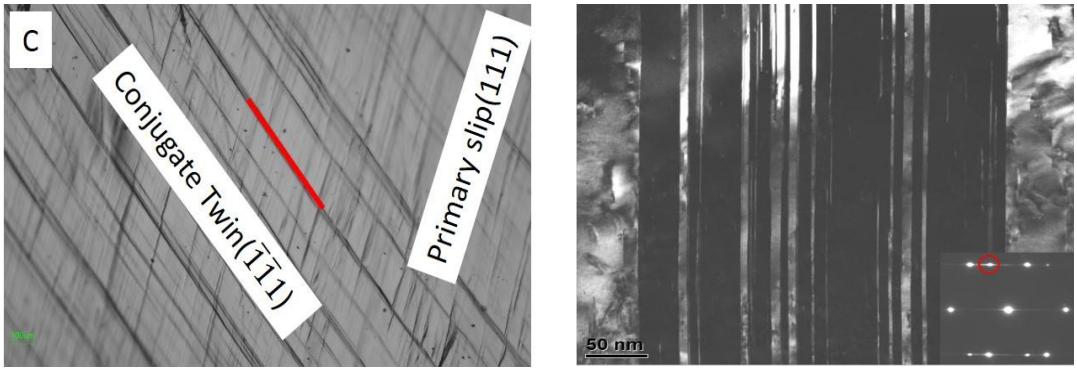

Figure 2.14. (a) Deformation Marking observed on a [$\bar{1}23$] deformed at 77K at point C in S-S curve (b) TEM dark-field image of deformation twins and SAD pattern

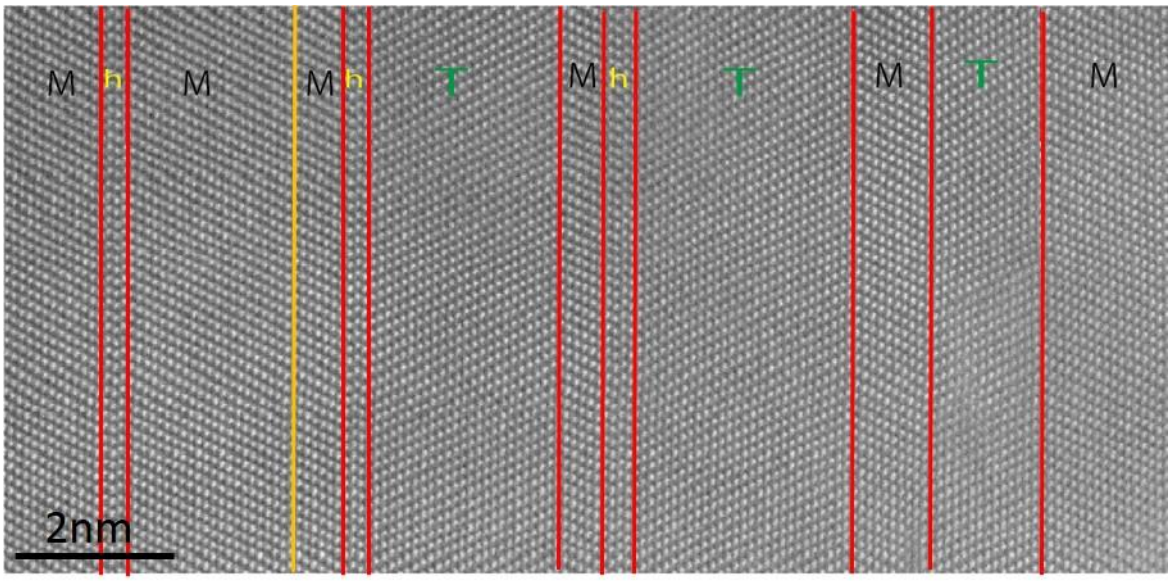

Figure 2.15. Atomic-resolution STEM image of deformation twins in a [$\bar{1}23$] oriented single crystal of the Cr-Fe-Co-Ni deformed in tension at 77 K.

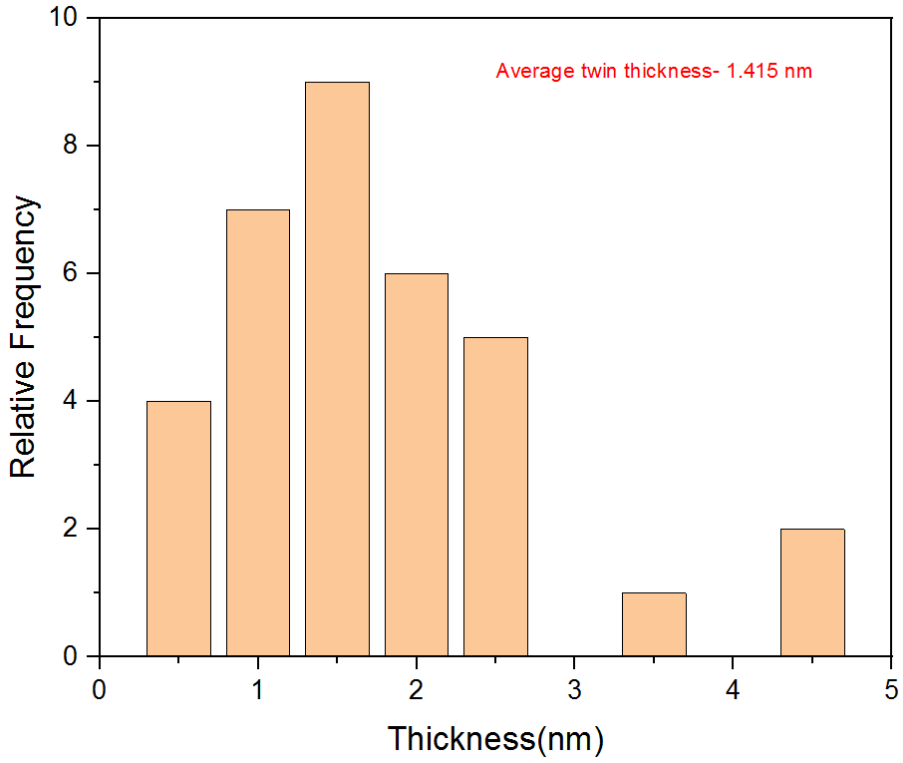

Figure 2.16(a). Average twin thickness of single crystal Cr-Fe-Co-Ni MEA deformed at 77K

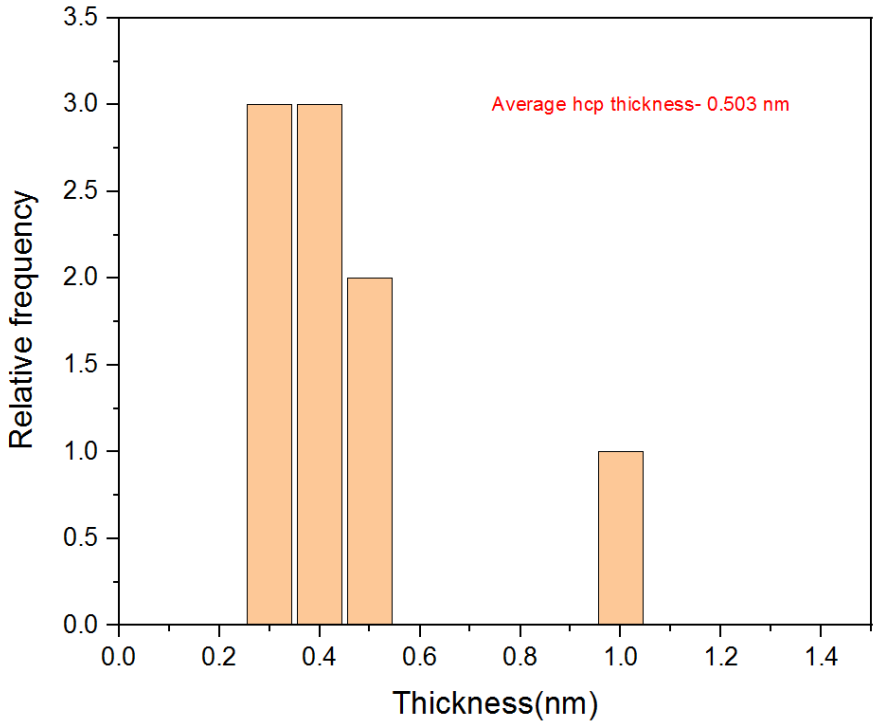

Figure 2.16(b). An average hcp layer thickness of single crystal Cr-Fe-Co-Ni MEA deformed at 77K

Q. Lin et al.[13] also reported similar findings in Cr-Fe-Co-Ni and suggested that the formation of hcp structure is achieved via the glide of Schockley partial dislocation on every other {111} FCC plane. Niu et al. [14] explained that thin HCP layers sometimes exist at the edge of twins since the formation of the HCP layer is more favoured than further twin thickening due to the very low stacking fault energy of the Cr-Co-Ni MEA. The same is the case might be for Cr-Fe-Co-Ni as SFE is lower than Cantor alloy. Kawamura et al. [7] conclude that the stacking fault energy (in other words, the energy difference between FCC and HCP structures) is not low enough to introduce thin HCP layers in the Cantor alloy. Figs. 2.17 (a-d) show fracture surfaces of [$\bar{1}23$] oriented single crystals tensile tested to failure at

77 K and room temperature, respectively. The specimens exhibit obvious necking and fracture surfaces are of the dimple type typical for ductile failure at both temperatures. These are clear indications that the Cr-Fe-Co-Ni MEA is a ductile failure.

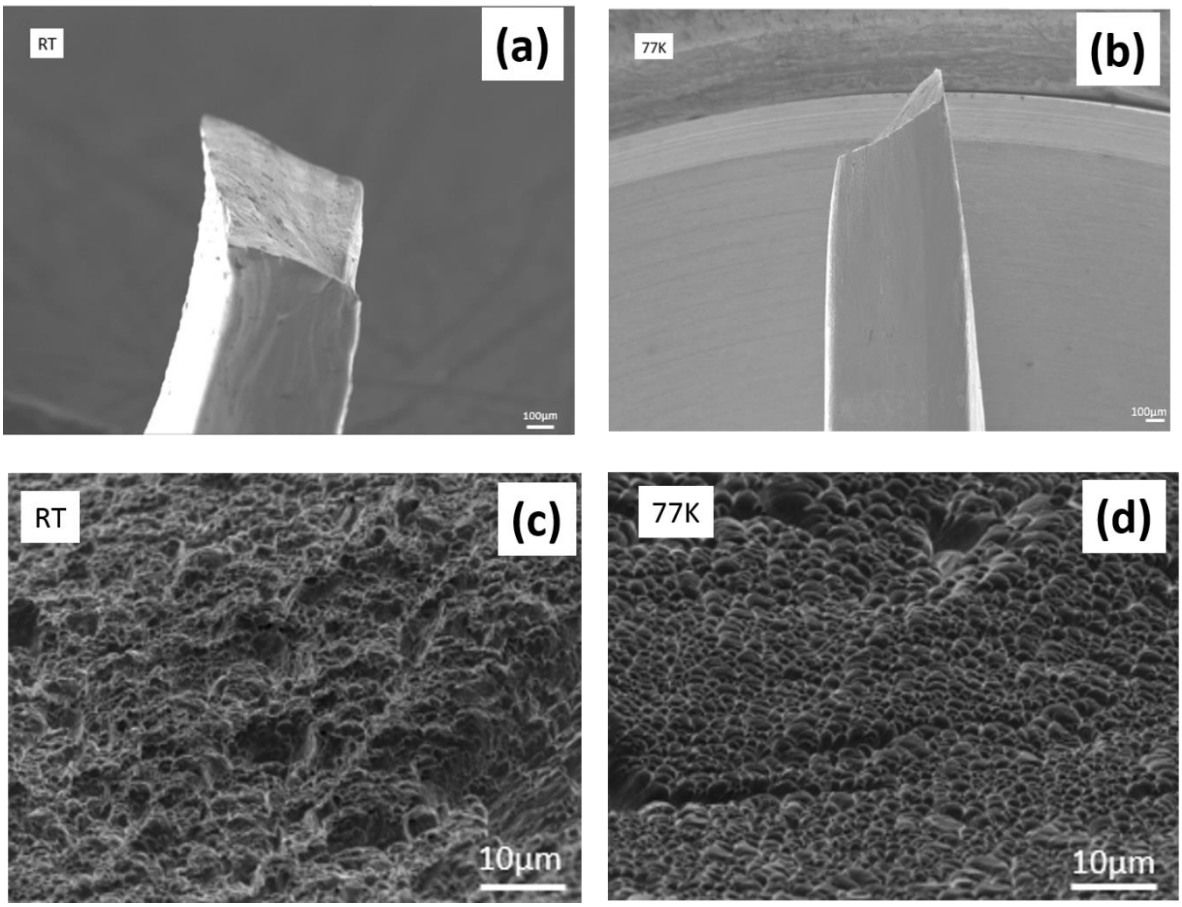

Figure 2.17. Side and top view of fracture surfaces in [$\bar{1}23$] oriented single crystals of the Cr-Fe-Co-Ni deformed in tension at room temperature ((a), (c)), and 77 K ((b), (d)).

2.4. Discussions

2.4.1. Mechanical Properties

The CRSS for {111} < 110 > slip in the present single crystals of the quaternary, equiatomic, Cr − Fe −Co −Ni MEA is in the range of 42- 45 MPa at room temperature, which is consistent with the CRSS values reported by Z. Wu et al. [3]. At 77K, the CRSS value is 135-140 MPa, higher than the value reported by Z. Wu et al. [3]. Below room temperature strength of this alloy increases, and strong temperature dependence occurs down to 0K. Around 50K, dullness in the dependence of CRSS is noticeable, implying an inertia effect found for many other FCC solid solution alloys. By extrapolating the CRSS to 0K, the CRSS value determined at 0K is 213MPa, which is higher than our study on Cr-Mn-Fe-Co-Ni single crystal alloy 168MPa at 0K. As in many conventional FCC alloys, a slight increase in yield stress is noted in the high-temperature region of the CRSS (yield stress) vs temperature curve. This is believed to be due to the PL effect as in other FCC alloys. All these mechanical properties of the Cr −Fe −Co −Ni MEA have also been observed in many other conventional FCC alloys, indicating that the present MEA is not a peculiar alloy but is simply a typical FCC solid-solution alloy with exceptionally high strength. The high strength of the present MEA could originate from the large extent of lattice distortion, as proposed in [15], where the mean-square atomic displacement (MSAD) was used to quantify the extent of lattice distortion and directly correlated with the 0 K CRSS.

Solid solution strengthening is considered as the main strengthening mechanism in FCC single crystal Cr-Fe-Co-Ni alloy. In connection with that, the concept of 'stress equivalence'

proposed for FCC solid-solution alloys a long time ago by Basinski [16–18] holds true in the present quaternary MEA single crystals. It states that (i) the yield strength at 77 K is proportional to the difference between the yield strength at 77 K and that at room temperature for all FCC solid-solutions (Fig. 2.18 (a)) and values of the activation volume measured at a given temperature all lie on a single master curve is plotted as a function of yield stress (Fig. 2.19) irrespective of their concentration. The present MEA and cantor alloy data at room temperature and 77 K are included in Figs. 2.18 and 2.19. As can be seen, the present MEA and cantor alloy falls on the extrapolated lines drawn through the data points of other conventional FCC alloys; however, the absolute values of stress (Fig. 2.18) and activation volume (Fig. 2.19) are much higher and lower, respectively, for the HEA than for conventional FCC alloys. This is clear evidence that the present MEA is not a peculiar alloy but is a standard solid-solution alloy, except for its very high strength at cryogenic temperature. This indicated that the thermal activation process for dislocation glide does not vary from one alloy to other regardless of the concentration and a single mechanism is responsible for the thermal activation process. To confirm this hypothesis in our MEA, we investigated the activation enthalpy for deformation by using the strain rate jump test. Activation Enthalpy can be calculated from the following equation:

$$\dot{\gamma} = Cexp[-U(\tau)/kT] \qquad 2.4\ (a)$$

Where $\dot{\gamma}$, k and T are shear strain rate, Boltzmann's constant and temperature, respectively. C is a constant and of the order of 10^8 /s. Also, without considering the constant C, we estimated the Activation Enthalpy by deriving the equation from the above equation,

$$U(\tau) = -k[\frac{\partial ln\dot{\gamma}}{\partial\left(\frac{1}{T}\right)}]$$

$$\approx -k\,[ln\dot{\gamma}(\tau, T_2) - ln\dot{\gamma}(\tau, T_1)]/(\frac{1}{T_2} - \frac{1}{T_1}) \quad 2.4\text{ (b)}$$

Figure 2.20 shows the plot between Enthalpy and shear stress by using the above two equations. The Activation Enthalpy calculated for this alloy is .65 eV at room temperature, consistent with the values of many other FCC solid solution alloys.

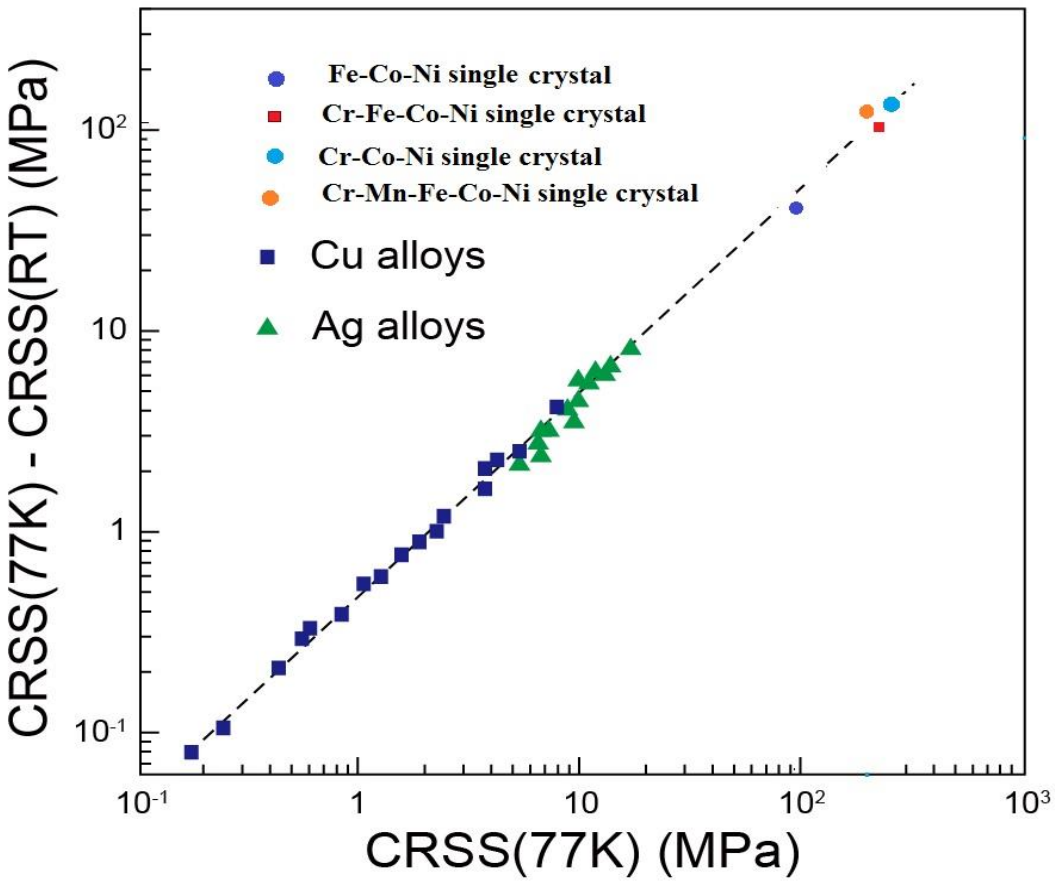

Figure 2.18. The difference between the yield strength at 77 K and that at room temperature plotted as a function of the yield strength at 77 K for FCC solid solutions.

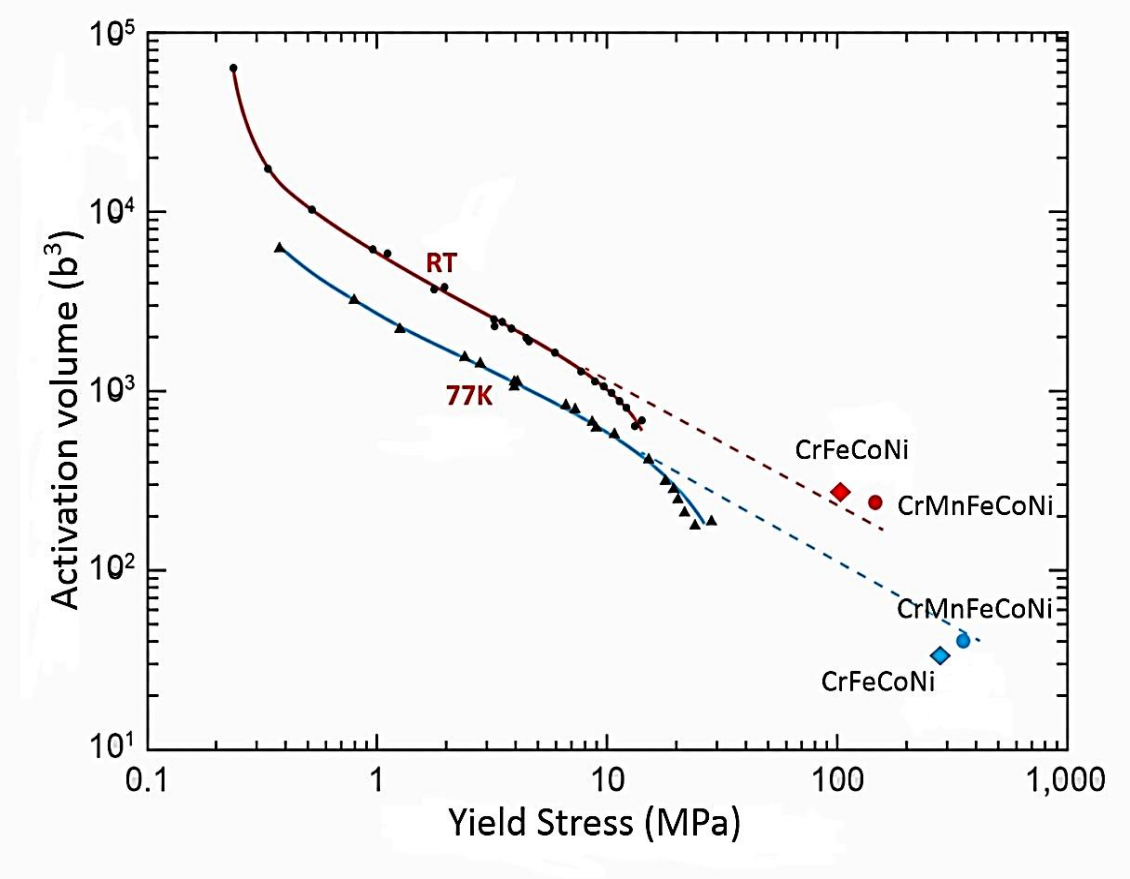

Figure 2.19. Activation volumes at room temperature and 77 K for FCC solid solutions plotted as a function of their yield strengths along with Cr-Fe-Co-Ni and Cr-Mn-Fe-Co-Ni

Activation volume at RT and 77K is found to be 248.7b and 33.74$b^{3,}$ respectively. Which is consistent with Cr-Mn-Fe-Co-Ni alloy. Laplanche et al.[19] reported that the activation volume for deformation obtained by strain-rate jump tests decreases with strain at room temperature because forest dislocations are introduced during plastic straining in Cantor alloy. This decrease in activation volume can be minimized if the test is made in the strain range of

easy glide as shown in the present study using single crystals (which is not possible with polycrystals as they lack a region of easy glide since hardening starts almost immediately after yielding). Kawamura et al.[7] estimated lower values of activation volume by using a single crystal. On the other hand, Hong et al.[20] reported that activation volume for deformation increases with strain at room temperature because the short-range ordering of constituent atoms that existed prior to deformation is gradually destroyed by the passage of dislocations (they did not mention the countervailing effect of forest dislocations, which would tend to decrease the activation volume). The relatively strain-independent activation volume measured in the present study (in the easy-glide region) implies either no significant short-range ordering in the alloy or that the flow stress is not significantly affected by short-range ordering, though a detailed investigation is still required for the presence of SRO.

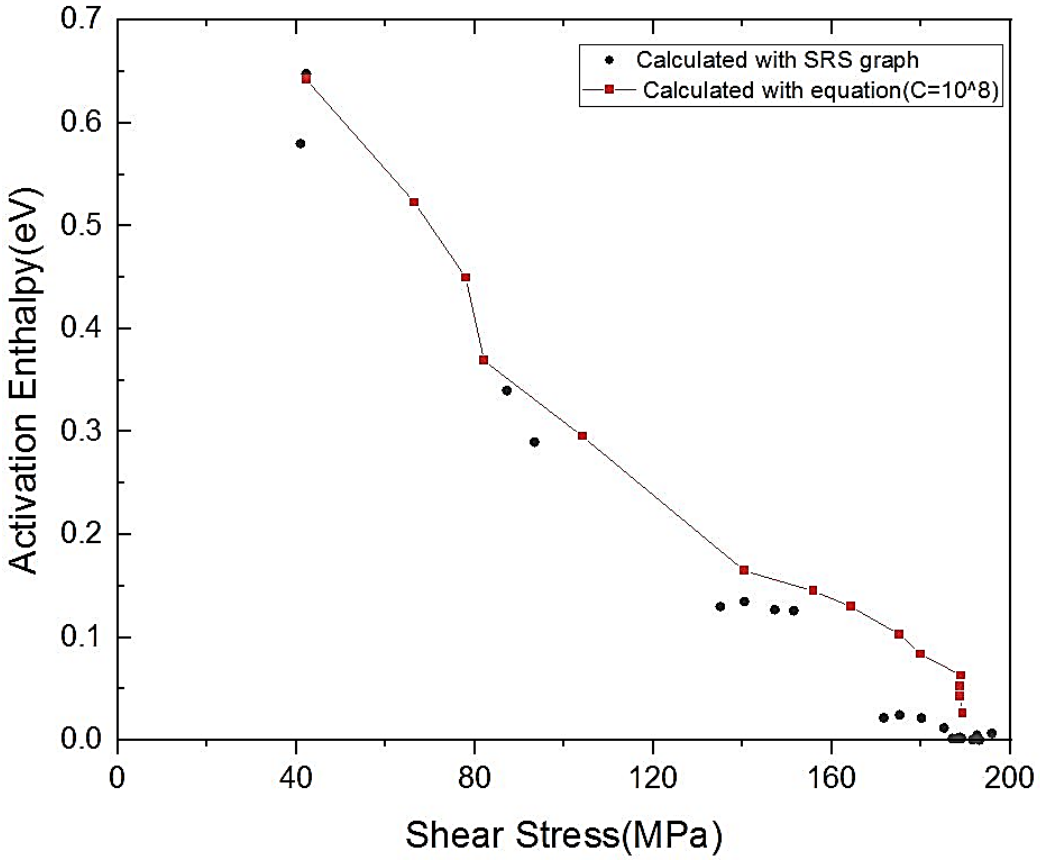

Figure 2.20 Activation Enthalpy of Cr-Fe-Co-Ni measured using the equation as a function of Shear stress

2.4.2. Dislocation behavior

Dislocations with the Burgers vector, $\boldsymbol{b}$ = 1/2 < 110 > are widely dissociated into coupled Shockley partials from which a relatively low stacking fault energy of 22 mJ/m^2 can be estimated; this contributes to the activation of deformation twinning at low temperatures. Recently, significant point-to-point variations in dislocation dissociation widths have been reported in the Cr −Mn −Fe −Co −Ni HEA and ascribed to dislocation interactions with solute atoms causing local fluctuations in the stacking fault energy [21]. However, variations in

dissociation widths similar in magnitude to those in the present MEA (Fig.2.8 (b)) have also been observed in elemental metals such as pure Cu[21,22]and pure Ag[21], indicating that concentrated solid solutions such as HEAs are not unique when it comes to local variations in dissociation widths. In this connection, it is vital to consider the extended jogs that form by forest cutting. Such jogged dislocations in Cu alloys can significantly change dislocation dissociation widths[23–25]. The jogs that form in low stacking fault energy materials (such as the present MEA) are extended jogs[23]. A slight increase in yield stress is noted in the high-temperature region of the CRSS (yield stress) vs temperature curve of the Cr- Fe −Co − Ni MEA, as in many other conventional FCC alloys (Fig.2.5(b)). In conventional FCC alloys, this is usually explained in terms of the PLC effect, in which solute atoms that have segregated to the stacking fault between coupled partial dislocations (if such segregation is energetically favourable through the Suzuki effect) move along with the dislocations provided the temperature is high enough to allow atomic diffusion to occur at speed comparable to that of the dislocations. Since the local stacking of four atomic layers across the stacking fault resembles HCP stacking, segregation of elements with the HCP structure (Co in the case of the present quaternary MEA) may occur and cause the PLC effect.

2.4.3. Twinning Behavior

The twinning shear stress for conventional FCC alloys increases with increases in stacking fault energy. In High Entropy alloys, this trend seems to be the opposite as Lapalanche et al.[26] reported that twinning stress is higher for polycrystalline Cr-Co-Ni MEA than for a Cr-Mn-Fe-Co-Ni HEA. We found a similar opposite trend in our group while investigating

three different FCC single crystal HEA/MEA and results shown in Figure 2.21 as a function of stacking fault energy. Twinning was not observed at RT but at 77K, consistent with Cr-Mn-Fe-Co-Ni single-crystal HEA reported by Kawamura et al.[7] Other than twins, a thin layer of HCP is also observed in this Cr-Fe-Co-Ni alloy though the fraction of HCP is relatively low as compared to twinning.

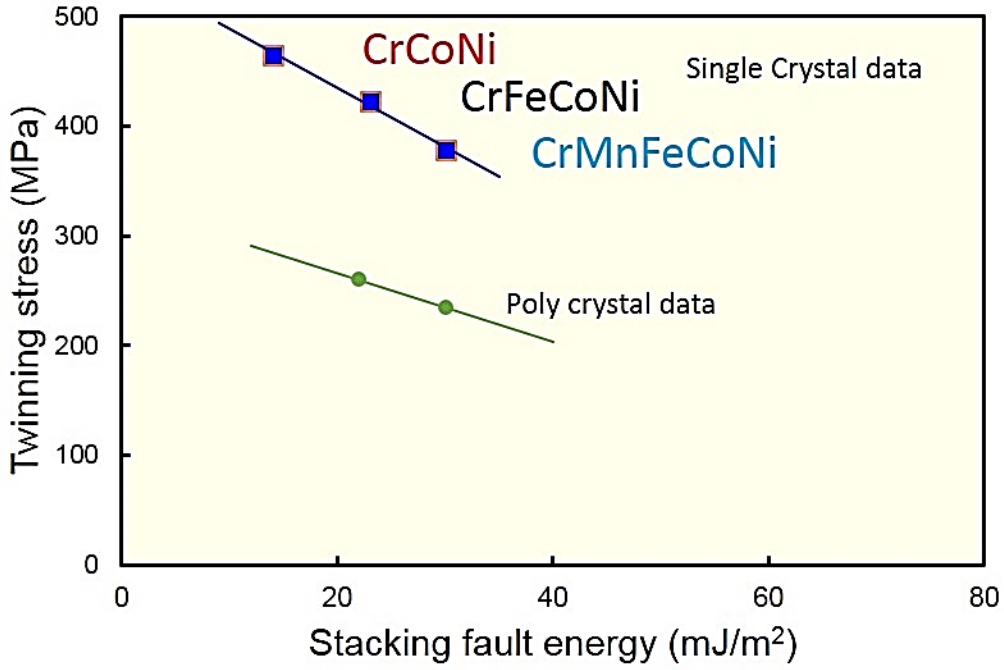

Figure 2.21. Twinning stress as a function of SFE of 3 different FCC single crystal HEA and MEA showing opposite trends than traditional FCC alloys

2.5. Conclusions

Plastic Deformation behavior of an equiatomic single-crystal Cr-Fe-Co-Ni MEA was systematically studied at temperatures ranging from 12.4K to 1373K and different strain rates from 10^{-5} s^{-1} to $5x10^{-3}$ s^{-1} in compression and tension. Based on the mechanical properties, the following conclusions were drawn in this chapter:

1. The CRSS for {111} < 110 > slip increases with decreasing temperature, with showing inertia effects at cryogenic temperatures (below 50 K). From an extrapolation to lower temperatures, the CRSS at 0 K is estimated to be 220 MPa. The concept of 'stress equivalence' originally proposed for conventional FCC solid-solution alloys holds true for the Cr −Fe −Co −Ni HEA, although the stress levels are much higher than those of conventional FCC alloys. The quaternary equiatomic Cr −Fe −Co −Ni MEA exhibits a higher strain-rate sensitivity of flow stress than binary FCC alloys such as Cu −Al, Cu-5Al consistent with its stronger temperature dependence CRSS than the binary alloys. Together, these observations indicate that solid-solution hardening is the major strengthening mechanism.
2. Dislocations with b = 1/2 < 110 > dissociate into two Shockley partials with b = 1/6 < 112 > bounding a stacking fault. The stacking fault energy deduced from the separation distance is about 20 mJ/m^2, which is low enough to account for the observed planar arrays of dislocations and the occurrence of deformation twinning at 77 K.
3. Deformation twinning does not occur at room temperature but does occur at 77 K at a high plastic strain of about 80% after the tensile axis overshoots to [$1\bar{3}$ 12 25] as a

result of plastic deformation, including stage I (easy glide) and stage II (linear work-hardening). Twinning occurs on conjugate (1 1 1) planes at an onset twinning shear stress of 423 MPa. Tensile elongation to failure is much more significant at 77 K than at room temperature because of deformation twinning.

4. Thin layers of HCP are observed locally at 77K deformed specimen, which happens because of the passage of Shockley partial dislocation along with the twin interface.

References

[1] Z. Li, S. Zhao, R.O. Ritchie, M.A. Meyers, Mechanical properties of high-entropy alloys with emphasis on face-centered cubic alloys, Prog. Mater. Sci. 102 (2019) 296–345. https://doi.org/10.1016/j.pmatsci.2018.12.003.

[2] B. Cantor, I.T.H. Chang, P. Knight, A.J.B. Vincent, Microstructural development in equiatomic multicomponent alloys, Mater. Sci. Eng. A. 375–377 (2004) 213–218. https://doi.org/10.1016/j.msea.2003.10.257.

[3] Z. Wu, Y.F. Gao, H. Bei, Single crystal plastic behavior of a single-phase, face-center-cubic-structured, equiatomic FeNiCrCo alloy, Scr. Mater. 109 (2015) 108–112. https://doi.org/10.1016/j.scriptamat.2015.07.031.

[4] Z. Wu, H. Bei, G.M. Pharr, E.P. George, Temperature dependence of the mechanical properties of equiatomic solid solution alloys with face-centered cubic crystal structures, Acta Mater. 81 (2014) 428–441. https://doi.org/10.1016/j.actamat.2014.08.026.

[5] C. Varvenne, A. Luque, W.A. Curtin, Theory of strengthening in fcc high entropy alloys, Acta Mater. 118 (2016) 164–176. https://doi.org/10.1016/j.actamat.2016.07.040.

[6] G. Bracq, M. Laurent-Brocq, C. Varvenne, L. Perrière, W.A. Curtin, J.M. Joubert, I. Guillot, Combining experiments and modeling to explore the solid solution strengthening of high and medium entropy alloys, Acta Mater. 177 (2019) 266–279.

https://doi.org/10.1016/j.actamat.2019.06.050.

[7] M. Kawamura, M. Asakura, N.L. Okamoto, K. Kishida, H. Inui, E.P. George, Plastic deformation of single crystals of the equiatomic Cr−Mn−Fe−Co−Ni high-entropy alloy in tension and compression from 10 K to 1273 K, Acta Mater. 203 (2021). https://doi.org/10.1016/j.actamat.2020.10.073.

[8] G. Laplanche, A. Kostka, C. Reinhart, J. Hunfeld, G. Eggeler, E.P. George, Reasons for the superior mechanical properties of medium-entropy CrCoNi compared to high-entropy CrMnFeCoNi, Acta Mater. 128 (2017) 292–303. https://doi.org/10.1016/j.actamat.2017.02.036.

[9] M. Pergamon, M. Plc, 1989 By, 71 (1989) 195–199.

[10] T.H. Wille, C. Schwink, Precision measurements of critical resolved shear stress in CuMn alloys, Acta Metall. 34 (1986) 1059–1069. https://doi.org/10.1016/0001-6160(86)90216-6.

[11] Z.S. Basinski, Thermally activated glide in face-centred cubic metals and its application to the theory of strain hardening, Philos. Mag. 4 (1959) 393–432. https://doi.org/10.1080/14786435908233412.

[12] S.F. Liu, Y. Wu, H.T. Wang, J.Y. He, J.B. Liu, C.X. Chen, X.J. Liu, H. Wang, Z.P. Lu, Stacking fault energy of face-centered-cubic high entropy alloys, Intermetallics. 93 (2018) 269–273. https://doi.org/10.1016/j.intermet.2017.10.004.

[13] Q. Lin, J. Liu, X. An, H. Wang, Y. Zhang, X. Liao, Cryogenic-deformation-induced

phase transformation in an FeCoCrNi high-entropy alloy, Mater. Res. Lett. 6 (2018) 236–243. https://doi.org/10.1080/21663831.2018.1434250.

[14] C. Niu, C.R. LaRosa, J. Miao, M.J. Mills, M. Ghazisaeidi, Magnetically-driven phase transformation strengthening in high entropy alloys, Nat. Commun. 9 (2018). https://doi.org/10.1038/s41467-018-03846-0.

[15] N.L. Okamoto, K. Yuge, K. Tanaka, H. Inui, E.P. George, Atomic displacement in the CrMnFeCoNi high-entropy alloy - A scaling factor to predict solid solution strengthening, AIP Adv. 6 (2016). https://doi.org/10.1063/1.4971371.

[16] C. Schwink, T. Wille, ON THE CONCENTRATION DEPENDENCE OF STRESS EQUIVALENCE IN SOLID SOLUTION HARDENING, 1980.

[17] M. 2 Butt, P. Feltham, SOLID-SOLUTION HARDENING, n.d.

[18] Z.S. Basinski, R.A. Foxall, R. Pascual, Stress equivalence of solution hardening, Scr. Metall. 6 (1972) 807–814. https://doi.org/10.1016/0036-9748(72)90052-X.

[19] G. Laplanche, J. Bonneville, C. Varvenne, W.A. Curtin, E.P. George, Thermal activation parameters of plastic flow reveal deformation mechanisms in the CrMnFeCoNi high-entropy alloy, Acta Mater. 143 (2018) 257–264. https://doi.org/10.1016/j.actamat.2017.10.014.

[20] J. Moon, S.I. Hong, J.W. Bae, M.J. Jang, D. Yim, H.S. Kim, On the strain rate-dependent deformation mechanism of CoCrFeMnNi high-entropy alloy at liquid nitrogen temperature, Mater. Res. Lett. 5 (2017) 472–477.

https://doi.org/10.1080/21663831.2017.1323807.

[21] D.J.H. Cockayne, M.L. Jenkins, I.L.F. Ray, The measurement of stacking-fault energies of pure face-centred cubic metals, Philos. Mag. 24 (1971) 1383–1392. https://doi.org/10.1080/14786437108217419.

[22] W.M. Stobbs, C.H. Sworn, The weak beam technique as applied to the determination of the stacking-fault energy of copper, 8086 (2006). https://doi.org/10.1080/14786437108217418.

[23] C.B. Carter, The Extension of Jogs on Dissociated Dislocations in F.C.C. Metals, Phys. Status Solidi. 54 (1979) 395–406. https://doi.org/10.1002/pssa.2210540150.

[24] C.B. Carter, I.L.F. Ray, Philosophical Magazine Observations of constrictions on dissociated dislocation lines in copper alloys, (n.d.). https://doi.org/10.1080/14786437408226609.

[25] C.B. Carter, P.B. Hirsch, Philosophical Magazine The formation and glide of jogs in low stacking-fault energy face-centred cubic materials, (n.d.). https://doi.org/10.1080/14786437708232974.

[26] G. Laplanche, A. Kostka, O.M. Horst, G. Eggeler, E.P. George, Microstructure evolution and critical stress for twinning in the CrMnFeCoNi high-entropy alloy, Acta Mater. 118 (2016) 152–163. https://doi.org/10.1016/j.actamat.2016.07.038.

Chapter 3

Deformation Mechanism of single crystal FCC Fe-Co-Ni Medium Entropy alloy

3.1. Introduction

High entropy alloys are a quest for the materials world because of their exceptional strength and ductility. Therefore, FCC high and medium entropy alloys, say, specially cantor alloys and their derivatives, have drawn significant attention from researchers around the globe. For example, Wu et al. [1] studied the temperature dependence of mechanical properties of equiatomic solid solution alloys with FCC crystal structures. In their study, he covered all the possible single-phase FCC medium entropy alloys and reported that the yield strength of these alloys increases strongly while decreasing the temperature. To understand the behaviour, they analyzed temperature-dependent yield strength and strain hardening separately. Lattice friction appeared to be the predominant component for the temperature dependence of yield stress because Peierls barrier height decreases with increasing temperature due to a thermally induced increase of dislocation width. Figure 3.1 shows the temperature dependence of yield stress of equiatomic medium entropy alloy.

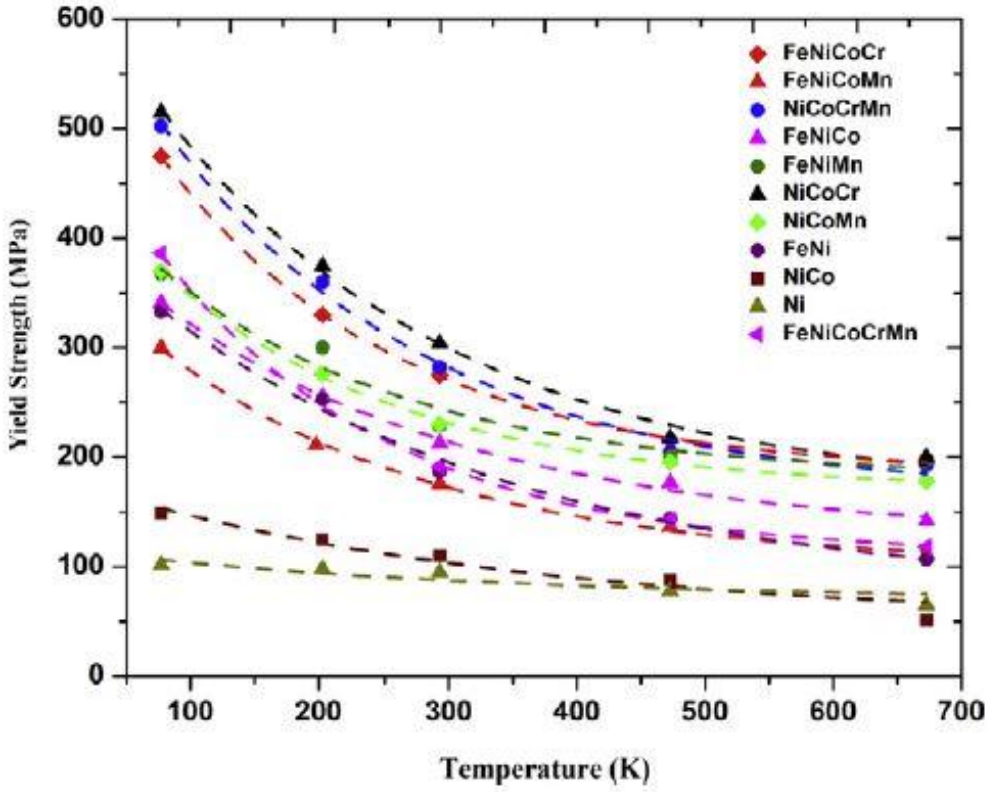

Fig.3.1 The temperature dependence of yield stress of equiatomic alloys and pure nickel

However, most of the research has been done on polycrystal. Therefore, to understand the fundamentals of the plastic deformation mechanism of the family of this alloy, it is essential to investigate through the single crystal as stated in Chapter 2.

This chapter aims to reveal the plastic deformation mechanism of equiatomic FCC Fe-Co-Ni Medium Entropy alloy in bulk single-crystal in tension and compression at temperature range 13K-1373K.

3.2. Experimental Procedures

3.2.1. Single crystal fabrication

Cylindrical ingots, 10 mm in diameter and 80 mm long, were prepared by arc-melting in argon atmosphere high-purity (> 99.9%) Fe, Co, and Ni in equiatomic ratios. Each ingot was flipped and re-melted at least four times to ensure chemical homogeneity. This ingot was then used to grow single crystals of the quaternary MEA by the Floating Zone method in the Ar atmosphere at the growth rate of 10 mm/h and 15 rpm. Figure 3.1 (a) shows a grown single crystal specimen after the floating zone. The single crystals were annealed at 1473 K for 72 h, followed by water quenching. A small piece of this sample was cut, and EBSD was done to check the quality of a single crystal.

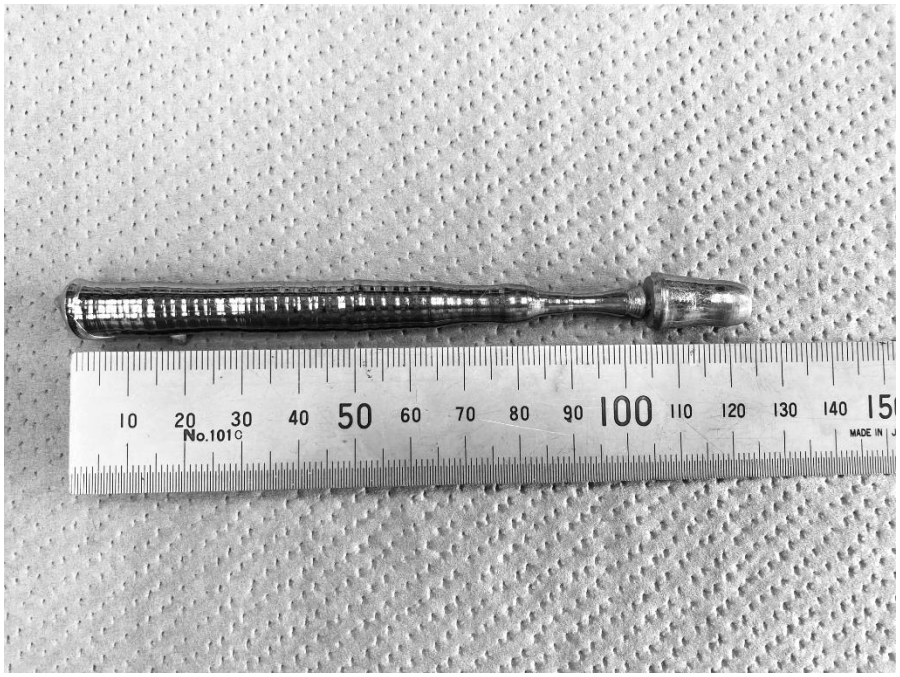

Figure 3.1 Single crystal of equiatomic FCC Fe-Co-Ni prepared by Optical floating zone method

3.2.2. Orientation determination and preparation of bulk samples for mechanical testing

Crystallographic orientations were determined by the X-ray back-reflection Laue method, and oriented test specimens were cut from the crystal by spark-machining for uniaxial tests in compression (dimensions: 2 ×2 ×5 mm 3) and tension (gage section dimensions: 2 ×2 ×5 mm 3). The surfaces of the compression and tensile test specimens were mechanically polished, followed by electro-polishing with a solution of nitric acid and methanol (1:3 by volume). The compression-axis orientations and tensile axis tested were $[\bar{1}23]$. Compression and tensile tests were conducted on an Instron-type testing machine in a vacuum in the temperature range from 13 to 1373 K at an engineering strain rate of 1×10^{-4} s^{-1}. The strain-rate sensitivity of flow stress was measured by strain rate jump test by changing the strain rate by one or two orders of magnitude in the range of 1×10^{-5} to 5×10^{-3} s^{-1} at selected temperatures.

3.2.3. Compression deformation

Rectangular specimens for compression tests in the range of 13K-1373K, having dimensions 2x2x5 mm^3, were cut from the $[\bar{1}23]$ oriented crystal using an electric discharge wire cutting machine. Uniaxial compression tests were carried out in the vacuum atmosphere at high temperatures (473K-1373K) and cryogenic temperature (13K- 212K). Room temperature and 77K compression test was done separately by using an Instron-type testing machine. The strain-rate sensitivity of flow stress was measured by suddenly changing the strain rate by one or two orders of magnitude in the range of 1×10^{-5} to 5×10^{-3} s^{-1} at selected

temperatures. Deformation offsets on the specimen surface (caused by slip) were examined by optical microscopy and in a scanning electron microscope (SEM) equipped with an electron backscatter diffraction (EBSD) detector. Dislocation structures and dislocation core structures were examined by transmission electron microscopy (TEM), respectively, with JEOL JEM-20 0 0FX electron microscopes operated at 200 kV. Thin foils for TEM observations were prepared by electro-polishing with a solution of methanol, nitric acid and ethylene glycol (20:5:2 by volume).

3.2.4. Tensile deformation

Dogbone shape specimens were cut from the oriented crystal using an electric discharge wire cutting machine. Next, uniaxial tensile tests were performed using an Instron-type testing machine at room temperature and 77K at a strain rate of $1x10^{-4}$ s^{-1}. For 77K, the tensile test specimen immersed in liquid nitrogen temperature and a pre-test was done before starting the actual test.

3.3. Results

3.3.1. Compression deformation behavior

Stress-strain curves of jump test of a single crystal with $[\bar{1}23]$ orientation deformed at the temperature range from 13K-1373K with is shown in Figure 3.2 (a-c). The strain rate was changed by one or two orders of magnitude in the range of 1×10^{-5} to 5×10^{-3} s^{-1} at selected temperatures. Slip markings on the surface of the compression specimen for RT and 77K are shown in Figures 3.3 (a) and (b). Optical microscopy images of slip markings confirm the $(111)[\bar{1}01]$ slip systems at room temperature and 77K. Slip markings on the surface are straight from one end to the other of the specimen. We couldn't find any traces of cross-slip in the easy-glide region, possibly because this alloy's high stacking fault energy is comparatively higher than Cr-Mn-Fe-Co-Ni and Cr-Fe-Co-Ni alloys. Strain rate sensitivity was measured in the easy-glide region to minimize the work hardening effect.

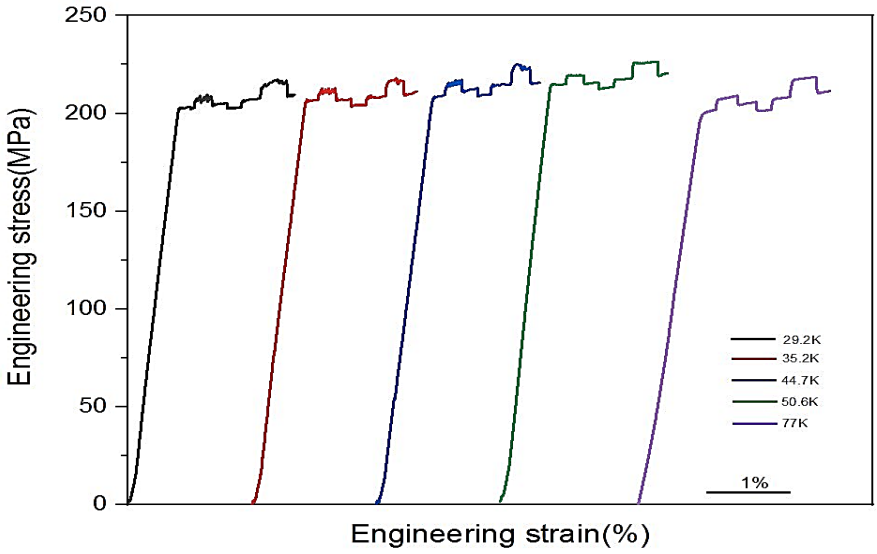

Figure 3.2 (a) S-S curve of compression of Fe-Co-Ni single crystal at different temperature

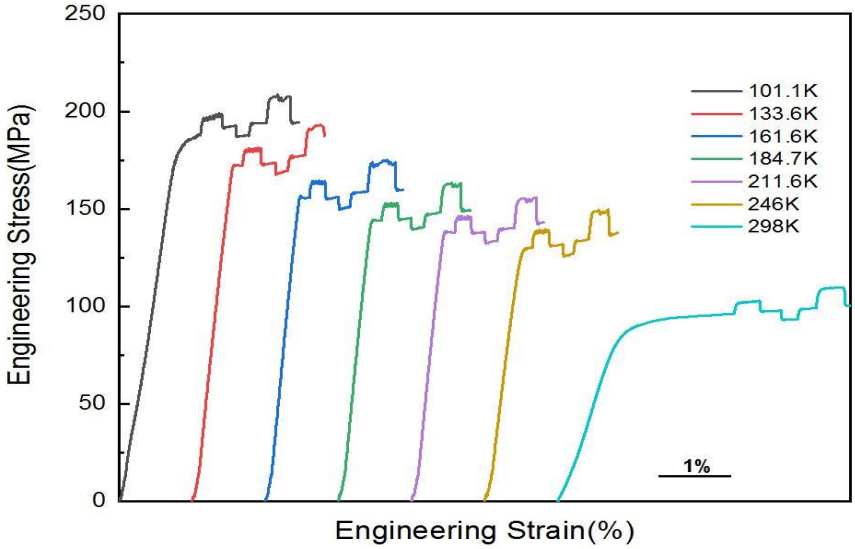

Figure 3.2 (b) S-S curve of compression of Fe-Co-Ni single crystal at different temperature

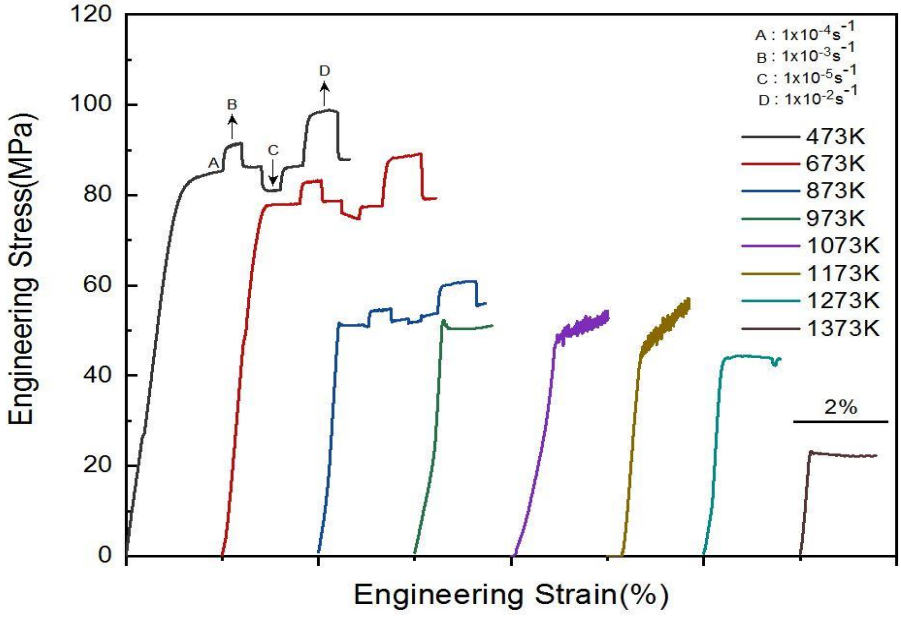

Figure 3.2 (c) S-S curve of compression of Fe-Co-Ni single crystal at different temperature

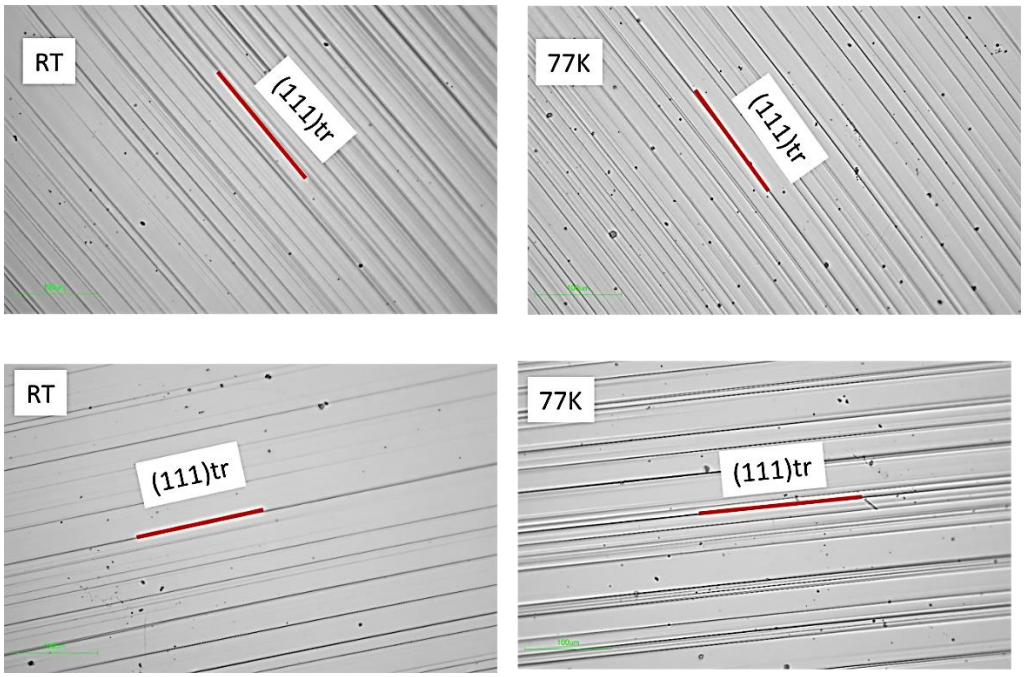

(a) (b)

Figure 3.3 (a)Slip Markings of single crystal Fe-Co-Ni at RT and (b)77K

3.3.2. Temperature dependence of CRSS

The temperature dependence of the CRSS curve at a strain rate of 1×10^{-4} s^{-1} is shown in Figure 3.4. The absolute values of CRSS at each temperature are much more extensive for the Fe-Co-Ni MEA than other binary FCC alloys reported previously, and the same phenomena are also reported for quaternary Cr-Fe-Co-Ni MEA and quinary Cr-Mn-Fe-Co-Ni HEAs. CRSS values were calculated by multiplying the 0.2% yield strength to the Schmid factor (0.46). CRSS increases while decreasing the temperature below room temperature. Below 50K temperature, the curve starts getting dull and such phenomena is `also observed in FCC binary alloys such as Cu-5Al and Cu-10Al alloys[2], which is described as inertia

effect[3,4]. A detailed explanation of inertia effects is introduced in Chapter 2. A slight increase in CRSS values is noticed around 1073K, and a serration is noticed in the S-S curve in Cr-Mn-Fe-Co-Ni and Cr-Fe-Co-Ni. Serration occurs at this temperature because there is an interaction between solute atoms and dislocation known as Portvin-Le Chatlier (PL) effect, and this is also described in Chapter 2 and by Kawamura et al.[5] for quinary Cr-Mn-Fe-Co-Ni. 0K CRSS for Fe-Co-Ni is estimated to be 125 MPa by extrapolating the temperature dependence curve using equation 3.1, which is less than single-crystal cantor alloy (0K CRSS 168MPa) and Cr-Fe-Co-Ni (0K CRSS 215MPa) and much higher than other binary FCC alloys.

$$\tau_{crss} = \tau_{ath} + \tau_{th} \times \left[1 - \left(\frac{T}{T_{TA}}\right)^{\frac{1}{q}}\right]^{\frac{1}{p}} \qquad (3.1)$$

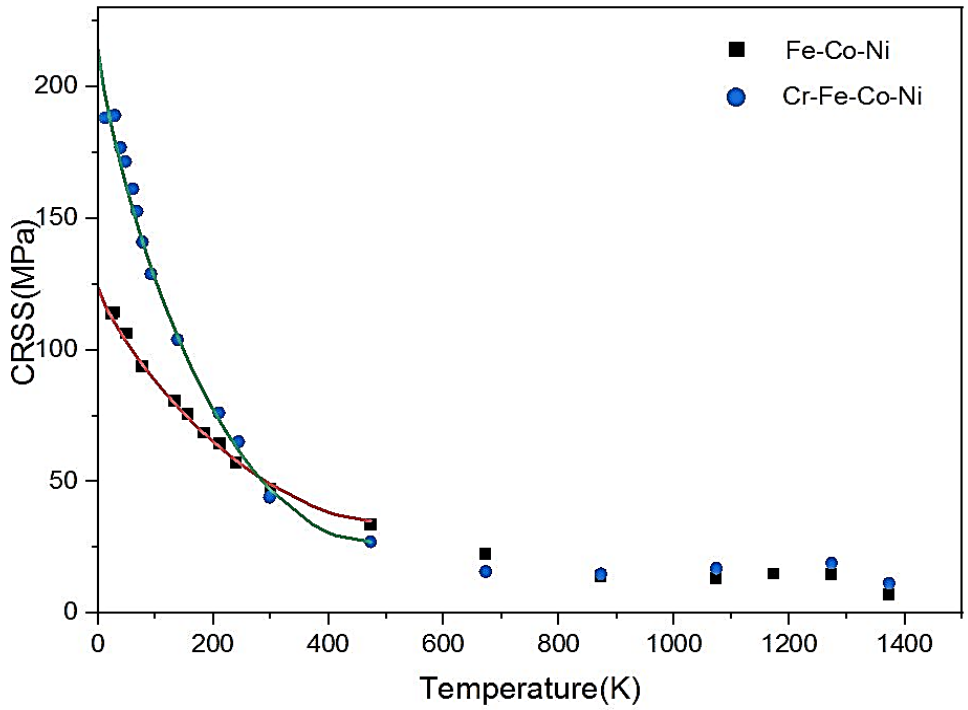

Figure 3.4. Temperature dependence of CRSS of Single-crystal Fe-Co-Ni and Cr-Fe-Co-Ni MEA

3.3.3. Strain rate sensitivity of flow stress and Activation Volume

The strain rate sensitivity of flow stress measured for $[\bar{1}23]$ oriented single crystal of equiatomic Fe-Co-Ni MEA in the easy-glide region at a temperature range between 12.4K and 473K are plotted in Fig 3.5 as a function of strain rate. Stress and strain are converted into shear stress and shear strain by multiplying to schmid factor (.467). The flow stress of Fe-Co-Ni equiatomic MEA increased at a higher strain rate, and strain rate sensitivity (SRS) is more prominent at low temperatures up to 60.7K also found in Cr-Fe-Co-Ni in chapter 2. Below this temperature, SRS of flow stress becomes smaller, as shown in Fig 3.5. This decrease in SRS of flow stress is strong evidence of the occurrence of the inertia effect [3],

through which the dullness of the temperature dependence of CRSS occurs in Fig 3.4. The activation volume (V) is determined with the strain rate sensitivity of flow stress measured at different temperatures by using equation 3.2

$$V = kT\delta \ln(\dot{\epsilon}) / \delta\tau \qquad (3.2)$$

Where k is Boltzmann's constant, T is test temperature, $\dot{\epsilon}$ is shear strain rate, and $\delta\tau$ is shear stress. The values of activation volume are measured at each temperature and compared with Cr-Fe-Co-Ni single crystal MEA and are plotted in Fig 3.6(a). Activation volumes at temperatures below 50K are less dependent on temperature. Fig 3.6(b) shows the more clear picture of extent of strain rate sensitivity of flow stress, which is deduced from the gradient of the SRS curves as a function of temperature. Graph shows a sharp decrease in the slope at temperature near about 60K which again confirms the inertia effects of this single crystal MEA and consistent with Cr-Fe-Co-Ni MEA. At room temperature, the activation volume is 256.46b^3, close to the activation volume measured for quinary Cr-Mn-Fe-Co-Ni equiatomic single-crystal HEA, which is 232.7 b^3. At 12.4K and 77K, activation volumes are 17.97b^3 and 72.79$b^{3,}$ which is more than Cr-Mn-Fe-Co-Ni HEA (5.4 b3 for 10K and 40.2 b3 for 77K).

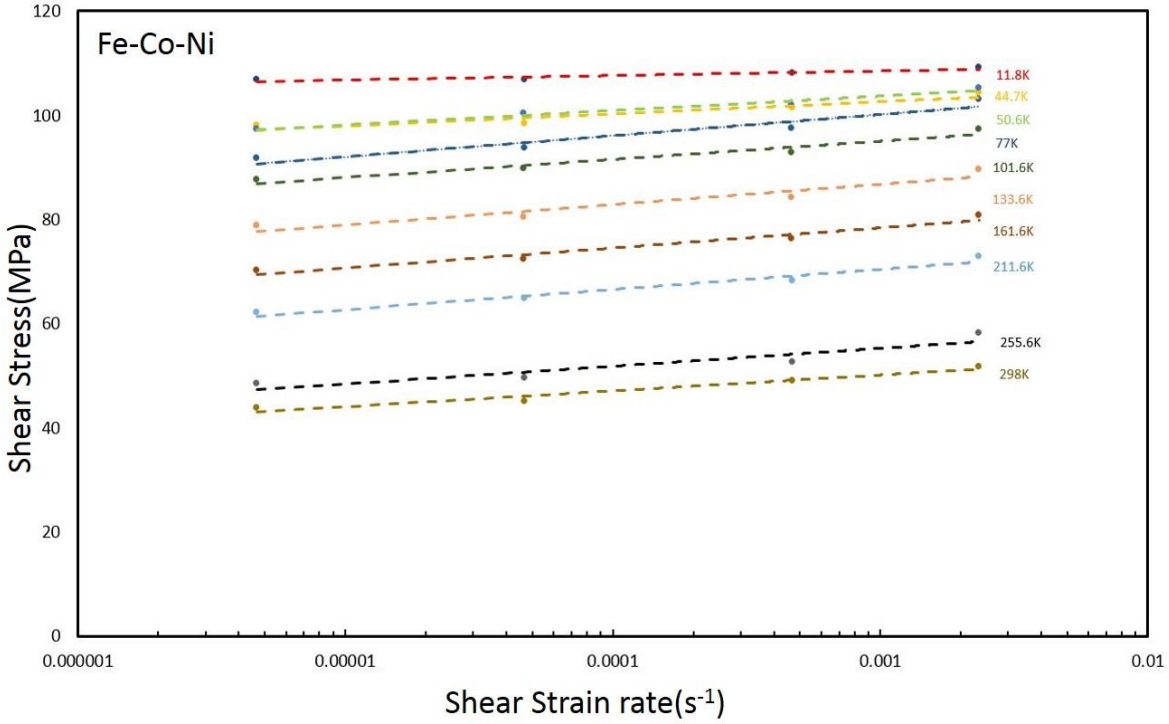

Figure 3.5. Strain rate sensitivity of the flow stress of Fe-Co-Ni at different temperature

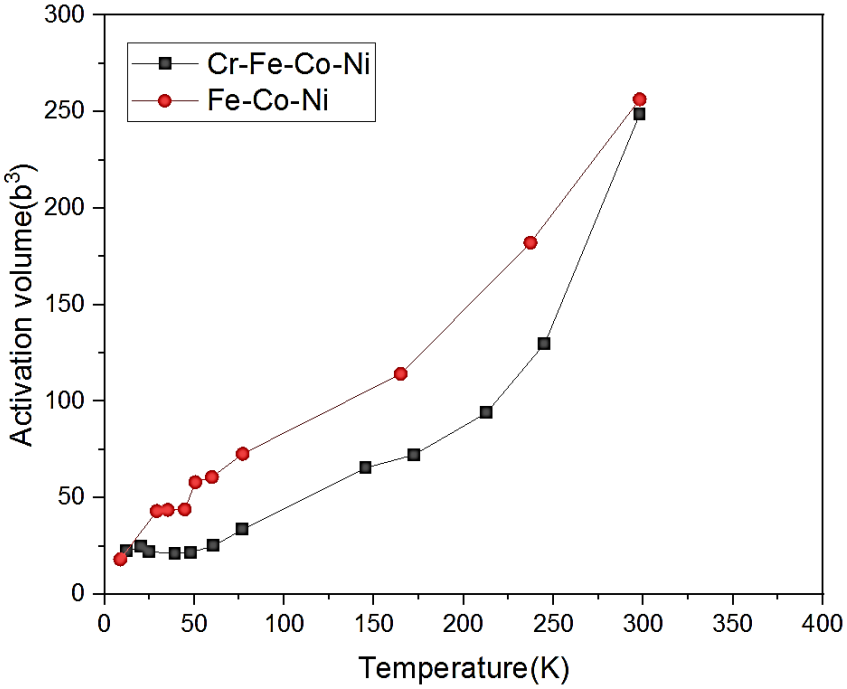

Figure 3.6(a) Activation Volume as a function of Temperature

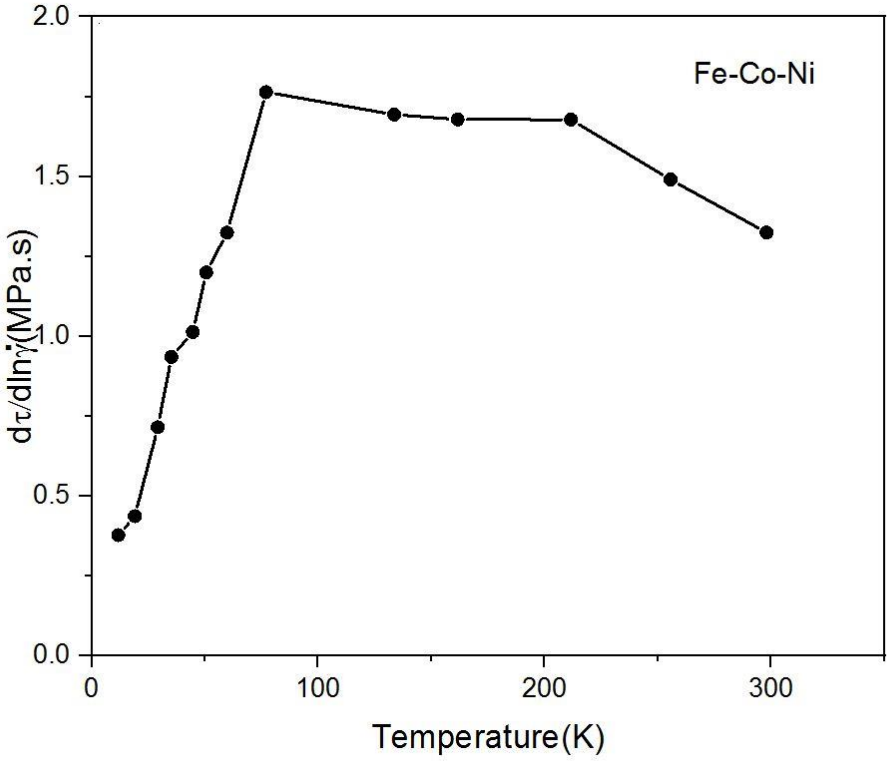

Figure 3.6(b) Gradient of SRS as a function of temperature

3.3.4. Dislocation Structures

A typical dislocation structure observed in an $[\bar{1}23]$ oriented equiatomic single crystal of ternary Fe-Co-Ni MEA deformed in compression up to 3% of plastic strain at RT is shown in Fig 3.7(a). A thin foil of deformed specimen was cut parallel to the (111) slip plane. Planar arrays of dislocations are observed of this MEA. However, a widespread partial dislocation is not visible in the weak beam image in Fig 3.7(b). The separation distance of this partial was beyond the measurement limit of the weak beam technique. This narrow separation width suggests a high stacking fault energy of equiatomic Fe-Co-Ni MEA.

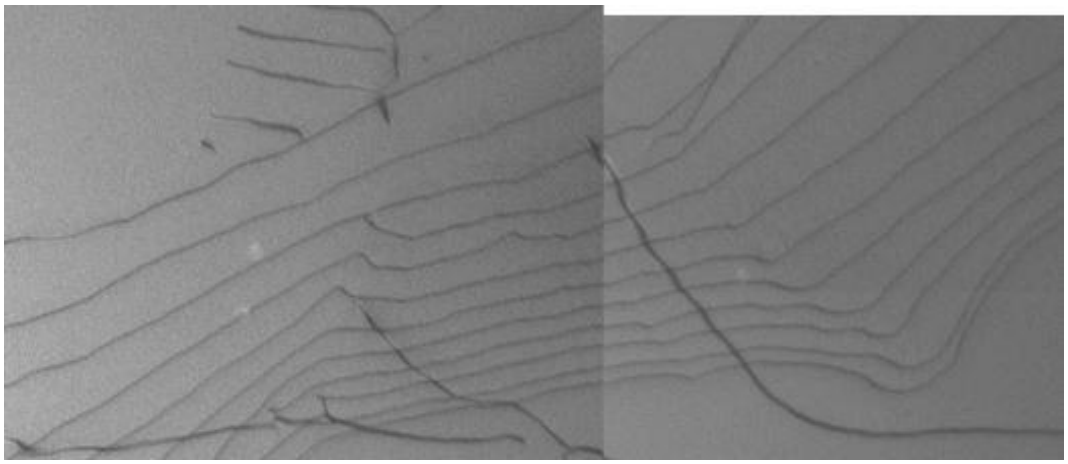

Figure 3.7(a) Bright-field image of the dislocation structure of single-crystal Fe-Co-Ni shows a planar dislocation array in the easy glide region.

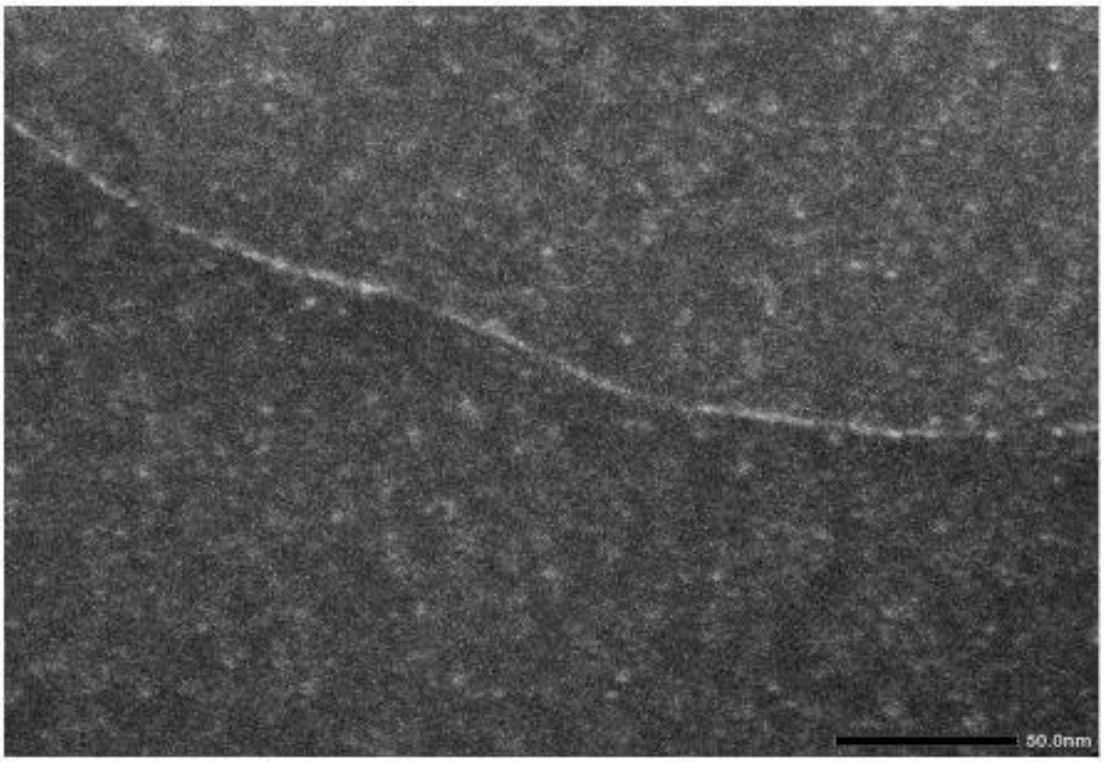

Figure 3.7(b) Weak beam image of partial dislocation of single-crystal Fe-Co-Ni.

3.3.5. Tensile deformation behavior

Stress-Strain curves of $[\bar{1}23]$ oriented Fe-Co-Ni single crystal deformed at RT and 77K are shown in Figure 3.8. These specimens were deformed at an engineering strain rate of 1×10^{-4}/s until fracture occurred. Stage 1 (easy glide, low work hardening) extends to about 20% plastic strain at room temperature, followed by stage 2 work hardening (high work hardening) until necking occurs at the ultimate tensile strength around 215 MPa. The hardening rate in stage 2 is about G/137 when normalized by shear modulus (G), which is less than single-crystal Cr-Mn-Fe-Co-Ni[5] and Cr-Fe-Co-Ni H/MEAs but in good agreement with FCC alloys with higher stacking fault energy[6]. For example, Cu-Al alloys with coarse grains show a low strain hardening rate and have high stacking fault energy[6]. On the other hand, Cu-Al alloys with fine grains show a relatively higher strain hardening rate and show the onset of twinning because of this alloy's low stacking fault energy[6]. During stage 1, slip markings corresponding to the (111)[110] primary slip system gradually fill the entire gage length. During stage 2, in addition to the primary slip system, the cross slip is observed. The CRSS in tension at room temperature is 46MPa, consistent with the CRSS obtained in compression deformation. This tension-compression symmetry in Fe-Co-Ni MEA suggests that its dislocation structure and response to applied stress is "normal" for the FCC metals, and this is also found true in Cantor alloy and 4-elements Cr-Fe-Co-Ni MEA. SEM- EBSD on the deformed specimen after facture shows no sign of twinning deformation at RT, as shown in Fig 3.11. At 77K, the CRSS increases significantly to 87 MPa from 44 MPa at RT while exhibiting no compression-tension asymmetry. Stage I (easy glide, low

work-hardening rate) extends up to 8%, followed by stage II (high work-hardening rate). The work hardening rate at 77 K in stage II (G /120) is similar to that at room temperature (G /137), as shown in Figures 3.9 and 3.10. Work hardening behavior curves were generated using true stress and true strain curves.

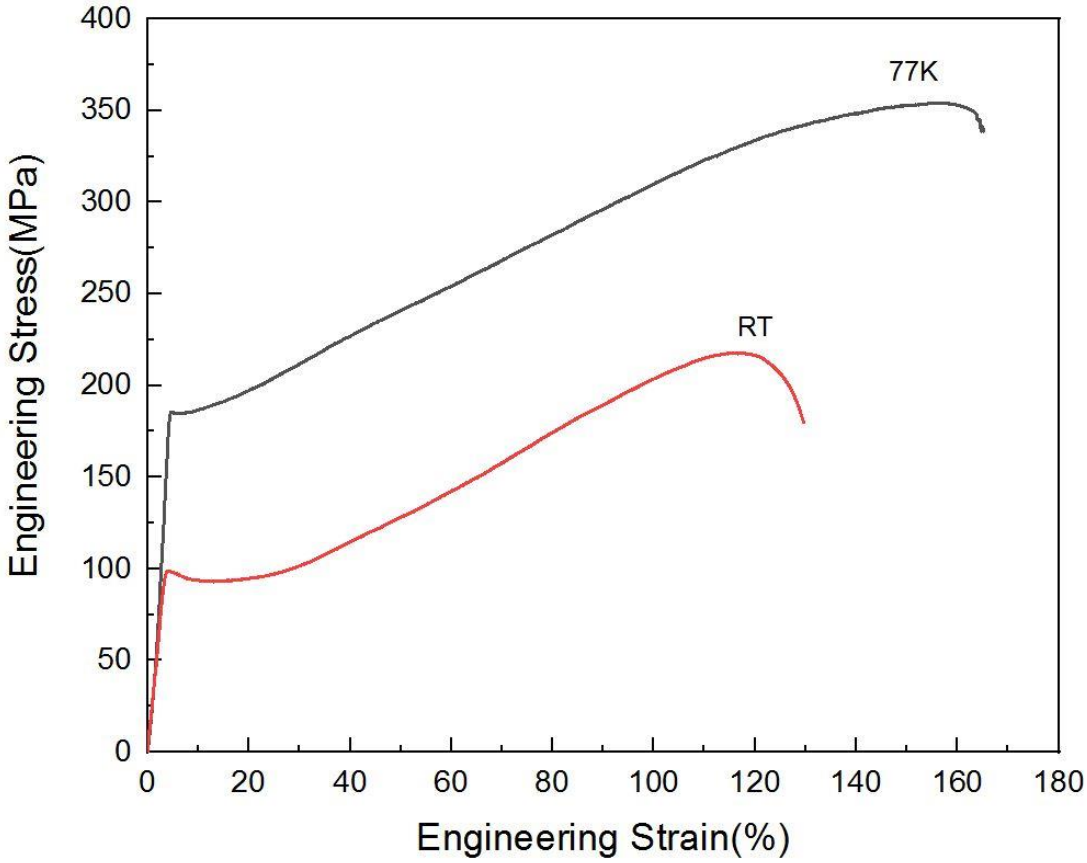

Figure 3.8 Stress-strain curves obtained for [$\bar{1}23$]-oriented single crystals of the Fe-Co-Ni deformed in tension to failure at 77 K and RT.

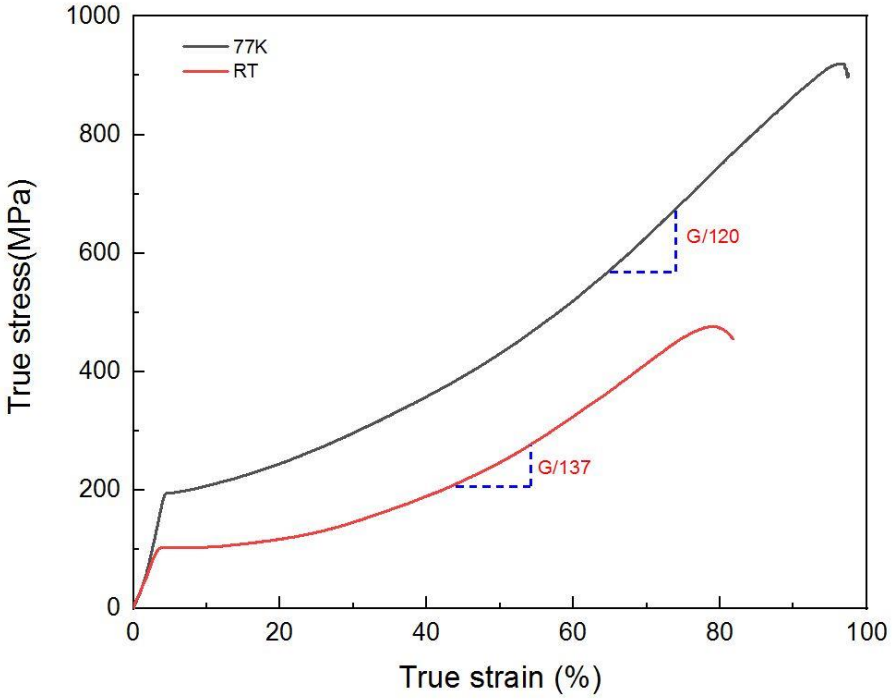

Figure 3.9 True S-S curve of single-crystal Fe-Co-Ni deformed at 77K and RT

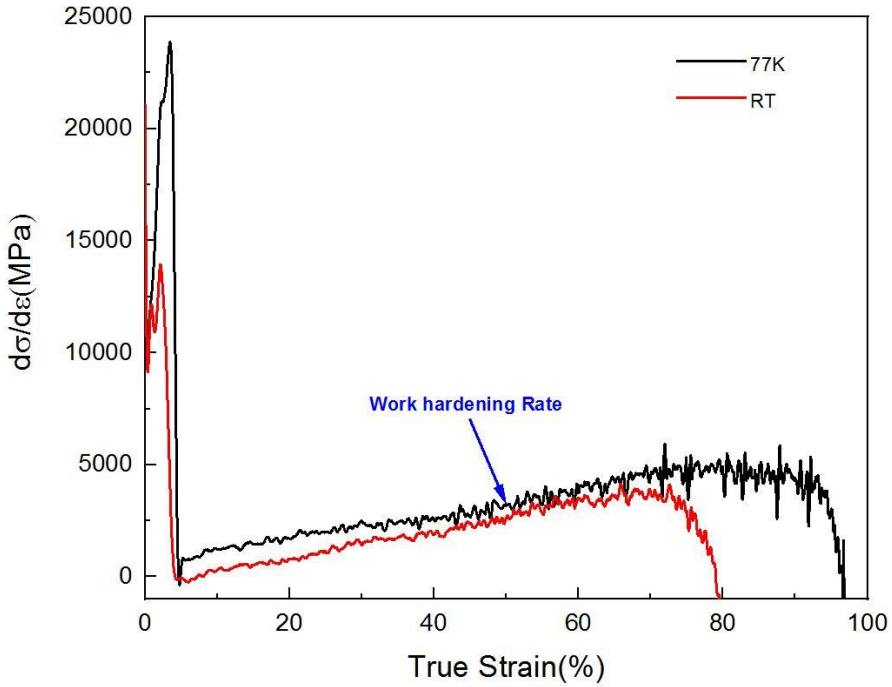

Figure 3.10 Work hardening rate(WHR) of single crystal Fe-Co-Ni at 77K and RT

It is well-known that materials with high stacking fault energy deformed by cross-slip mechanism after easy glide region, and that's why we could observe a planar array of dislocation after 3% of dislocation in bright field image (Fig.3.7(a)). In that case, the strain hardening rate is monotonously decreased with increasing the strain, as shown in Figure 3.10.

In Fe-Co-Ni single-crystal MEA, we couldn't find any evidence of twinning deformation both at RT and 77K. EBSD map of deformed specimens in Figure 3.11 shows the only matrix without having any band of twinning. Stacking fault energy, which is relatively higher for this Fe-Co-Ni, is responsible for the absence of twinning in this alloy.

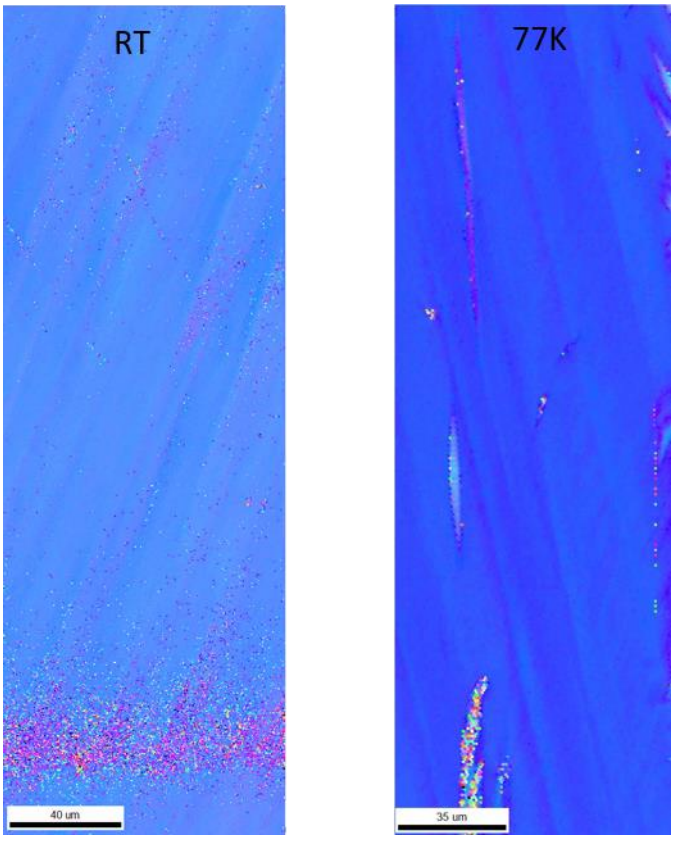

Figure 3.11 EBSD of single-crystal Fe-Co-Ni fractured surface after tensile deformation at RT and 77K

In the case of Fe-Co-Ni, as we couldn't observe any twinning phenomena, we investigated the fractured specimen after tensile deformation to reveal the deformation mechanism. It is already observed that low work hardening rate and high stacking fault energy are responsible for the absence of twinning suggest that cross slip is a major deformation mechanism in stage 2 deformation. We could observe fractured surfaces by optical microscopy to see the microstructure, and we found the occurrence of cross slip at RT deformed specimen. As cross slip is a thermally activated process, we couldn't see cross slip at 77K as intense as in RT. Figure 3.12 (a) and (b) shows optical images of slip marking after deformation. Figure 3.13 shows fracture surfaces of room temperature and 77K tensile deformation samples. A top view shows a dimple-like character at 77K deformed specimen suggesting ductile failure, which is often observed in typical FCC alloys[7] but the top surface of room temperature does not show prominent dimples indicating brittle fracture.

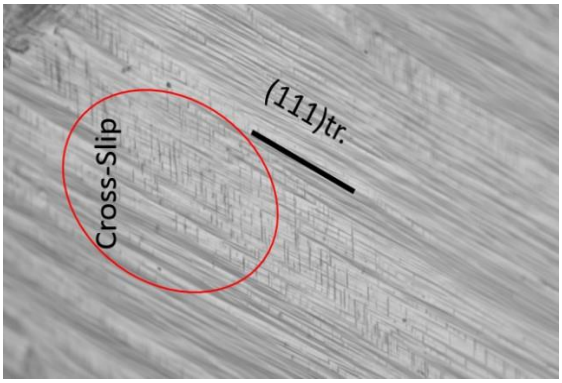

Figure3.12(a) Optical micrograph of Cross-slip markings of Fe-Co-Ni deformed at RT

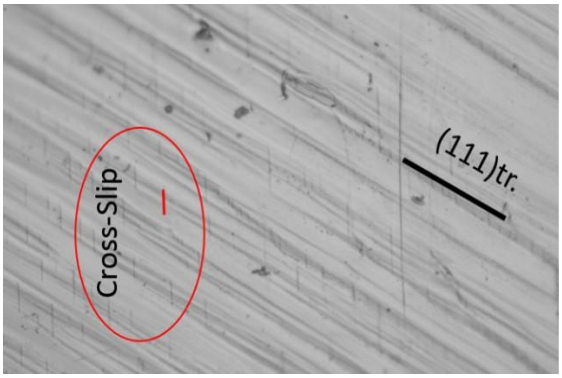

Figure3.12(b) Optical micrograph of Cross-slip markings of Fe-Co-Ni deformed at 77K

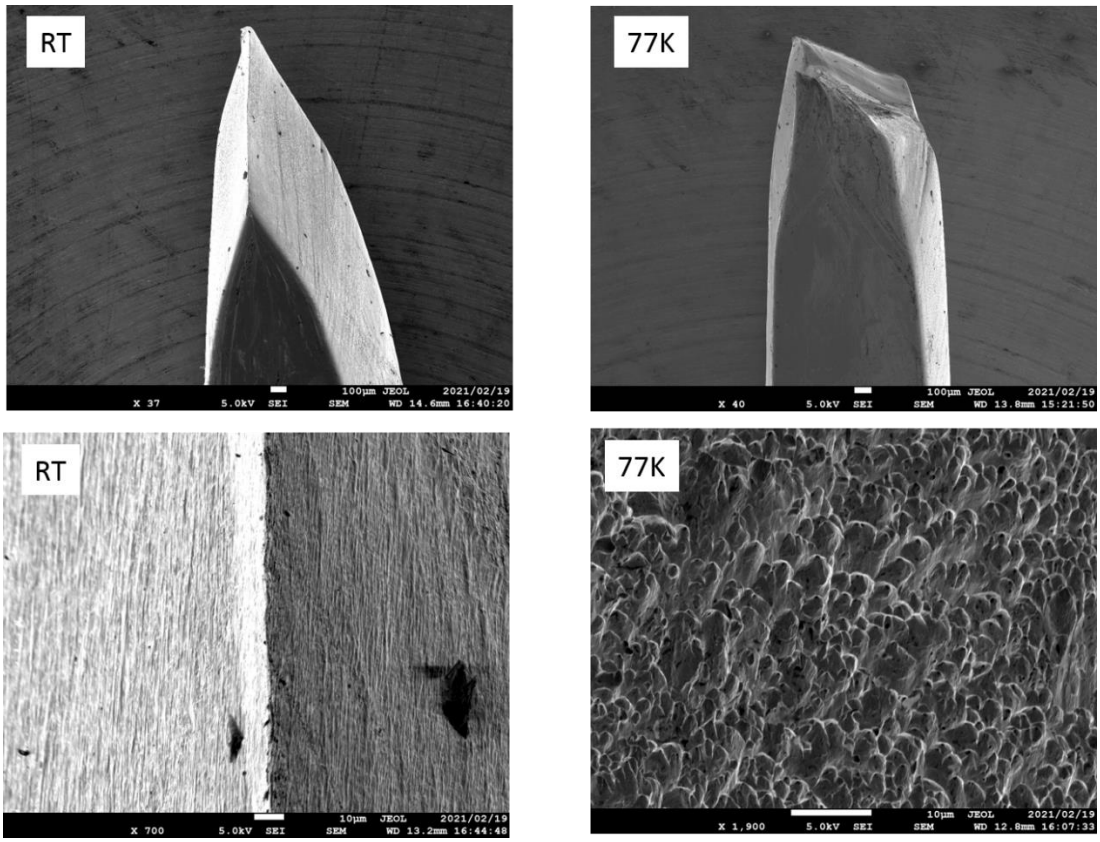

Figure 3.13 Side and top view of fracture surfaces in [$\bar{1}23$] oriented single crystals of the Fe-Co-Ni deformed in tension at RT and 77K.

3.4. Discussions

3.4.1. Mechanical Properties

The CRSS for {111} < 110 > slip in the present single crystals of the quaternary, equiatomic, Fe −Co −Ni MEA is in the range of 44- 47 MPa at room temperature, At 77K, the CRSS value is 90-95 Mpa. Below room temperature strength of this alloy increases, and strong temperature dependence occurs down to 0K consistent with Cr-Mn-Fe-Co-Ni[5] and Cr-Fe-Co-Ni single crystal alloys. Around 50K, dullness in the dependence of CRSS is noticeable, implying an inertia effect found for many other FCC solid solution alloys[4,8–10] By extrapolating the CRSS to 0K, the CRSS value determined at 0K is 130MPa, which is less than our study on Cr-Mn-Fe-Co-Ni single crystal alloy 168MPa at 0K.[5] As in many conventional FCC alloys, a slight increase in yield stress is noted in the high-temperature region of the CRSS (yield stress) vs temperature curve. This is believed to be due to the PL effect as in other FCC alloys. All these mechanical properties of the Fe −Co −Ni MEA have also been observed in many other conventional FCC alloys, indicating that the present MEA is not a peculiar alloy but is simply a typical FCC solid-solution alloy with exceptionally high strength. The high strength of the present MEA could originate from the large extent of lattice distortion, as proposed in [11], where the mean-square atomic displacement (MSAD) was used to quantify the extent of lattice distortion and directly correlated with the 0 K CRSS.

Solid solution strengthening is considered as the main strengthening mechanism in FCC single crystal Cr-Fe-Co-Ni alloy and cantor alloy. Fe-Co-Ni MEA is no different with them.

In connection with that, the concept of 'stress equivalence' proposed for FCC solid-solution alloys a long time ago by Basinski[12] holds true in the present ternary MEA single crystals. It states that (i) the yield strength at 77 K is proportional to the difference between the yield strength at 77 K and that at room temperature for all FCC solid-solutions (Fig. 3.14 (a)), and figure 3.15 values of the activation volume measured at a given temperature all lie on a single master curve is plotted as a function of yield stress (Fig. 3.14 (a)) irrespective of their concentration. The present MEA and cantor alloy data at room temperature and 77 K are included in Fig 3.14. As can be seen, the present MEA and cantor alloy fall on the extrapolated lines drawn through the data points of other conventional FCC alloys; however, the absolute values of stress and activation volume (Fig. 3.15) are much higher and lower, respectively, for the HEA than for conventional FCC alloys. This is clear evidence that the present MEA is not a peculiar alloy but is a standard solid-solution alloy, except for its very high strength at cryogenic temperature. This indicated that the thermal activation process for dislocation glide does not vary from one alloy to other regardless of the concentration and a single mechanism is responsible for the thermal activation process. To confirm this hypothesis in our MEA, we investigated the activation enthalpy for deformation by using the strain rate jump test. Activation Enthalpy can be calculated from the following equation:

$$\dot{\gamma} = Cexp[-U(\tau)/kT] \qquad 3.4(a)$$

Where $\dot{\gamma}$, k and T are shear strain rate, Boltzmann's constant and temperature, respectively. C is a constant and of the order of 10^8 /s. Also, without considering the constant C, we estimated the Activation Enthalpy by deriving the equation from the above equation,

$$U(\tau) = -k[\frac{\partial ln\dot{\gamma}}{\partial\left(\frac{1}{T}\right)}]$$

$$\approx -k\,[ln\dot{\gamma}(\tau, T_2) - ln\dot{\gamma}(\tau, T_1)]/(\frac{1}{T_2} - \frac{1}{T_1}) \quad 3.4(b)$$

Figure 3.15 shows the plot between activation enthalpy and shear stress by using the above two equations. The Activation Enthalpy calculated for this alloy is .65 eV at room temperature, consistent with the values of many other FCC solid solution alloys[13–15]

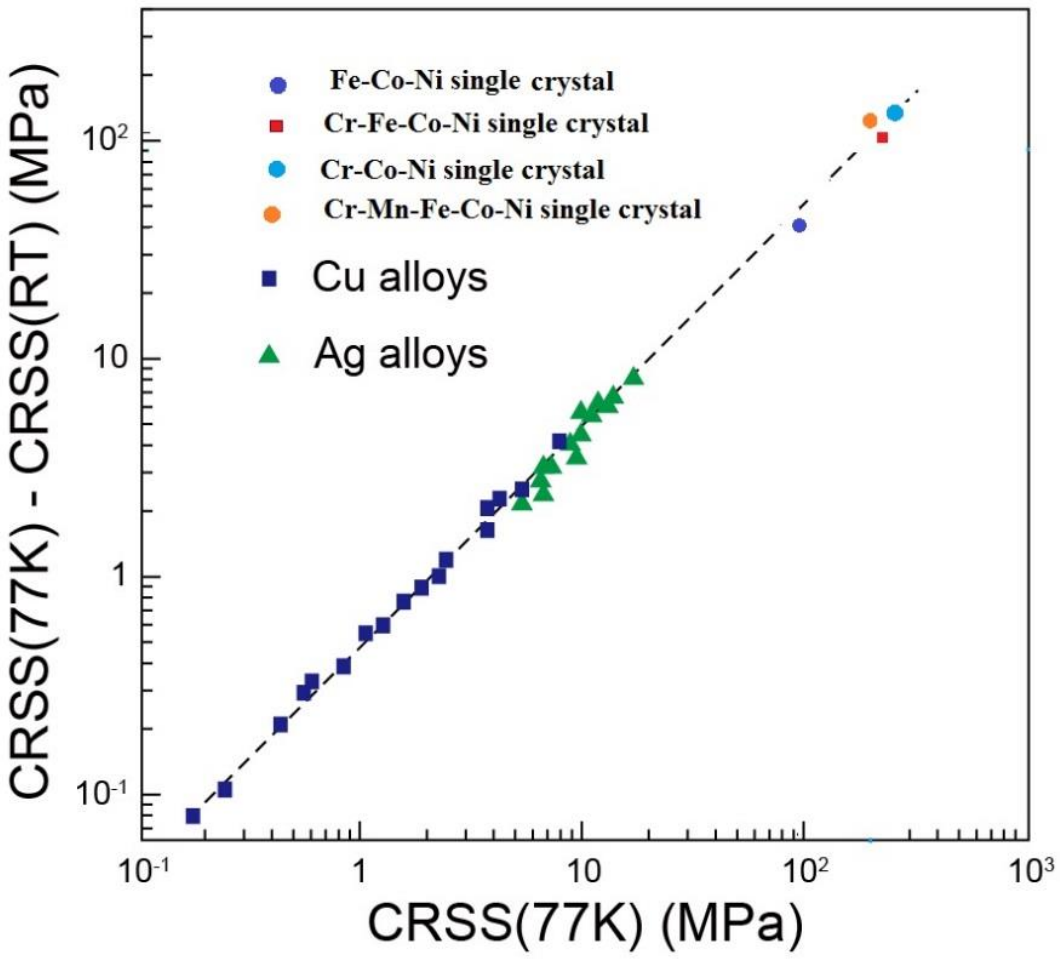

Figure 3.14. The difference between the yield strength at 77 K and that at room temperature plotted as a function of the yield strength at 77 K for FCC solid solutions.

Activation volume at RT and 77K is found to be 256.46 b^3 and 77.79 $b^{3,}$ respectively. Which is consistent with Cr-Mn-Fe-Co-Ni alloy. Laplanche et al.[16] reported that the activation volume for deformation obtained by strain-rate jump tests decreases with strain at room temperature because forest dislocations are introduced during plastic straining in Cantor alloy. This decrease in activation volume can be minimized if the test is made in the strain range of easy glide as shown in the present study using single crystals (which is not possible with polycrystals as they lack a region of easy glide since hardening starts almost immediately after yielding). Kawamura et al.[5] estimated lower values of activation volume by using a single crystal. On the other hand, Hong et al.[17] reported that activation volume for deformation increases with strain at room temperature because the short-range ordering of constituent atoms that existed prior to deformation is gradually destroyed by the passage of dislocations (they did not mention the countervailing effect of forest dislocations, which would tend to decrease the activation volume). The relatively strain-independent activation volume measured in the present study (in the easy-glide region) implies either no significant short-range ordering in the alloy or that the flow stress is not significantly affected by short-range ordering, though a detailed investigation is still required for the presence of SRO.

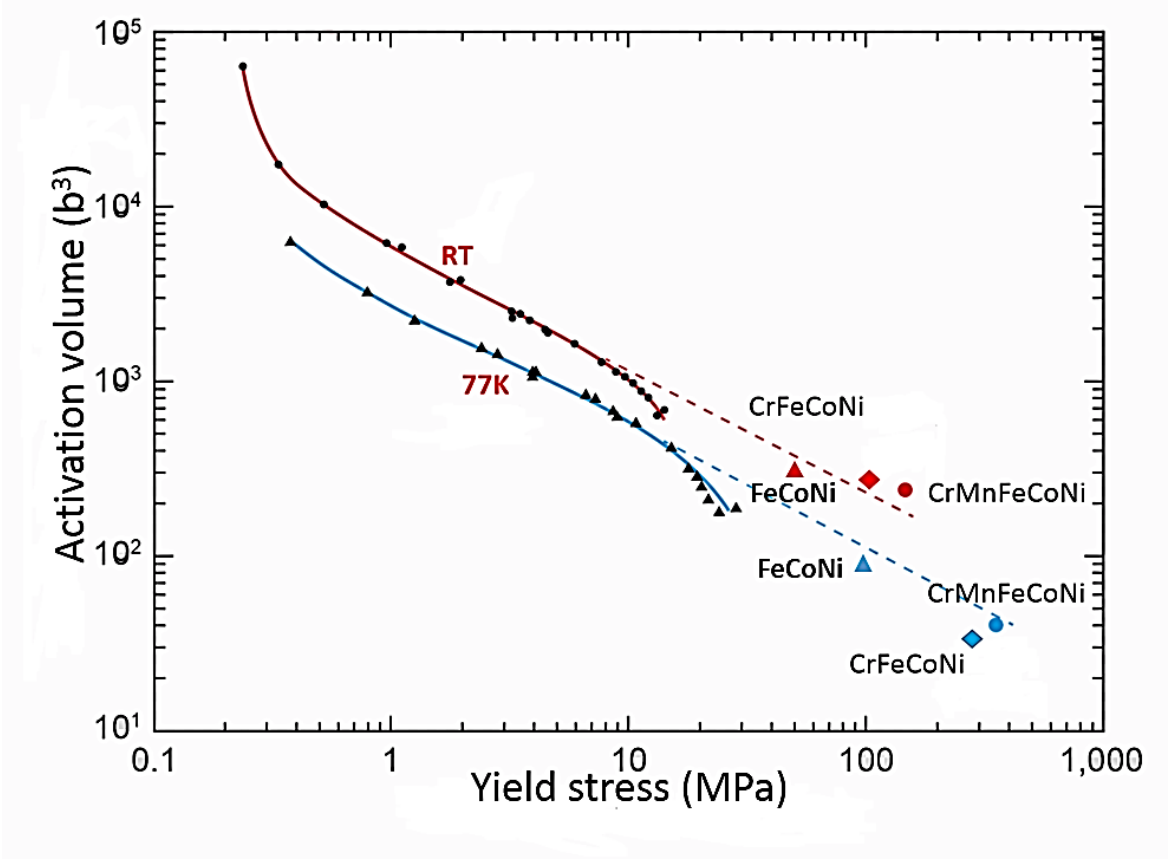

Figure 3.15. Activation volumes at room temperature and 77 K for FCC solid solutions plotted as a function of their yield strengths along with Fe-Co-Ni, Cr-Fe-Co-Ni and Cr-Mn-Fe-Co-Ni.

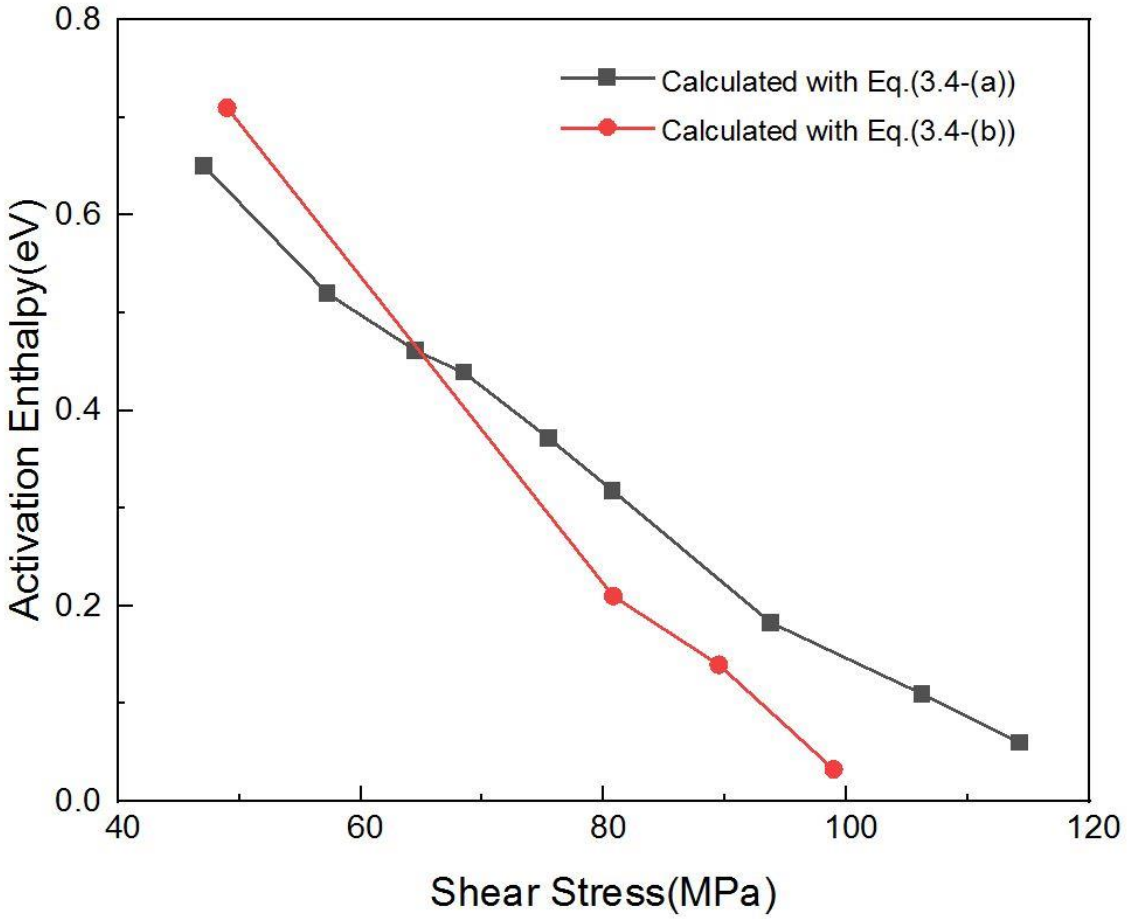

Figure 3.16. Activation Enthalpy of single-crystal Fe-Co-Ni MEA as a function of shear stress.

3.4.2. Dislocation behavior

Dislocations with the Burgers vector, $\boldsymbol{b}$ = 1/2 < 110 > are dissociated into coupled Shockley partials that are narrow enough to measure a relatively lower dissociation width, which indicates high stacking fault energy of this alloy. This leads to the absence of deformation twinning even at low temperatures. Recently, significant point-to-point variations in dislocation dissociation widths have been reported in the Cr −Mn −Fe −Co −Ni

HEA and ascribed to dislocation interactions with solute atoms causing local fluctuations in the stacking fault energy[18]. A slight increase in yield stress is noted in the high-temperature region of the CRSS (yield stress) vs temperature curve of the Fe −Co −Ni MEA, as in many other conventional FCC alloys[2] .In conventional FCC alloys, this is usually explained in terms of the PLC effect, in which solute atoms that have segregated to the stacking fault between coupled partial dislocations (if such segregation is energetically favourable through the Suzuki effect) move along with the dislocations provided the temperature is high enough to allow atomic diffusion to occur at speed comparable to that of the dislocations[19].

3.4.3. Tensile deformation and strain hardening

Fe-Co-Ni single-crystal MEA shows no trace of twinning after failure at tensile deformation. The Stress-Strain curve of tensile deformation indicates a low strain hardening rate of G/137 and G/120 at room temperature and 77K. The low work hardening rate and high stacking fault energy of this alloy are responsible for the absence of twinning as the stress required for twinning nucleation could never reach, and the main deformation mechanism in stage 2 of tensile deformation is slip deformation rather than twinning. It is well reported for FCC alloys with high stacking fault energy materials and a low strain hardening rate[20,21]. Figures 3.12 (a) and (b) show optical images of Fe-Co-Ni slip markings after fracture, which offers evidence of cross-slip mechanism as the main deformation mechanism in Fe-Co-Ni single-crystal MEA. The process of cross-slip involves the formation of constrictions in the dislocation ribbons, and therefore depends on the stacking-fault energy of the metal[20].

As cross slip is a thermally activated process, cross slip is more favourable at room temperature. Figure 3.16 shows that at 77K, cross-slip markings are less intense as compared to room temperature. The most prominent mechanism for cross-slip in FCC is the Friedel-Escaig (F-E) mechanism[22]. The F-E mechanism assumes that the initial dislocation, dissociated into Shockley partial dislocations on an initial glide plane, shown in Figures 3.7 (a) and (b), must constrict locally to form a Stroh constriction from which the dislocation can cross-slip and begin dissociating on another glide plane.

3.5. Conclusions

Plastic Deformation behavior of an equiatomic single-crystal Fe-Co-Ni MEA was systematically studied at temperatures ranging from 12.4K to 1373K and different strain rates from 10^{-5} s^{-1} to $5x10^{-3}$ s^{-1} in compression and tension. Based on the mechanical properties, the following conclusions were drawn in this chapter:

1. The CRSS for {111} < 110 > slip increases with decreasing temperature, with showing inertia effects at cryogenic temperatures (below 50 K). From an extrapolation to lower temperatures, the CRSS at 0 K is estimated to be 130 MPa. The concept of 'stress equivalence' originally proposed for conventional FCC solid-solution alloys holds true for the Fe −Co −Ni MEA, although the stress levels are much higher than those of conventional FCC alloys. The ternary equiatomic Fe −Co −Ni MEA exhibits a higher strain-rate sensitivity of flow stress than binary FCC alloys such as Cu −Al, Cu-5Al consistent with its stronger temperature dependence CRSS than the binary alloys. Together, these observations indicate that solid-solution hardening is the major strengthening mechanism.
2. Dislocations with b = 1/2 < 110 > dissociate into two Shockley partials with b = 1/6 < 112 > bounding a stacking fault. Separation width of partials are narrow and measurement of width is beyond the limit of weak beam technique.
3. Second stage work hardening rate of single crystal Fe-Co-Ni MEA is low in compare to Cr-Fe-Co-Ni and cantor alloy but well within the range of FCC alloys with high stacking fault energy.

4. Twinning was not observed in single crystal Fe-Co-Ni MEA at room temperature and 77K, reason being the high stacking fault energy of this alloy.

References

[1] Z. Wu, H. Bei, G.M. Pharr, E.P. George, Temperature dependence of the mechanical properties of equiatomic solid solution alloys with face-centered cubic crystal structures, Acta Mater. 81 (2014) 428–441. https://doi.org/10.1016/j.actamat.2014.08.026.

[2] P. Jax, P. Kratochvils, P. Haasent, SOLID SOLUTION HARDENING OF GOLD AND OTHER F.C.C. SINGLE CRYSTALS*, n.d.

[3] Z.S. Basinski, Thermally activated glide in face-centred cubic metals and its application to the theory of strain hardening, Philos. Mag. 4 (1959) 393–432. https://doi.org/10.1080/14786435908233412.

[4] T.H. Wille, C. Schwink, Precision measurements of critical resolved shear stress in CuMn alloys, Acta Metall. 34 (1986) 1059–1069. https://doi.org/10.1016/0001-6160(86)90216-6.

[5] M. Kawamura, M. Asakura, N.L. Okamoto, K. Kishida, H. Inui, E.P. George, Plastic deformation of single crystals of the equiatomic Cr−Mn−Fe−Co−Ni high-entropy alloy in tension and compression from 10 K to 1273 K, Acta Mater. 203 (2021). https://doi.org/10.1016/j.actamat.2020.10.073.

[6] Y.Z. Tian, L.J. Zhao, S. Chen, A. Shibata, Z.F. Zhang, N. Tsuji, Significant contribution of stacking faults to the strain hardening behavior of Cu-15%Al alloy with different grain sizes, Sci. Rep. 5 (2015) 2–10. https://doi.org/10.1038/srep16707.

[7] W.S. Lee, T.H. Chen, C.F. Lin, Z.Y. Li, Effects of strain rate and temperature on shear

properties and fracture characteristics of 316L stainless steel, Mater. Trans. 53 (2012) 469–476. https://doi.org/10.2320/matertrans.M2011274.

[8] T.H. Wille, W. Gieseke, C.H. Schwink, Quantitative analysis of solution hardening in selected copper alloys, Acta Metall. 35 (1987) 2679–2693. https://doi.org/10.1016/0001-6160(87)90267-7.

[9] E.O. Hall, Yield Point Phenomena in Metals and Alloys, Springer US, 1970. https://doi.org/10.1007/978-1-4684-1860-6.

[10] M. 2 Butt, P. Feltham, SOLID-SOLUTION HARDENING, n.d.

[11] N.L. Okamoto, K. Yuge, K. Tanaka, H. Inui, E.P. George, Atomic displacement in the CrMnFeCoNi high-entropy alloy - A scaling factor to predict solid solution strengthening, AIP Adv. 6 (2016). https://doi.org/10.1063/1.4971371.

[12] Z.S. Basinski, R.A. Foxall, R. Pascual, Stress equivalence of solution hardening, Scr. Metall. 6 (1972) 807–814. https://doi.org/10.1016/0036-9748(72)90052-X.

[13] W.A. Curtin, New interpretation of the Haasen plot for solute-strengthened alloys, Scr. Mater. 63 (2010) 917–920. https://doi.org/10.1016/j.scriptamat.2010.07.003.

[14] H. Conrad, THERMALLY ACTIVATED DEFORMATION OF METALS, n.d.

[15] M.Z. Butt, P. Feltham, Review Solid-solution hardening, 1993.

[16] G. Laplanche, J. Bonneville, C. Varvenne, W.A. Curtin, E.P. George, Thermal activation parameters of plastic flow reveal deformation mechanisms in the CrMnFeCoNi high-entropy alloy, Acta Mater. 143 (2018) 257–264. https://doi.org/10.1016/j.actamat.2017.10.014.

[17] J. Moon, S.I. Hong, J.W. Bae, M.J. Jang, D. Yim, H.S. Kim, On the strain rate-

dependent deformation mechanism of CoCrFeMnNi high-entropy alloy at liquid nitrogen temperature, Mater. Res. Lett. 5 (2017) 472–477. https://doi.org/10.1080/21663831.2017.1323807.

[18] T.M. Smith, M.S. Hooshmand, B.D. Esser, F. Otto, D.W. Mccomb, E.P. George, M. Ghazisaeidi, M.J. Mills, Atomic-scale characterization and modeling of 60°dislocations in a high-entropy alloy, Acta Mater. 110 (2016) 352–363. https://doi.org/10.1016/j.actamat.2016.03.045.

[19] N.R. Dudova, R.O. Kaibyshev, V.A. Valitov, Short-range ordering and the abnormal mechanical properties of a Ni-20% Cr alloy, Phys. Met. Metallogr. 108 (2009) 625–633. https://doi.org/10.1134/S0031918X0912014X.

[20] P.R. Thornton, T.E. Mitchell, P.B. Hirsch, The dependence of cross-slip on stacking-fault energy in face-centred cubic metals and alloys, Philos. Mag. 7 (1962) 1349–1369. https://doi.org/10.1080/14786436208213168.

[21] V. Shterner, I.B. Timokhina, H. Beladi, The correlation between stacking fault energy and the work hardening behaviour of high-mn twinning induced plasticity steel tested at various temperatures, Adv. Mater. Res. 922 (2014) 676–681. https://doi.org/10.4028/www.scientific.net/AMR.922.676.

[22] W.G. Nöhring, W.A. Curtin, Dislocation cross-slip in fcc solid solution alloys, Acta Mater. 128 (2017) 135–148. https://doi.org/10.1016/j.actamat.2017.02.027.

Chapter 4

Mean Square Atomic Displacement: A scaling factor to predict Solid Solution Strengthening in HEAs/MEAs and determine the fitting parameters of the equation used to determine 0K CRSS.

4.1. Introduction

Solid solution strengthening (SSS) is one of the strengthening mechanisms in which alloying elements strengthen metals. Solute atoms dissolved in a solvent matrix offer resistance to dislocations' motion, thereby making the material stronger. Many different models are given to understand the SSS in the materials. SSS mechanisms are usually defined in terms of randomly dispersed substitutional solute atoms interacting with dislocations through misfits in the atomic size and elastic modulus of solute and solvent atoms[1,2]. Theoretical Models that treat stationary solute atoms acting on moving dislocations are of a frictional type and can be divided into two groups based on solute spacing, range of interaction and solute-dislocation interaction energy. In very dilute alloys, solute atoms adjacent to glide planes are assumed to come in contact with dislocation at full interaction force and termed as strong pinning described by Fleischer-Friedal Model.[3,4] On the other hand, in concentrated alloys(several at. % of solute), a range of interaction force is assumed to account for spatial fluctuation of solute density, Where maximum value is the same order as the full interaction force and termed as weak pinning as described by the Mott-Labusch model.[5] The key parameters in these models are solute dislocation interaction energy.

Curtin et al.[6] have explained the solute concentration and temperature dependences of the critical resolved shear stress of certain dilute Al and Mg alloys using an analytical model of the weak-pinning type. The solute-dislocation interaction energy is calculated from the first principles. This approach cannot readily be applied to HEAs/MEAs because of the difficulties in estimating the solute- dislocation interaction energy; in an equiatomic HEA, "solute" and "solvent" atoms cannot be defined separately. In a quaternary MEA such as Cr-Mn-Fe-Co-Ni, the concentration of the constituent atoms is as high as 20 at.%. Alternative methods to SSS are needed to pronounce the strength of HEAs. Recently, Toda-Caraballo et al.[7] have anticipated an extension of a classical SSS model for the binary system to a multi-component system. They used alloy's unit cell parameters as key parameters and their variations with compositions. Curtin and co-workers[8] proposed a parameter-free and predictive SSS theory by approximating the multi-component matrix as an effective medium having the average properties of the alloy and then calculated the solute-dislocation interaction energy from first principles for a multitude of configurations.

An alternative approach is to consider the displacement of the atoms in a solid solution from their ideal lattice positions. Solute dislocation interaction energy calculations have an assumption that solvent atoms around solute atoms are displaced from their ideal lattice positions because of atomic size misfit, as shown in Figure 4.1(a). Accordingly, averaged atomic displacement over the entire crystal is expected to increase with high solute concentration. (Figure 4.1(b)). Therefore, it is essential to understand the relationship between the average atomic displacement and the strength of solid solution alloys. In the case of HEAs, it is expected that all atoms are displaced from their ideal lattice position since

multiple principal elements with different sizes interact with each other, unlike dilute alloys where only those in close vicinity of the solute atoms are displaced.

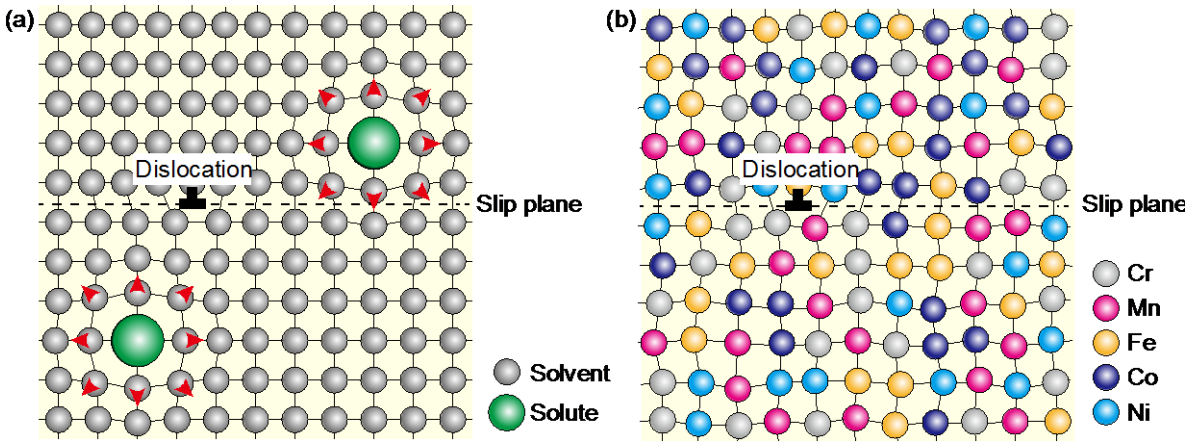

Figure 4.1. Schematic illustrations of atomic arrangements in (a) dilute solid solutions and (b) HEAs.[1]

This chapter aims to investigate the average atomic displacement in the equiatomic Cr-Mn-Fe-Co-Ni with other derivatives of cantor alloys using first-principle calculations to determine an alternative scaling factor to predict solid solution strengthening and to choose the fitting parameters of the equation used to determine 0K CRSS.

4.2. Experimental procedures

4.2.1. First-principles calculations

All calculations for the derivation of MSAD were performed based on the density functional theory (DFT) formulated within the generalized gradient approximation (GGA) by Perdew, Burke, and Ernzerhof (PBE).18) The Kohn-Sham equations were solved with the Vienna Ab initio simulation package (VASP) code.19-21) We used the special quasirandom structure (SQS) package22,23) to model the atomic configurations with a 3 x 3 x 3 extension of the FCC unit cell for the ternary and quaternary alloys listed elsewhere[9].

The first and second nearest neighbours were taken into account for pair correlation functions. The plane wave energy cut off was set to 400 eV. The Methfessel-Plaxton technique with a smearing value of 0.1 eV and k point grids of 4 x 4 x 4 with Monkhorst-Pack scheme was used. The SQS structures were relaxed until the residual forces became less than 10^{-3} eV/Å with fixed global FCC symmetry. The calculations were iterated with independently relaxed cell volume and atomic positions and terminated when convergence was reached. MSAD was derived as $MSAD = \sum_i c_i \, MSAD_i$ using the MSAD of element i ($MSAD_i$) that can be obtained as an average of atomic displacements for i atoms from regular lattice points.

4.3. Results and Discussions

4.3.1. Correlation of MSAD and CRSS at 0K

Okamoto et al. [1] determined the magnitude of the atomic displacement parameter (ADP) obtained by X-ray diffraction at finite temperatures. ADP is a sum of the squares of the dynamic displacements of all constituent atoms from their mean (equilibrium) positions due to thermal vibration (dynamic disorder) and the static displacement of the mean positions from the ideal lattice points (static disorder) (Fig.4.2). Therefore, the ADP becomes increasingly dominated by the static component as the temperature is decreased down to cryogenic temperatures. The refined ADP values obtained in the present study diffraction experiment from which these ADP values were obtained at 25K and 300 K are 23.5±0.4 and 58.7±0.5 pm2.

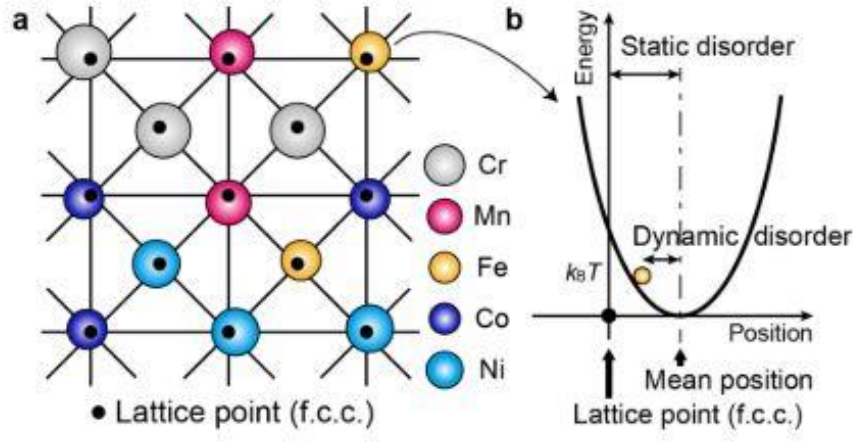

Figure 4.2. Static disorder in the CrMnFeCoNi HEA. (a) Schematic illustration of the FCC lattice of the CrMnFeCoNi HEA. (b) Schematic illustration of an energy-position curve for a harmonic oscillator in thermal equilibrium[1].

MSADs values estimated above correlate with the strengths of a family of complex, equiatomic, FCC alloys. For this, we utilize the results of single crystal experimental data in our group. We investigated the temperature dependence of the CRSS of the quinary Cr-Mn-Fe-Co-Ni HEA and some of its derivative FCC quaternary and ternary equiatomic alloys. The values of CRSS extrapolated to 0 K by fitting their temperature dependences with a fitting function $\tau_{crss} = \tau_{ath} + \tau_{th} \times \left[1 - \left(\frac{T}{T_{TA}}\right)^{\frac{1}{q}}\right]^{\frac{1}{p}}$. It is interesting to evaluate how the CRSS of these alloys at 0 K correlates with their MSAD values averaged over the constituent elements. For this purpose, first-principles total-energy calculations were made to deduce MSAD values for four different FCC equiatomic alloys (Cr-Mn-F-eCo-Ni, Cr-Co-Ni, Cr-Fe-Co-Ni and Fe-Co-Ni). are tabulated in Table.

Our group published the results[1] related to the correlation of MSAD and strength by utilizing results of Wu et al. [10]. As seen in Fig. 4.3, when normalized by shear modulus, the CRSS at 0 K for these equiatomic ternary, quaternary and quinary alloys scale linearly with the square root of the average MSAD values and can be described by the following equation:

$$\tau_{CRSS}/\mu = k \cdot MSAD^{1/2} \text{ (k = constant)}$$

Figure 4.3 suggests that MSAD can be a scaling parameter to predict the strength at 0K of these solid solution alloys. This was done with polycrystalline 0K CRSS data derived from Wu et al. [10] temperature dependence plot. We did different compression tests for different possible FCC HEAs/MEAs using equiatomic single-crystal bulk samples and evaluated

CRSS at 0K by extrapolation using the equation mentioned above. Single crystal data were not consistent with Okamoto et al. [1], and it is presented in Figure 4.5 below.

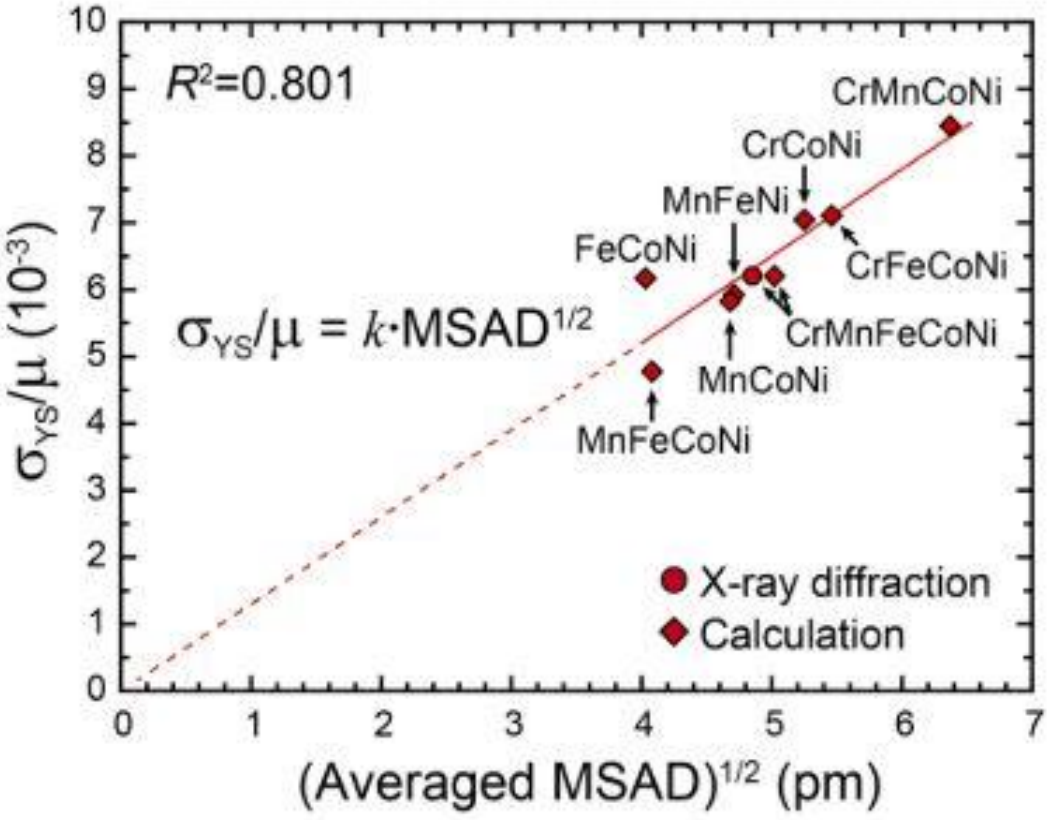

Figure 4.3. Yield strengths of the quinary CrMnFeCoNi HEA and its derivative quaternary and ternary equiatomic alloys extrapolated to 0 K and normalized by shear modulus plotted against the square root of the MSAD value averaged over the constituent[1].

Some more calculations were done for a single crystal for a possible combination of Cantor alloys by using first-principle calculations to determine the MSAD values. Calculated values of MSAD and CRSS at 0K for different single-crystal equiatomic HEAs/MEAs are summarized in the table below.

Alloys	CRSS at 0K	Shear Modulus (μ)	CRSS/μ	$MSAD^{0.5}$
CrMnFeCoNi	175	85.77	2.0403	5.8566
CrFeCoNi	215	88.23	2.4368	6.0745
CrCoNi	220	93.12	2.3625	6.7379
FeCoNi	130	67.59	1.9233	3.5637

Table 4.1

0K CRSS values were determined by extrapolating the temperature dependence of CRSS curves for given single crystal alloys considering the best possible fitting functions, which is described in section 4.3.2. Figure 4 shows a plot between MSAD of H/MEAs and CRSS (0K).

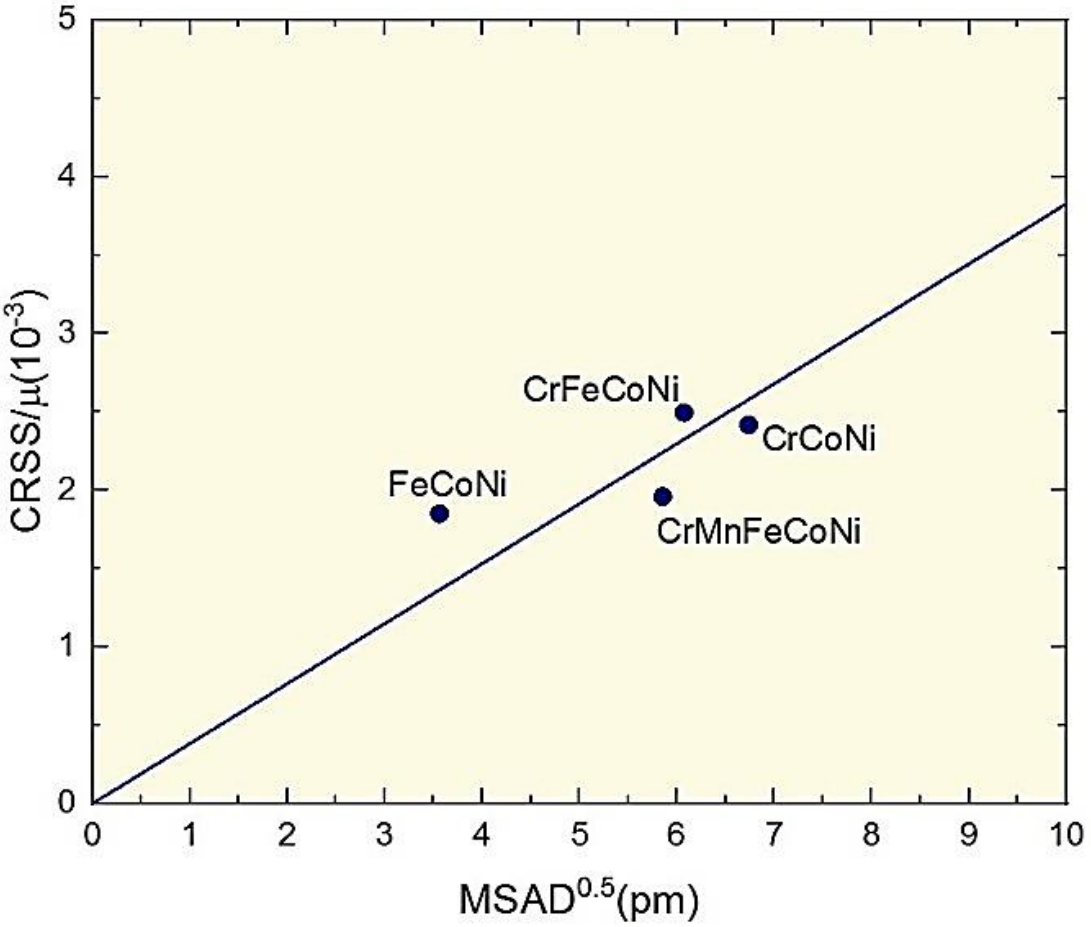

Figure 4.4. CRSS of the single crystal quinary Cr-Mn-Fe-Co-Ni HEA and its derivative quaternary and ternary equiatomic alloys extrapolated to 0 K and normalized by shear modulus plotted against the square root of the MSAD value averaged over the constituent

We need more data set of CRSS at 0K for other possible derivatives of FCC single crystal H/MEAs to determine the possible scaling factor of MSAD for strength. More calculations are needed to calculate the MSAD of derivatives of Cantor alloys, and then we can have a clear picture of this scaling factor.

4.3.2. Determination of fitting parameters

Temperature dependence of CRSS of FCC single crystal H/MEAs has been investigated in detail down to 0K temperature. In Chapter 2 and Chapter 3, it is described that there is a dullness of CRSS curve or say anomaly occurs near about 50K. This anomaly can be explained by the inertial model for dislocation motion[11–13]. Theoretically, this behaviour has been studied as a result of the decrease of thermal activation[14]. However, we found that the change in CRSS at low temperature is non monotonically in these equiatomic single-crystal FCC H/MEAs. We have used a fitting equation 4.1 to determine the 0K CRSS of these alloys using our experimental data at selected temperatures.

$$\tau_{crss} = \tau_{ath} + \tau_{th} \times \left[1 - \left(\frac{T}{T_{TA}}\right)^{\frac{1}{q}}\right]^{\frac{1}{p}} \quad (4.1)$$

Figure 4.5 shows the temperature dependence of CRSS on different derivatives of equiatomic FCC single crystal cantor alloy. 0K CRSS is determined by extrapolating the experimental data by using equation 4.1. Temperature dependence of CRSS shows a sharp increase in CRSS values at low temperature, and near 473K, an infection is observed in all the derivatives of cantor alloys. The exact reason for this infection is still under investigation, but it is plausible that vacancies are introduced during quenching of these single-crystal alloys after homogenization at 1473K.

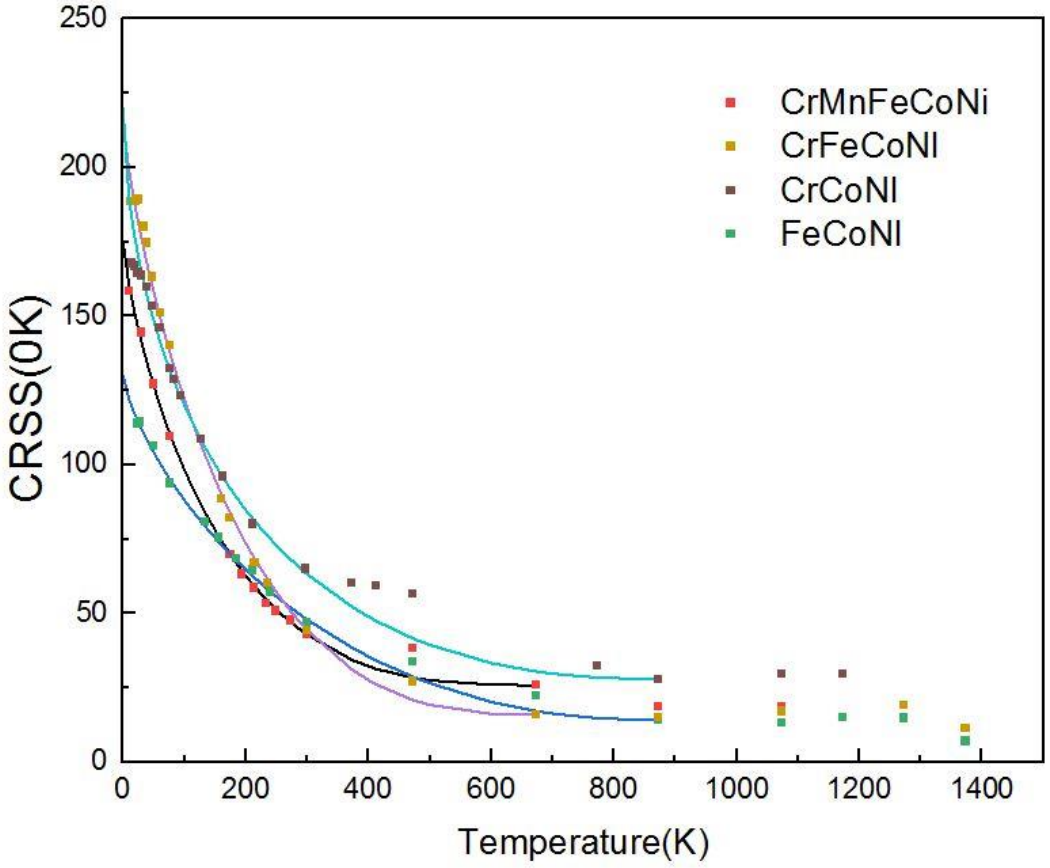

Figure 4.5. Temperature dependence of CRSS of equiatomic FCC single crystal Cantor alloy and its derivatives.

Table 4.2 shows transition temperatures and p and q values for each of the derivatives found while extrapolating the experimental data using equation 4.1.

Alloys	$\tau_{athermal}$	$\tau_{thermal}$	T_{TA}	CRSS(0K) MPa	p	q
CrMnFeCoNi	25.85	142.15	673	168	.34	1.25
CrFeCoNi	15.96	199.04	673	215	.37	1.21
CrCoNi	27.81	192.19	873	220	.45	1.73
FeCoNi	14	116	873	130	.47	1.31

Table 4.2

In equation 4.1, fitting parameters were $\boldsymbol{\tau_{crss}}$, T_{TA}, p and q. By disregarding the athermal stress component for the fit, we calculated the fitting functions and confirmed the values by plotting the data τ/τ_{crss} vs T/T_0. Figure 4.6 (a-d) shows the plot assuring the best fit for the determination of CRSS at 0K. We have found that the range of p and q values of these High and medium entropy alloys are in good agreement with the values reported by Kocks et al. [14] for their typical obstacles that are $0 < p < 1$ and $1 < q < 2$.

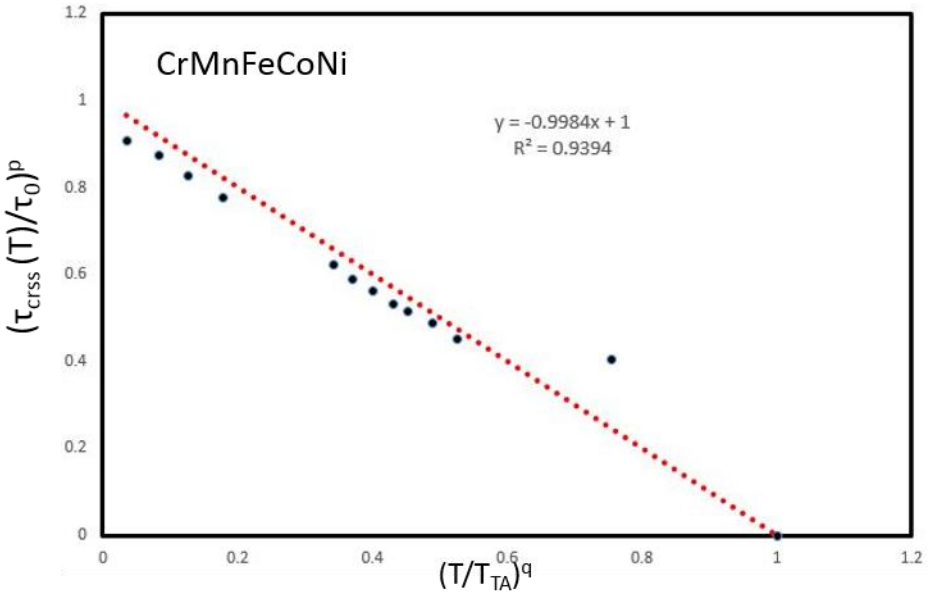

Figure 4.6 (a). Reduced effective stress vs reduced temperature according to equation 4.1

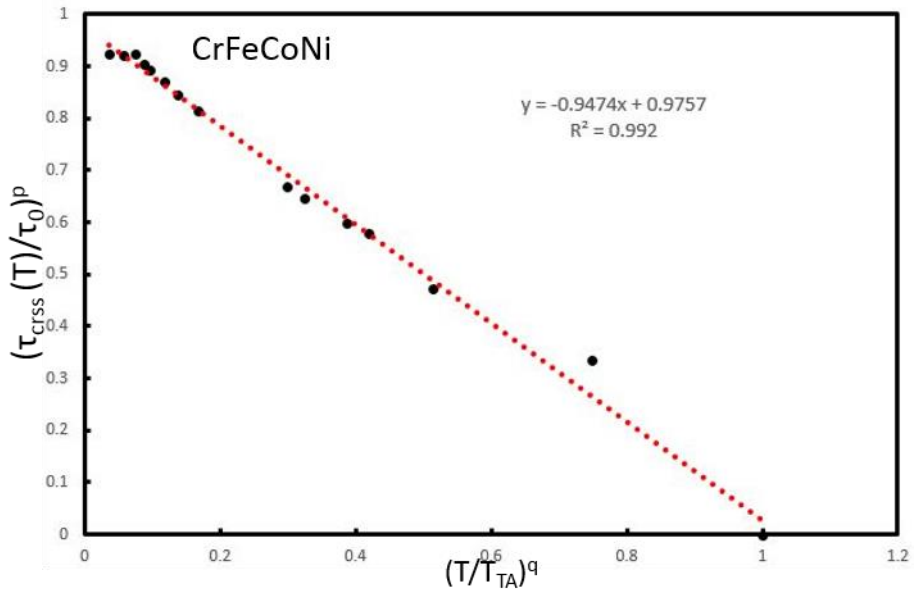

Figure 4.6 (b). Reduced effective stress vs reduced temperature according to equation 4.1

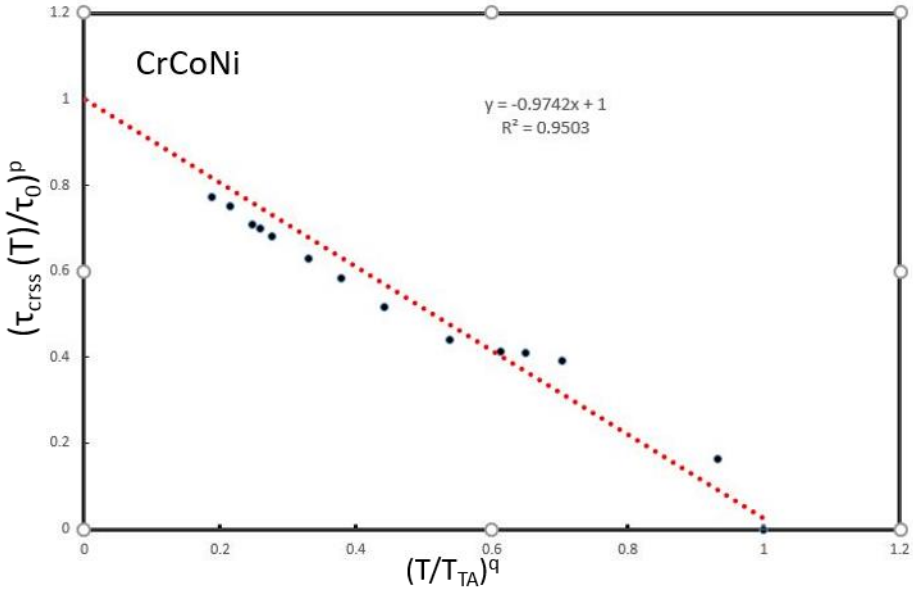

Figure 4.6 (c). Reduced effective stress vs reduced temperature according to equation 4.1

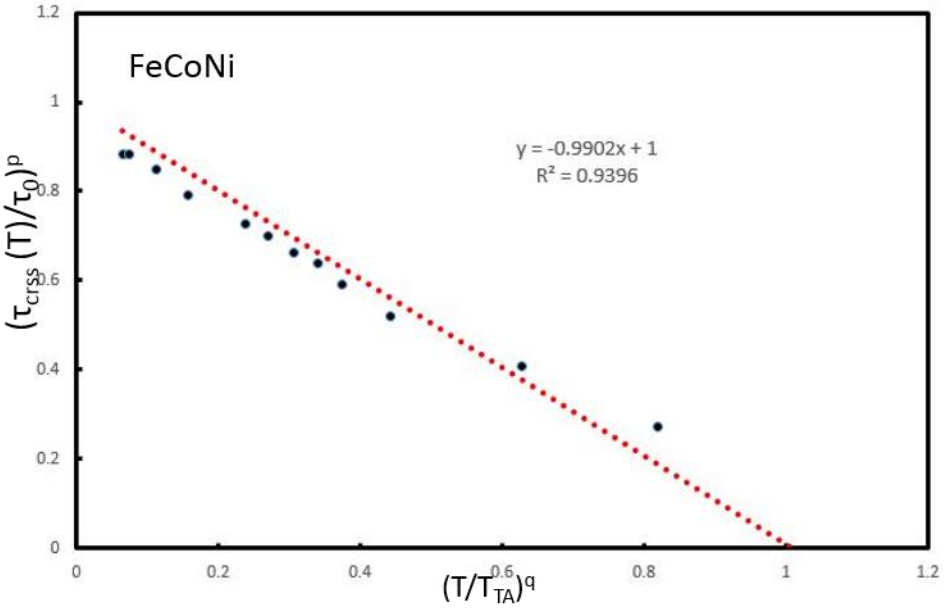

Figure 4.6 (d). reduced effective stress vs reduced temperature according to equation 4.1

Values of these fit parameters in Table 4.2 and the CRSS data scaled with equation 4.1 are consistent with dilute FCC solid solution alloys. The solid solution strengthening behaviour of High and medium entropy alloys is similar to (conventional) dilute alloys.

4.4. Conclusion

Mean square atomic displacement and fitting function of CRSS at 0K was investigated for different derivatives of equiatomic single-crystal FCC cantor alloy, and the following conclusions were drawn:

1. Mean square atomic displacement can be a scaling parameter to predict the strength of these high and medium entropy alloys and other FCC solid solutions. However, a detailed investigation is due to make this claim.
2. p and q values were determined for the fitting equation for the temperature dependence of CRSS of high and medium entropy alloys, and it is found that like dilute solid solution alloys, the range of $0 < p$ 1 and $1 < q < 2$ are similar for these FCC high and medium entropy alloys.

References

[1] N.L. Okamoto, K. Yuge, K. Tanaka, H. Inui, E.P. George, Atomic displacement in the CrMnFeCoNi high-entropy alloy - A scaling factor to predict solid solution strengthening, AIP Adv. 6 (2016). https://doi.org/10.1063/1.4971371.

[2] R.S. Mishra, N. Kumar, M. Komarasamy, Lattice strain framework for plastic deformation in complex concentrated alloys including high entropy alloys, Mater. Sci. Technol. (United Kingdom). 31 (2015) 1259–1263. https://doi.org/10.1179/1743284715Y.0000000050.

[3] R.L. Fleischert, SUBSTITUTIONAL SOLUTION HARDENING*, n.d.

[4] F.R.N. Nabarro, The theory of solution hardening, Philos. Mag. 35 (1977) 613–622. https://doi.org/10.1080/14786437708235994.

[5] R. Labusch, R. LABUSCH: A Statistical Theory of Solid Solution Hardening A Statistical Theory of Solid Solution Hardening, 1970.

[6] G.P.M. Leyson, L.G. Hector, W.A. Curtin, Solute strengthening from first principles and application to aluminum alloys, Acta Mater. 60 (2012) 3873–3884. https://doi.org/10.1016/j.actamat.2012.03.037.

[7] I. Toda-Caraballo, P.E.J. Rivera-Díaz-Del-Castillo, Modelling solid solution hardening in high entropy alloys, Acta Mater. 85 (2015) 14–23. https://doi.org/10.1016/j.actamat.2014.11.014.

[8] C. Varvenne, G.P.M. Leyson, M. Ghazisaeidi, W.A. Curtin, Solute strengthening in random alloys, Acta Mater. 124 (2017) 660–683.

https://doi.org/10.1016/j.actamat.2016.09.046.

[9] T. Ohmura, Ad va nc Ad eV, (2021).

[10] Z. Wu, H. Bei, G.M. Pharr, E.P. George, Temperature dependence of the mechanical properties of equiatomic solid solution alloys with face-centered cubic crystal structures, Acta Mater. 81 (2014) 428–441. https://doi.org/10.1016/j.actamat.2014.08.026.

[11] T.H. Wille, C. Schwink, Precision measurements of critical resolved shear stress in CuMn alloys, Acta Metall. 34 (1986) 1059–1069. https://doi.org/10.1016/0001-6160(86)90216-6.

[12] T.H. Wille, W. Gieseke, C.H. Schwink, Quantitative analysis of solution hardening in selected copper alloys, Acta Metall. 35 (1987) 2679–2693. https://doi.org/10.1016/0001-6160(87)90267-7.

[13] jpsj.56.3941.pdf, (n.d.).

[14] H. Mecking, U.F. Kocks, Kinetics of flow and strain-hardening, Acta Metall. 29 (1981) 1865–1875. https://doi.org/10.1016/0001-6160(81)90112-7.

Chapter 5

Summary and Conclusions

The present thesis studied "Deformation mechanism of Single crystals FCC Medium Entropy alloys(MEA)". The present study revealed many essential and unique behaviour of FCC Cr-Fe-Co-Ni and Fe-Co-Ni medium entropy alloy in the temperature range of 13K-1373K. Each of the behaviour was thoroughly analyzed and experimentally verified. The main results from every chapter are briefly summarized and concluded below:

In **Chapter 1**, the relevant introduction and background of high entropy alloys, deformation mechanism of FCC alloys and objective and outlines of the thesis are reported.

In **Chapter 2**, the Deformation mechanism of FCC single crystal equiatomic Cr-Fe-Co-Ni MEA was reported in the temperature range of 13K-1373K. Compression and tensile deformation behaviour were studied at different strain rates (10^{-5} s^{-1} 10^{-4} s^{-1}, 10^{-3} s^{-1} and $5x10^{-3}$) and at selected temperatures.

Strong temperature dependence of CRSS of single-crystal FCC Cr-Fe-Co-Ni was observed in the low-temperature region. CRSS at 0K was found to be 220MPa. The activation volume of Cr-Fe-Co-Ni was observed at RT and 77K, and values were 248.70 b^3 and 33.74 b^3, consistent with the quinary equiatomic Cr-Mn-Fe-Co-Ni high Entropy alloy. Temperature dependence of CRSS, Strain rate sensitivity and gradient of strain rate sensitivity curves

suggest inertia effect at a temperature lower than 60K, typically seen in other FCC solid solution alloys. Stress-equivalence was also observed in good agreement with other FCC binary solid solution alloys. The activation enthalpy of Cr-Fe-Co-Ni at RT was found to be .71eV, which is in the range of typical FCC alloys. All these findings suggest that solid solution hardening is the principal strengthening mechanism of this single crystal FCC Cr-Fe-Co-Ni. A planar array of dislocation was observed in a bright field image of Cr-Fe-Co-Ni. The stacking fault energy of Cr-Fe-Co-Ni MEA is measured to be 22mJ/m^2 by using the weak beam technique.

Tensile deformation of single crystal Cr-Fe-Co-Ni MEA was studied at room temperature and 77K. At room temperature, deformation twinning was not observed as stress needed for twinning could never reach to that value, but at 77K, twinning was observed. In stage 2 of tensile deformation at 77K, an inflecion point was noticed responsible for the onset of twinning. Twinning stress was found to be 423MPa. A high-resolution atomic image showed a thin layer of the hcp phase along with twinning. Twin thickness was found to be 1.41nm and for hcp thickness was 0.50nm.

In **Chapter 3** the Deformation mechanism of FCC single crystal equiatomic Fe-Co-Ni MEA was reported in the temperature range of 13K-1373K. Compression and tensile deformation behaviour were studied at different strain rates (10^{-5} s^{-1} 10^{-4} s^{-1}, 10^{-3} s^{-1} and $5x10^{-3}$) and at selected temperatures.

Strong temperature dependence of CRSS of single-crystal FCC Fe-Co-Ni was observed in the low-temperature region. CRSS at 0K was found to be 130MPa. The activation volume of Fe-Co-Ni was observed at RT and 77K, and values were 256.46 b^3 and 77.79 b^3, consistent with the quinary equiatomic Cr-Mn-Fe-Co-Ni High Entropy alloy. Temperature dependence of CRSS, Strain rate sensitivity and gradient of strain rate sensitivity curves suggest inertia effect at a temperature lower than 60K, typically seen in other FCC solid solution alloys. Stress-equivalence was also observed in good agreement with other FCC binary solid solution alloys. The activation enthalpy of Fe-Co-Ni at RT was found to be .65eV, which is in the range of typical FCC alloys. All these findings suggest that solid solution hardening is the principal strengthening mechanism of this single crystal FCC C Fe-Co-Ni. A planar array of dislocation was observed in a bright field image of Fe-Co-Ni. The stacking fault energy measurement of Fe-Co-Ni MEA is beyond the range of weak beam technique as the separation width is too narrow and considered to be high stacking fault energy.

Tensile deformation behaviour does not show twinning because of its high stacking fault energy and low strain hardening rate in stage 2. Cross–slip was observed and considered as the primary deformation mechanism in stage 2 of tensile deformation.

In **Chapter 4**, Mean square atomic displacement was introduced as a scaling factor to predict the strength of FCC high and medium entropy alloys. A correlation was developed between MSAD and CRSS at 0K for derivatives of Cantor FCC alloys. First principal

calculations determined MSAD and CRSS was deduce by extrapolating the temperature dependence of the CRSS curve. Fitting parameters were deduced for the fitting equation used to deduce the CRSS at 0K and was found in good agreement with the values reported for dilute alloys.

The present study is a systematic study of plastic deformation of different derivatives of equiatomic FCC single crystal of cantor alloy in a wide temperature range. The first detailed study of temperature dependence of CRSS of medium entropy alloys. This study gives an insight into operative deformation mechanism of single crystal FCC medium Entropy alloys.

In **Chapter 5**, this thesis has reported experimental findings from every chapter briefly summarized and concluded.

Acknowledgements

I would like to quote Dr APJ Kalam sir, here " If you fail, never give up because FAIL means "First Attempt In Learning." This very quote kept me going towards my PhD journey. I feel blessed to have great support from my family. There are not enough words to express my gratitude toward my Mother and elder brothers. I am forever grateful to Allah SWT, who gives me enough strength and courage that kept me moving forward.

I would like to express my sincere gratitude to my thesis advisor Prof. Haruyuki Inui, for giving me an opportunity to pursue my higher studies with him. I am indebted to him to teach me all the fundamentals related to the plastic deformation of FCC alloys. I admire his way of teaching; the encouragement he gave me constantly to learn as much as possible. I sincerely acknowledge his invaluable suggestions and productive discussions during my research.

I would like to extend my sincere gratitude to Associate Prof. Kyushike Kishida and assistant Professor Kodai Niitsu of Inui laboratory for their invaluable suggestions and most effective discussions during my PhD at Kyoto University. I would like to thank Dr Zhenghao Chen, Dr Afandi, and Mr Li for fruitful discussion from time to time and for helping me with my experiments. I would like to thank Hazui Miki san, secretary of Inui lab, for her continuous help during my day to day activities and for processing all the official documents regarding my PhD. I would like to thank Dr Bhaskar Paul for his kind support while his stay in Inui Lab. and my seniors Sai Chandra Teja, Mohit Joshi and my friends Soumya Sethi, Siddharth Gavhale, Surya

and Hardik, Rutvika, Richards, Kaushik, Richa and Tushar for their unconditional help during my stay in Japan. Thanks are due to all the previous and current lab members for creating a healthy research atmosphere.

I would like to express my sincere appreciation to Prof. Nobuhiro Tsuji and Prof. Hideyuki Yasuda of Kyoto University for their acceptance to evaluate my thesis.

Most importantly, acknowledgements are due to the Japan International Cooperation Agency (JICA) - FRIENDSHIP scholarship for financial support during the course of my study at Kyoto University, Japan. I will always be owing gratitude to the JICA for invaluable support.